A Study of Vibration Control of Truck Seat Suspension System

A thesis submitted in fulfillment of the requirements for the Degree of Master of Engineering

Yuli Zhao

Bachelor of Automotive Engineering & Mechanical Engineering, RMIT University, 2014

School of Engineering

College of Science, Technology, Engineering and Maths

RMIT University

September 2020

Declaration

I certify that except where due acknowledgment has been made, the work is that of the author alone; the work has not been submitted previously, in whole or in part, to qualify for any other academic award; the content of the thesis is the result of work which has been carried out since the official commencement date of the approved research program; any editorial work, paid or unpaid, carried out by a third party is acknowledged; and, ethics procedures and guidelines have been followed. I acknowledge the support I have received for my research through the provision of an Australian Government Research Training Program Scholarship

Yuli Zhao

29th September 2020

Acknowledgments

First of all, I would like to extend my sincere gratitude to my supervisor, Professor Xu Wang, for his constant encouragement and patience with me for these years. He has walked me through all the stages of my Master degree study and he also has contributed to this thesis with a major impact. Thank you as well for those wise advice, for my research life.

Second, I would like to express my heartfelt gratitude to my second supervisor Associate Professor Yongmin Zhong, for his support and suggestions.

I am also deeply indebted to Mr. Huw James, for his assistance in the NVH Lab and workshop. I also want to thank Mrs. Mary Tomlinson for her administration related helps.

Special thanks should go to those people in my office for their help in academics and life. To all my colleagues: Ran Zhang, Zhenwei Liu, Han Xiao, Latih Egab, Elie Al Shami, and Linchuan Guo.

Last, my thanks would go to my beloved family for their loving considerations and great confidence in me all through these years.

Statement of impact from COVID19

Due to the impact of COVID19, Melbourne went into lockdown from March 2020. Due to the school blockade, my scheduled experiments cannot be completed. I cannot use laboratory equipment to verify the mathematical model, and at the same time, I cannot provide training data for the artificial neural network model. Due to the closure of the workshop, the active suspension system for the truck seat cannot be manufactured, even if the related motor, gearbox, belts, and pulleys have been purchased. All these have had a significant impact on my research work.

Table of Contents

List of Figures

List of Tables

Abstract

The research has designed a novel active truck seat suspension system for a further study of active vibration control. A 5-degree-of-freedom driver and seating suspension system model for active vibration control has been developed. A novel fast system parameter identification method from vibration measurement data has been proposed for the seat-occupant system based on the multi-objective Genetic Algorithm optimization (GA). This system parameter identification method can identify the system parameters of a 5 degree-of-freedom lumped mass-spring-dashpot biodynamic seat-occupant model from vibration test results quickly and accurately. Without calculation and measurement of materials, the physical parameters of the seating suspension system such as mass (m), stiffness (k) and damping coefficients (c) are estimated by matching the measured resonant frequency and peak transmissibility amplitude at a specific frequency with the simulated ones. This is one of the main contributions of this paper. The characteristics of the human body vibration in the low-frequency range are analyzed through the seat to head transmissibility (STHT) ratio. The experimental and simulation results of the STHT values have been compared to verify each other. The sensitivity analysis of the seat effective amplitude transmissibility (SEAT) values over the seating system parameters have been conducted and validated by the measured results of the transmissibility ratios. This has answered the first research question.

A response surface method (RSM) model has been developed to establish a relationship between the vibration isolation performance target and input design parameters from any measurement or simulation results. The statistical significance of the RSM model has been validated by analysis of variance (ANOVA). The sensitivity analysis of design parameters and their interaction effects have been conducted. The design parameters have been optimized through RSM modeling and the genetic algorithm (GA). It is concluded that to mitigate the low-frequency vibration, the addition of a seat cushion with small stiffness and damping coefficients and use of the commercial vehicle seat with the small seat structure

stiffness and damping coefficients are most effective for the system vibration isolation. The results of the response surface method have been verified by those of the artificial neural network modeling and linear regression modeling in this thesis. This has answered the second research question.

Finally, a novel type of active seating suspension system combining timing belt, servo motor, and traditional x-shaped seat structure has been proposed and designed for vibration control. The design fully considers the packaging space of the seating suspension system, including the reduction of the system volume and noise. This has answered the third research question.

Nomenclature

A_I effective cross-section area of the inlet valve, m^2

A_E effective cross-section area of the outlet valve, m^2

A_{ef} effective area of the pneumatic spring, m^2

a, b distances of the axles to the centre of gravity of the vehicle body (m)

c_{si} ith damping coefficient of suspension (N s/m)

c_{s5} damping coefficient of the passenger seat (N s/m)

d_m variable diameter

d(n) disturbance signal as calculated in the feedback controller

e, f distances of the passenger seat to the centre of gravity of the vehicle body (m)

e(n) error signal

Fc_{1x} force of the mechanical springs, N

Fc_{2x} force of the end-stop buffers, N

Fd_{1x} force of the hydraulic shock-absorber, N

Fd_{2x} overall friction force, N

$\widehat{F_d}$ disturbance observer

k_{si} ith spring constant of suspension (N/m)

k_{s5} spring constant of the passenger seat (N/m)

k_{ti} ith stiffness coefficient of the tyre (N/m)

M mass of the vehicle body (kg)

m suspended mass, kg

m_s mass of suspension system affixed to suspended mass, kg

m_I mass flow rate for inflating of the air-spring, kg/s

m_E mass flow rate for exhausting of the air-spring, kg/s

m_i ith mass of axle (kg)

m_5 mass of the passenger (kg)

p_{as} air pressure inside the air-spring, Pa

p_{m1}, p_{m2} air pressure into the left and right muscles, Pa

p_s air pressure of the power supply, Pa

p_0 atmospheric pressure, Pa

$P(z)$ primary path

$W(z)$ adaptive filter

q_{1x}, displacement of the seat upper part frame, m

q_{2x} displacement of the sitting part of the human body in contact with the back support, m

T_s air temperature of the power supply, K

T_0 atmospheric air temperature, K

F_{as} air-spring force, N

F_{bd} bottom end stop buffers force, N

F_{bu} top end stop buffers force, N

F_d shock-absorber force, N

F_{ff} friction force, N

F_g gravity force, N

$G_{IS(z)}$ internal model system of the feedback controller

p_m absolute air pressure

$S(z)$ secondary path dynamic

u desired control input

u_{m1}, u_{m2} predicted control signals, V

u_{min}, u_{max} minimum and maximum values of the signal, V

V_m cylindrical volume

$W(z)$ adaptive controller

x displacement of the suspended mass, m

$\tilde{x}$ acceleration of the suspended mass, m

x_s displacement of the excitation, m

$\tilde{x}_{set}$ setting value of the acceleration control loop, m/s^2

$x(n)$ reference signal

x_i ith state variable (m)

$y(n)$ filter output

z_v cabin floor displacement

z_s mass displacement

$z_i(t)$ ith road excitation (m)

Introduction

How to reduce the harm damage to human health caused by the vibration of trucks and other commercial vehicles has become a popular research topic. The motivation of the research is to develop a truck seat with a compact active suspension to improve the ride comfort and manufacturing readiness.

This thesis is composed of 8 chapters, which aims to answer the research questions raised from the research gaps based on the literature review. 1. How is a reliable and accurate biodynamic model developed based on vehicle measurement data? 2. How is the influence of system parameters and their interactions on the vibration isolation performance determined using the system sensitivity analysis method? 3. How is the actuator mechanical structure integrated with traditional seat structure to reduce the size of an active seat system and packed into a vehicle cab for vibration control?

The thesis focuses on a study of the parameter identification method of the seating suspension system and design parameter optimisation method for the best vibration isolation performance rather than focuses on the active vibration control research which will be conducted by another Ph.D. student.

The major assumptions of the thesis are: the driver seating suspension system is a small displacement, time non-variable parameter, and linear system. The main focused frequency range is around 4 Hz (1.6 ~ 10 Hz), as this frequency is close to the human body critical resonant frequency. The vibration at this frequency will most cause the sickness and discomfort of human passengers. Although a five degrees of freedom biodynamic human seating suspension system model is adopted and the motion platform of CKAS has three degrees of freedom of the roll, pitch, and heave, the main focused vibration mode or degree of freedom is the vertical or heave mode. This is because the vertical vibration would most degrade the ride comfort which reflects common sense. In order to consider the effect of the truck suspension on the ride comfort of the human seating suspension, a seven degrees of freedom truck vehicle suspension plus human seating suspension model has been adopted by combining the five degrees of freedom biodynamic human seating suspension system with the two degrees of freedom truck suspension system. The excitation signals in this thesis can be either the measured truck cab floor accelerations for the five degrees of freedom biodynamic human seating suspension system or the road class profile displacement random excitations defined in the ISO 8606 standard for the seven degrees of freedom truck vehicle suspension plus human seating suspension model. It is assumed that the idle vibration of the truck human seating system is stationary.

1 Literature Review

1.1 Introduction

Modern research has shown that whole-body vibration (WBV) can lead to potential hazards. Based on existing studies, there are many medical reports regarding the diseases that may be caused by WBV, including back and neck pain, neuropathy, cardiovascular disease, digestion disorders, and cancer [1].

As a risky occupation, the drivers of heavy commercial vehicles are prone to prolonged exposure to low-frequency WBV generated from road excitation, which could influence drivers' comfort and affect their health. According to Ref. [2], the long-term operations of heavy commercial vehicles under low-frequency vibrations can cause diseases of the muscles, bones, digestive system, and the visual system. This is because low-frequency vibrations can lead to resonance of the organs and tissues in the human body, and this type of vibration energy is absorbed and dissipated by the body. According to Ref. [3], due to the high social cost of musculoskeletal diseases caused by the working environment under low-frequency vibrations, Europe has issued regulations requiring that the vibration level of a working vehicle's driver must be evaluated to provide a healthy and safe operation environment, where the maximum accelerations of 0.5 and $1.5\ \mathrm{m/s^2}$ are set for 8 hours of action and limit values, respectively. In Ref. [4], it was reported that the WBV may induce changes in the posture of the human body and cause health risks to the muscular system and spine. In Ref. [5], it was shown that conventional vehicle seats with passive suspension would fail to protect the driver's body from the health risks of WBVs if the exposure to low-frequency vibrations produced by commercial vehicles was more than 8 hours every day. It was claimed in a medical research report [6] that back pain disease is one of the most common occupational injuries, because the lower back of the human body is sensitive to low-frequency vibrations of 4–10 Hz. Therefore, long-term exposure to large amplitude low-frequency vibrations can cause back pain disorders, especially common diseases of the lumbar joints. These diseases include degenerative spinal changes, lumbar disc herniation, and sciatic nerve injuries. According to ongoing medical reports, these diseases are common among tractor drivers, truck drivers, bus drivers, and other commercial heavy machinery operators who are often exposed to vibrations throughout the body.

The diagram (Figure 1.1) shows the vibration amplitude orders of commonly used heavy commercial machinery. According to the international standard ISO 2631-1 1997, as the vertical acceleration increases, the ride comfort decreases, and the WBV level increases, which also increases health risks. Therefore, the development of an efficient vibration reduction seat system is a practical and effective way to protect drivers. Researchers have studied the vibration control of vehicle seat systems as well as various effects that vibrations and vibration transmission exerted on the human body. In Ref. [7], the seats of 100 commercial heavy-duty vehicles from 14 different categories were tested and evaluated for vibration isolation performance. Two groups of Seat Effective Amplitude Transmissibility (SEAT) values calculated through the weighting parameters of different standards (BS6841 and ISO2631) showed that the median SEAT values of these seats were all less than 100%, indicating that they provided a certain degree of isolation and protection. This study also proposed to improve the dynamic performance of seats by reducing the severity of WBV exposure in many working environments. In addition to the dynamic characteristics of seats, the dynamic response of the human body under vibration excitation is also a topic of considerable interest. In Ref. [8], 41 male and 39 female subjects between 18 and 65 years of age were selected to participate in an experiment to study the factors that may affect the apparent mass of the human body, which is a method that can be used to present comfort levels and WBV levels and their relationship. According to this study, aging can affect the resonant frequency of the human body and the transmission ratio of vibration. Further, gender and body mass index (BMI) are factors that affect vibration transmissibility. In addition to research on the whole seat, the seat cushion, as an important vibration isolation device, was examined in Ref. [9]. The authors investigated the seat cushion–body interaction by measuring and analyzing the contact force distributions and the contact area between the human body and the seat cushion when vibration is experienced. It was found that the pressure distribution at the interface between the body and the cushion showed strong asymmetry in terms of the dynamic contact force, and the effective contact area was affected by the nonlinear characteristics of the cushion itself and the characteristics of soft tissues of the human body. Further, under large vibration excitation, a seat cushion with high stiffness, a large damping coefficient, and large static deflection are able to effectively reduce the transmission of vibrations. It can be seen from the figure that the human head, in the sitting state, has the largest acceleration ratio under vibration excitation of about 4 Hz, followed by the shoulders.

Figure 1.1 Contents page from paper Diagnosis of whole-body vibration related health problems in occupational medicine. *J. Low Freq. Noise Vib. Act. Control* 2011, *30*, 207–220. Johanning, E.

<Image removed due to copyright restrictions>

Figure 1.1 (a) Vibration amplitude orders from the measurement of examples of on- and off-road vehicles [6] (b) Vibration sensitive frequencies of different parts of the sitting posture of the human body.

In terms of seat vibration isolation measurements, an active dummy was developed (Figure

1.2), which adopted lateral and longitudinal actuators to produce forces in the vertical and longitudinal directions, respectively, to simulate the dynamic response of three different human body mass by reproducing the equivalent dynamic mass [10].

Figure 1.2 Contents page from paper
MEMOSIK V—An active dummy for
determining three-directional transfer
functions of vehicle seats and vibration
exposure ratings for the seated occupant.
Int. J. Ind. Ergon. 2008, *38*, 471–482.
Mozaffarin, A.; Pankoke, S.; Wölfel, H.-P.

<Image removed due to copyright restrictions>

Figure 1.2 The schematic diagram of MEMOSIK V [10].

Of course, in all of these works, determining how to mitigate vibrations is the most critical aspect. Three current mainstream research directions in this area are passive, semi-active, and active seat suspensions.

The passive seat suspension system can reduce vibrations by using conventional spring and damper components, but due to its characteristic limitations, vibration control that targets multiple frequencies cannot be achieved even with a well-tuned traditional positive spring-damper system. Therefore, a quasi-zero static stiffness seat suspension system based on the combination of negative stiffness and positive stiffness springs was proposed [10] to improve the vibration control efficiency of a seating system, as the characteristics of high static stiffness and low dynamic stiffness can be used to eliminate seat vibrations. In Ref. [12], a poly-optimal solution was sought for a seating system combined with a pneumatic spring and damper. This improved the performance of the traditional passive seat system by attenuating low-frequency vibrations in the frequency range of 0–4 Hz.

Semi-active vibration control of a seating system utilizes the characteristics of magnetorheological [13-16] and the electrorheological materials [17], which can change the stiffness or Young's modulus under magnetic field variations and achieve vibration control in a specific frequency range. In Ref. [18], a negative stiffness seat suspension system combined with a pneumatic spring stiffness control mechanism was proposed, and the related control algorithm that affects device stiffness variations associated with position and velocity data evaluation was designed. The semi-active vibration control method can achieve vibration control in a relatively certain frequency bandwidth with less energy consumption and fewer costs than the other two methods.

In Ref. [19], the difference between seat systems with active electromagnetic seat suspension and passive seat air suspension in reducing the WBV level and improving comfort was compared. The experimental results showed that the active electromagnetic suspension performed better for vibration reduction than the passive air spring suspension. In particular, passive suspensions may increase the amplitude of lateral vibration, which also harms driver comfort.

In terms of structure, in addition to traditional shock absorbers, semi-active seat suspensions have also been designed in different styles. An integrated semi-active seat suspension that included a swing mechanism (Figure 1.3) that converts longitudinal and vertical motion into rotational motion and a torque-controlled rotary magnetorheological (MR) damper operated in a pure shear mode to attenuate vertical and longitudinal vibrations was designed [14]. Additionally, a new semi-active seat suspension based on the variable admittance (VA) concept and designed a rotating VA device based on the MR damper was proposed to control the seat vibration. A random vibration test showed that the semi-active seat suspension had excellent low-frequency vibration cancellation performance. The frequency-weighted root-mean-square (FW-RMS) acceleration of the seat was reduced by 43.6%, indicating that ride comfort was greatly improved. Otherwise, a semi-active vibration control seat system based on an energy harvest device with variable external resistance was also developed. In the design, the energy regeneration seat device included a three-phase generator and a gear reducer mounted at the centre of the scissor-like structure of the seat, and the vibrational energy was collected directly from the rotational motion of the scissor-like structure. An H-infinity-state feedback controller was designed for a semi-active vibration control seat system, and the FW-RMS acceleration was reduced by 22.84% compared with passive vehicle suspension. At the same time, the generated RMS power was 1.21 W.

Figure 1.3 Contents page from paper Integrated semiactive seat suspension for both longitudinal and vertical vibration isolation. *J. Intell. Mater. Syst. Struct.* 2017, *28*, 1036–1049. Bai, X.-X.; Jiang, P.; Qian, L.-J.

<Image removed due to copyright restrictions>

Figure 1.3 Semi-active seat system vibration controls with a magnetorheological (MR) damper [14].

For the controller design, Sky-hook control theory [22–25], H-infinity control algorithm [26–32], non-resonance theory [15], on-off control strategy [33], fuzzy control theory [34–36], optimal control theory [37–39], Lyapunov control scheme [40], PID control algorithm [41] and sliding-mode control algorithm [42] are applied for the design of the controllers.

Compared with controller designs based on a single traditional adaptive control algorithm, an increasing number of controllers integrating multiple control algorithms built with semi-active seat vibration control systems have been proposed to improve vibration attenuation performance. In Ref. [43] a new adaptive fuzzy controller combining the H-infinity and sliding-mode control algorithms for a semi-active seat suspension with an MR fluid damper. This controller features a fuzzy control method that does not require an accurate dynamic model, even in a dynamic system with an uncertain environment. After that, a new adaptive hybrid controller was developed integrating the H-infinity control algorithm, the sliding-mode control algorithm, and the Proportional-Integral-Derivative (PID) control algorithm with the vibration attenuation of a semi-active seat system [44]. This controller features a combination of the Hurwitz constant matrix as components of the sliding surface and the H-infinity algorithm with robust stability. Also, a fuzzy logic module based on the interval type-2 fuzzy logic system was established, and a model was characterized by on-line clustering considering external interference. In Ref. [44], a new hybrid controller was proposed combining a neural fuzzy control module, a Proportional-Integral (PI) control module, and a sliding mode control module to control a semi-active seat suspension with an MR damper. The interval type-2 fuzzy model with an on-line rule updating function was adopted, and a granular clustering method was used to find data for the initial fuzzy set used to support the fuzzy model. Compared with conventional controllers, the proposed controller can provide better stability for vibration control performance. In Ref. [46], a novel neuro-fuzzy controller (NFC) was designed for a semi-active seat suspension system with an MR damper. This adaptive neuro-fuzzy inference system (ANFIS) is based on an algorithm called B-ANFIS, which is combined with a fuzzy inference system (FIS). Compared with the skyhook control theory, the NFC is better at improving the ride comfort of the vehicle. Besides, the NFC's ability to track trajectories and transient response characteristics is superior to that of conventional skyhook controllers. In Ref. [45], a new adaptive fuzzy controller based on inversely fuzzified values related to the H-infinity control algorithm to control the vibration of a semi-active seat suspension system was designed for an MR damper where a Riccatilike equation with fuzzified values was applied to enhance system robustness.

In summary, people are constantly studying new vehicle seat systems or applying advanced technology on vehicle seat system design to eliminate vibration to the human body and improve ride comfort. Meanwhile, people also have to face the design constraints of the limited space in the vehicle cabin and being very sensitive to energy consumption. For the passive seat system, the quasi-zero static stiffness structure has been applied to improve the low-frequency vibration isolation performance with zero energy consumption [11]. However, this suspension structure consists of three sets of springs, so this bloated structure obviously cannot meet the packaging requirements of a traditional vehicle cab which has a small space to place the structure. The semi-active suspension has shock absorbers consisting of magnetic rheological materials, which can replace the hydraulic or pneumatic shock absorbers in the traditional vehicle seat system. However, due to the characteristics of magnetorheological materials, the vibration control performance of semi-active suspension is not particularly improved compared with that of traditional passive seat system, and also the semi-active suspension needs electrical power to be driven. The active seat suspension uses a traditional motor or a linear motor as a force actuator to generate the resistant torque to mitigate the vibration. This solution is the most efficient, but making a practical and compact seat system with active seat suspension is becoming a big challenge.

Therefore, firstly, this chapter aims to reviewing and benchmarking the development and progress of active seat suspension in the previous literature published. An active vibration control seat system will be designed in a reduced size, then analyzed and discussed to be finalized with a design direction of significant advantage. Finally, the research gaps will be identified and questions will be raised and discussed.

1.2 Seat Systems with Active Suspension

1.2.1 Experiments with Prototypes

Active seat suspension prototypes in several previous research projects used electromagnetic, hydraulic, or air actuators to generate a corresponding compensation force for vibration cancellation in a finite number of frequencies, thereby reducing the vibration acceleration amplitude and improving the comfort of the seat system. According to Ref. [48], an active vibration control suspension in a vehicle has better vibration cancellation performance than a passive seat suspension. In Ref. [49], comparative experiments demonstrated that active and semi-active seat suspensions could improve comfort by approximately 50% compared with the passive seat suspensions.

The actuators used for active seat suspensions generally fall into three categories: electromagnetic actuators using linear or conventional rotating motors, hydraulic actuators using hydraulic servos, and air actuators using air springs. Among these three types of actuators, electromagnetic actuators have attracted the most attention because they have good dynamic responses, do not require an additional hydraulic servo system, tubes, or compressors, and satisfy small space requirements. The large output of hydraulic actuators makes them easy to carry with greater mass. The air actuator has a good vibration isolation effect in high frequencies.

1.2.1.1 Pneumatic Actuator

For vibration control, people developed an active seat suspension using a pneumatic spring and a corresponding feedback controller [50]. According to the results, the active seat suspension using vibration compensation can reduce the vibration amplitude by 10 dB, which is about 3 times. The vibration transmission rate of the active seat suspension is reduced by 30%–40% compared with that of a conventional passive seat suspension.

In another research project [51], an active seat suspension system was designed to attenuate low-frequency vibration. The active seat suspension system is composed of a pneumatic spring and a related linear control system as shown in Figure 4. The conventional metal spring in the system is used to carry the static load, and the pneumatic spring is used to generate damping and compensating forces to mitigate vibration. The pneumatic spring is driven by compressed air which is controlled through a proportional valve. The benefit of such a parallel structure is that the energy consumption of the whole system can be reduced. Two acceleration sensors and one displacement sensor were used in the experimental equipment, and the electric signals generated by the excitation were respectively collected by the corresponding controller and summed to control the actuator. There is no actual damper in this system, and the function of the damper is replaced by absolute damping, which is generated from the air spring through the skyhook control method. The complex state and parameters of the entire pneumatic subsystem need to be considered and the state equation of the compressed air needs to be considered in this active seat suspension. Besides, the flow rate of the air, the corresponding pressure changes in the air spring, and the corresponding forces also need to be considered. For the control system, a simple and practical linear control system is used where the controller is based on feed-forward and feed-back algorithms to reduce the effect of vibration on the human body by controlling the static position, damping force, and compensation force of the seat system. It was found that this active pneumatic spring seat suspension can reduce vibration transmissibility by approximately 8–10 dB with the feed-forward compensation path for a mass of 80 kg. In an experiment, by adjusting the parameters of the pneumatic spring, it was found that the active seat system performed well for vibration control in a frequency range of less than 4 Hz. However, this control system needs to work under an ideal condition.

Figure 1.4 Contents page from paper Vibration control system with a proportionally controlled pneumatic actuator. In Proceedings of the 1997 European Control Conference (ECC), Brussels, Belgium, 1–7 July 1997; pp. 1814–1818. Stein, G.J.

<Image removed due to copyright restrictions>

Figure 1.4 Active seat system vibration controls with a parallel spring structure [51].

An active seat suspension incorporating a hydraulic shock absorber and an active pneumatic spring (Figure 1.5) was developed in Ref. [52–54]. In this seating system, a hydraulic shock absorber is connected to a scissor-like frame for vibrational energy absorption, while a pneumatic spring is attached to the bottom of the seat and a rod of the frame to produce the corresponding compensation force. Among them, 1 represents the body mass; 2 is the upper part of the vibration control system; 3 is the steel spring; 4 is the lower part of the control system; 5 is the proportional electro-pneumatic transducer; 6 is the air spring; 7 represents the relative displacement sensor; 8 and 9 represent the two accelerometer sensors; uS, uZ, uB represent the output voltage signal; RS, RC, RB represent the corresponding transfer functions; uC is the actuator control voltage; AC, AB AS are transducing coefficients associated with two accelerometer sensors 8 and 9 and the relative displacement sensor 7; N is the actuator amplifier stage. The air spring is inflated and deflated by using compressed air and a proportional air valve. The advantage of this configuration is that configurations of the currently existing vehicle seat systems can be used without large modifications. Based on this type of active seat suspension system, a robust controller that can work with different mass loads was proposed for an active seat suspension as shown in Figure 1.6. In the design of the controller, the author used a triple feedback loop system to detect the acceleration, the relative speed, and the displacement of the suspension system and to control the system [52]. The results of the experiment demonstrated that an active seat system could be used to reduce the amplitude of the vibration by half compared with conventional passive seat systems at a resonant frequency. According to the previous research, when the human body is exposed to the vertical and horizontal whole-body vibration of 1.6 ~ 10Hz in the sitting state, the subjective discomfort and dynamic equivalent mass are both affected. The pitch and roll vibrations of the vehicle will cause the pitch and roll vibrations of the seat and driver which would cause discomfort, especially at 4 Hz. The human body is most sensitive to vibration around 4 Hz, so controlling the vibration of this low-frequency range can greatly improve seat comfort. The system can control the suspension well in the range of 0.5–4 Hz and can reduce response amplitudes under different mass load conditions, which means will improve the riding comfort.

Figure 1.5 Contents page from paper The vibration damping effectiveness of an active seat suspension system and its robustness to varying mass loading. *J. Sound Vib.* 2010, *329*, 3898–3914. Maciejewski, I.; Meyer, L.; Krzyżyński, T.

<Image removed due to copyright restrictions>

Figure 1.5 A seating system with an active pneumatic spring suspension [52].

Figure 1.6 Contents page from paper The vibration damping effectiveness of an active seat suspension system and its robustness to varying mass loading. *J. Sound Vib.* 2010, *329*, 3898–3914. Maciejewski, I.; Meyer, L.; Krzyżyński, T.

<Image removed due to copyright restrictions>

Figure 1.6 Schematic of the triple feedback loop controller [52].

With the same active seat suspension, an adaptive controller was developed as shown in Figure 1.7 [54]. This is a multi-controller approach to control the entire system, where the primary controller is used to calculate the force required to reduce the vibration. The inverse model is used to calculate the effective area of the proportional control valve. The application of the inverse model in the controller can directly derive the input signal according to the required force. The Proportional-Derivative (PD) predictor is used to generate the corresponding control signal to speed up the controller. Finally, the adaptive mechanism can estimate the load mass based on the inflation and deflation of the pneumatic spring. This active seat suspension can achieve good vibration control performance compared with a passive system, having a load range from 50 to 150 kg at a resonant frequency of 1.3 Hz. The advantage of this controller is that the adaptive control itself makes the system quickly return to stability by estimating the initial suspended load. The shortcoming of the controller is that the complexity of the multi-controller may delay signals, and in the case of high road roughness, the vibration control performance of the seat system will be degraded.

Figure 1.7 Contents page from paper Active control of a seat suspension with the system adaptation to varying load mass. *Mechatronics* 2014, *24*, 1242–1253. Maciejewski, I.; Glowinski, S.; Krzyżyński, T.

<Image removed due to copyright restrictions>

Figure 1.7 Schematic of the multi-controller [54].

A horizontal active seat suspension was designed using pneumatic muscles for horizontal vibration control as shown in Figure 1.8 [55]. This original control system combined a primary controller and an inverse model module to provide a control signal to the pneumatic muscles, and a PD control module was used to speed up the signal as shown in Figure 1.9. According to the final results, the proposed active seat suspension performed better than a passive seat suspension for vibration attenuation in the 1–10 Hz frequency range.

Figure 1.8 Contents page from paper Modeling and vibration control of an active horizontal seat suspension with pneumatic muscles. *J. Vib. Control* 2018, *24*, 5938–5950. Maciejewski, I.; Krzyżyński, T.; Meyer, H.

<Image removed due to copyright restrictions>

Figure 1.8 (a) The pneumatic muscle at the nominal length and (b) After contraction [55].

Figure 1.9 Contents page from paper Modeling and vibration control of an active horizontal seat suspension with pneumatic muscles. *J. Vib. Control* 2018, *24*, 5938–5950. Maciejewski, I.; Krzyżyński, T.; Meyer, H.

<Image removed due to copyright restrictions>

Figure 1.9 Block diagram of the control structure of the vibration control system [55].

The utilization of pneumatic springs as actuators has some advantages, such as being simple, reliable, and compact. At the same time, their low response speed, poor control precision, and dependence on a compressor pipeline hinder their actual use.

1.2.1.2 Hydraulic Actuator

In Ref. [56], an active seat suspension using a hydraulic actuator was developed as shown in Figure 1.10 [56]. In this system, the hydraulic actuator is controlled by a solenoid valve to control the direction of the force generated by the actuator. The control system generates a corresponding compensation force to reduce the vibration based on signals collected by two acceleration sensors and a displacement sensor. A PI controller was designed for the active seat suspension. Since the acceleration sensor and amplifier are integrated for the displacement of the positioning system, the system can be simplified using only one accelerometer placed on the chassis. This structure greatly simplifies the control system. This structure can also be achieved by connecting two first-order low-pass filters in series or by using a second-order analog circuit to adopt a very low resonant frequency as shown in Figure 1.11.

Figure 1.10 Contents page from paper Active Vibration Control System for the Driver's Seat for Off-Road Vehicles. *Veh. Syst. Dyn.* 1991, *20*, 57–78. Stein, G.J.; Ballo, I.

<Image removed due to copyright restrictions>

Figure 1.10 Active hydraulic control of a seat suspension system [56].

Figure 1.11 Contents page from paper Active Vibration Control System for the Driver's Seat for Off-Road Vehicles. *Veh. Syst. Dyn.* 1991, *20*, 57–78. Stein, G.J.; Ballo, I.

<Image removed due to copyright restrictions>

Figure 1.11 Schematic of the control system [56].

In this study, the delay of hydraulic performance was also considered and solved by using the cut-off frequency method. Also, the hysteresis effect of the hydrodynamic device was also carefully considered in the process of controller design. Depending on the result, the active seat suspension with the controller can reduce the acceleration Power Spectral Density (PSD) amplitude up to 16 dB at a frequency of 2 Hz compared with a passive system. The reduction of the acceleration Power Spectral Density (PSD) amplitude up to 16 dB at a frequency of 2 Hz by the active seat suspension with the controller is very important as the vibration frequency of 2 Hz is within the resonant frequency range where the vibration largely influences human comfort.

Active hydraulic control has the advantages of a large output force and high control precision, but the hydraulic pipeline and servo system of hydraulic control may also greatly limit its application.

1.2.1.3 Electromagnetic Actuator

A new active seat vibration reduction structure as shown in Figure 1.12) was proposed in Refs. [57–60]. This active seat system is based on the common scissor-like structure of commercial vehicle seat systems, using an inexpensive conventional rotary electric motor instead of an expensive linear motor as the actuator. The 1:40 gear ratio of the gearbox allows the electric motor to produce a torque output of 52 Nm. Moreover, due to the enlarged gearbox, the internal friction of the active seat suspension is greater than that of a conventional seat suspension system. The system can save some space because there is no need to install a conventional shock absorber. Also, the spring stiffness of the seat is carefully selected to keep the resonant frequency of the whole seat system lower than 4 Hz, which is the most sensitive vibration frequency range of the human body and may cause an uncomfortable feeling.

Figure 1.12 Contents page from paper Active control of an innovative seat suspension system with acceleration measurement based friction estimation. *J. Sound Vib.* 2016, *384*, 28–44. Ning, D.; Sun, S.; Li, H.; Du, H.; Li, W.

<Image removed due to copyright restrictions>

Figure 1.12 (a) The schematic of the seat structure (b) Front view of the seat structure [58].

In terms of the control system, an H-infinity algorithm based on output feedback was developed to reduce the seat system vibration [57]. The key feature of this design was the estimation of the friction generated by the active vibration control system. A special controller with friction compensation was employed to improve the precision of the control, which can affect the performance of the vibration control. The test results showed that in the low-frequency range, from 3 to 5 Hz, the driver's body RMS acceleration can be reduced by more than 35%.

In another study [58], an H-infinity controller with friction compensation was proposed to actively control the previously mentioned seat suspension. Due to the usage of the friction observer based on the acceleration measurement, the H-infinity controller can be more sensitive to the response of vibration excitation and can also improve the vibration control performance. The results of the experiment showed that the entire vibration control system could reduce vibration in a frequency range from 1 to 4.5 Hz. According to the ISO 2631 standard, the FW-RMS value of the vibration was reduced up to 35.5% by the vibration control system compared with a conventional well-tuned passive suspension system.

In Ref. [59], a terminal sliding mode controller based on a state observer and a disturbance observer was proposed to control an active seat suspension system as shown in Figure 1.13 where the state observer in this article is a program used to predict the state of space, and the disturbance observer is a friction observer which is a program for real-time prediction of friction. In the case where the suspension acceleration and relative displacement are measurable, but the absolute seat speed is unmeasurable, the settings of the disturbance and state observers can reduce the switching gain of the controller. The controller proposed in this paper had better control performance than the state feedback terminal sliding mode controller and could improve the comfort of the seat system. According to the experimental results, FW-RMS and Vibration Dose Value (VDV) were reduced by 34% and 33%, respectively.

Figure 1.13 Contents page from paper Vibration reduction of seat suspension using observer based terminal sliding mode control with acceleration data fusion. *Mechatronics* 2017, *44*, 71–83. Ning, D.; Sun, S.; Wei, L.; Zhang, B.; Du, H.; Li, W.

<Image removed due to copyright restrictions>

Figure 1.13 The experimental setup of the system with the terminal sliding mode controller [59].

With the same active seat suspension system, a disturbance observer based on the Takagi–Sugeno (TS) fuzzy controller was proposed for vibration control as shown in Figure 1.14 [60]. The controller used a closed-loop feedback control with acceleration and seat suspension displacement measurement signals to achieve good adaptability and robustness. The disturbance observer can estimate disturbances caused by friction and model simplification. The TS fuzzy control improves the vibration reduction performance of the controller by estimating load changes. During the experiment, the controller worked well in the vibration frequencies below 4 Hz. Two different loads of 55 and 70 kg could achieve a good response through the controller. The active seat suspension control was able to reduce the RMS acceleration by more than 45% compared to a well-tuned passive seat suspension.

Figure 1.14 Contents page from paper Disturbance observer based Takagi-Sugeno fuzzy control for an active seat suspension. *Mech. Syst. Signal Process.* 2017, *93*, 515–530. Ning, D.; Sun, S.; Zhang, F.; Du, H.; Li, W.; Zhang, B.

<Image removed due to copyright restrictions>

Figure 1.14 Block diagram of the Takagi–Sugeno (TS) controller with a disturbance observer [60].

Based on previous research, active vibration control of a multi-degree-of-freedom (multi-DOF) seat system was designed with a double-layer structure and an associated controller as shown in Figure 1.15 [61]. A second layer was added to the preceding scissor-like structure to control the vibration of pitching and rocking. The second layer consists of a universal joint and four support springs. The universal joint connects two conventional rotating motors and a gearbox to generate a torque of 52 Nm to remove the rolling and pitching vibrations. The spring system is responsible for supporting the static load. This is a simple and efficient active vibration control of a multi-DOF seat system compared with other active vibration controls of multi-DOF seat systems. For the control system, a sliding mode controller to reduce the roll vibration was designed. This algorithm has the advantages of fast convergence and good robustness and can be used to control the vibration in the swinging direction. In the design, for the swaying and pitch, the controller uses the minimum lateral acceleration and the minimum rolling angle as the control target, while the vertical vibration control uses the vertical acceleration as the control target.

Figure 1.15 Contents page from paper Control of a multiple-DOF vehicle seat suspension with a roll and vertical vibration. *J. Sound Vib.* 2018, *435*, 170–191. Ning, D.; Sun, S.; Du, H.; Li, W.; Li, W.

<Image removed due to copyright restrictions>

Figure 1.15 (a) The double-layer seat suspension prototype with a multi-DOF vibration control mechanism (b) The universal joint [61].

In another paper [62], with the same double-layer active seat suspension, an associated motion controller was designed to reduce the WBV of commercial vehicle drivers. The proposed active seat suspension could attenuate vibrations in 5-DOF, except the yaw vibration. The experimental results showed that when the seat system was fully controlled, the WBV could be reduced by over 40% vibration amplitude in the vertical direction.

An active seat system vibration control as shown in Figure 1.16 [63] adopted an electromagnetic linear actuator and a related controller which was designed. The system adopted a combination of active and passive suspensions, where the passive suspension is primarily responsible for static load-bearing, while two electromagnetic active suspensions (XTA-3806) that can produce a peak force of 1116 N are placed at both ends of the seat to generate the force needed to reduce vibration. In the next step, an adaptive controller based on the traditional filtered-X least mean square (FXLMS) algorithm combined with an on-line fast-block LMS identification method was developed and shown in Figure 1.17. In this study, the conventional FXLMS method was used to deal with the time-varying and nonlinear nature of the system, and the narrowband feed-forward FXLMS algorithm was employed to reduce the narrowband vibration caused by mechanical equipment. Finally, as shown in Figure 1.17, the usage of an additional LMS filter can identify the secondary path $S(z)$ online, which can generate a low-level white noise $u(n)$ being added to the control signal to drive the actuator. "Online" means when the active seat suspension system is operated in a running vehicle. "identification" means "measurement".

Figure 1.16 Contents page from paper Adaptive control of an active seat for occupant vibration reduction. *J. Sound Vib.* 2015, *349*, 39–55. Gan, Z.; Hillis, A.J.; Darling, J.

<Image removed due to copyright restrictions>

Figure 1.16 The model of the active seat system [63].

Figure 1.17 Contents page from paper Adaptive control of an active seat for occupant vibration reduction. *J. Sound Vib.* 2015, *349*, 39–55. Gan, Z.; Hillis, A.J.; Darling, J.

<Image removed due to copyright restrictions>

Figure 1.17 (a) The block diagrams of the filtered-X least mean square (FXLMS) controller (b) Fast-block least-mean-square FBLMS controller [63].

In the relevant research, an active seat system and the related displacement compensation controller was proposed for vibration control [64]. The seat was mounted on a hemispherical motion base to attenuate the 4-DOF vibration control through the active seat suspension as shown in Figure 1.18. The acceleration on each axis was measured by a set of acceleration sensors mounted on the seat, and the displacement in the corresponding direction was calculated by the controller as shown in Figure 1.19. The controller then sent a signal to drive the actuator for displacement compensation to eliminate vibration. The experimental results proved that this active seat system could reduce low-frequency vibration (2–6 Hz) which frequency is close to the human body resonant frequencies and which most influences the comfort of drivers.

Figure 1.18 Contents page from paper ACTISEAT: Active vehicle seat for acceleration compensation. *Proc. Inst. Mech. Eng. Part D J. Automob. Eng.* 2004, *218*, 925–933. Frechin, M.M.; Ariño, S.B.; Fontaine, J.

<Image removed due to copyright restrictions>

Figure 1.18 The semi-spherical motion base [64].

Figure 1.19 Contents page from paper ACTISEAT: Active vehicle seat for acceleration compensation. *Proc. Inst. Mech. Eng. Part D J. Automob. Eng.* 2004, *218*, 925–933. Frechin, M.M.; Ariño, S.B.; Fontaine, J.

<Image removed due to copyright restrictions>

Figure 1.19 Control algorithm design [64].

Table 1.1 Summary of the actuators of active seat suspension systems

Author	Actuator and Driver	Degree-of-Freedom (-DOF) Control	Max Output	Work Load	Pros and Cons
Stein (1997)	Pneumatic spring Proportional electro-pneumatic transducer	Vertical 1-DOF			Pros Simple structure The characteristics of the pneumatic spring itself help to reduce vibration Cons The pneumatic

					structure responds slowly Low control accuracy
Maciejewski et al. (2014)	Pneumatic spring	Vertical 1-DOF		55 kg 98 kg	Pros Common structure Traditional shock absorbers reduce energy consumption Cons Slow dynamic response Need pipeline and compressor
Maciejewski et al. (2010)	Pneumatic spring	Vertical 1-DOF		50 kg 80 kg 120 kg	Pros Common structure Traditional shock absorbers reduce energy consumption Cons Slow dynamic response Need pipeline and compressor
Maciejewski (2012)	Pneumatic spring	Vertical	Force = 400 N	51 kg 102	Pros

		1-DOF		kg	Common structure Traditional shock absorbers reduce energy consumption Cons Slow dynamic response Need pipeline and compressor
Ning et al. (2016)	400 W Panasonic servo motors×2 (MSMJ042G1U)×2	Vertical 1-DOF	Torque = 104 Nm	80 kg	Pros Simple structure Responsive Easy to control Con Bulky
Ning et al. (2017)	400 W Panasonic servo motors servo motor drivers (MBDKT2510CA1)	Vertical 1-DOF	Torque = 26 Nm	55 kg 70 kg	Pros Simple structure Responsive Easy to control Con Bulky
Ning et al. (2017)	400 W Panasonic servo motors servo motor drivers (MBDKT2510CA1)	Vertical 1-DOF			Pros Simple structure Responsive

					Easy to control Con Bulky
Ning et al. (2016)	400 W Panasonic servo motors servo motor drivers (MBDKT2510CA1)	Vertical 1-DOF	Torque = 52 Nm	55 kg	Pros Simple structure Responsive Easy to control Con Bulky
Ning et al. (2018)	400 W Panasonic servo motors ×4 servo motor drivers (MBDKT2510CA1) ×4	Vertical and roll 2-DOF	Torque = 52 Nm Force = 350 N	80 kg	Pros Simple structure Responsive Easy to control Con Bulky
Stein and Ballo (1991)	Electrohydraulic	Vertical 1-DOF		75 kg	Pros High output power High control precision Con Bulky
Gan et al. (2015)	Electromagnetic linear actuator (XTA-3086) ×2	Vertical 1-DOF	Force = 1116 N	55 kg	Pros Simple structure

	Responsive Easy to control Con High power consumption

1.2.2 Simulation

In the study of active seat suspension of vehicles, in addition to testing a prototype to verify the control algorithm, conducting simulations is also a common method to verify the feasibility of the controller design.

In Ref. [65], a model combining automotive chassis suspension, active seat suspension, and the driver’s body to analyze and achieve integrated vibration control was developed. A static output feedback controller considering driver weight changes and actuator saturation was designed for an active seat system. The simulation results showed that this integrated control strategy for an active seat suspension system could improve comfort and robustness.

Different controllers are always compared to find out the most suitable control method for the active vibration control of the seat system. In Ref. [66], a Very High-Speed Integrated Circuit Hardware Description Language that Includes Analog and Mixed-Signal Extensions (VHDL-AMS) model was proposed for vibration control of a car seat system, including an active electromechanical actuator. In that study, five different controllers were compared and analyzed, and the optimal control (OC) algorithm was identified as it provided the best results for vibration control. In another study [67], a seat system model under active vibration control was proposed based on the System C-A modeling technique as shown in Figure 1.20. Four control algorithms were compared with the OC algorithm for vibration mitigation performance. In Figure 1.20, the vehicle chassis (sprung mass) looks to be connected directly to the wheel without any vehicle suspension, which is incorrect.

Figure 1.20 Contents page from paper SystemC-A Modeling of an Automotive Seating Vibration Isolation System. In Proceedings of the Forum on Specification and Design Languages (FDL 2006), Darmstadt, Germany, 19–22 September 2006. Al-Junaid, H.; Kazmierski, T.; Wang, L.

<Image removed due to copyright restrictions>

Figure 1.20 The schematic diagram of the model used in System C-A [67].

In Ref. [68], a parameter identification method to identify the system parameters of a 5-DOF discrete spring-mass-damper seat system model of a truck-based on truck field test data. The parameter identification method is based on trial and error to match the measured natural resonant frequencies and vibration acceleration amplitude at the selected frequencies with the simulated ones of the 5-DOF discrete spring-mass-damper seat system model. The disadvantage of the trial-and-error method is the inefficient parameter identification process, which requires much time and effort. The 5-DOF discrete spring-mass-damper seat system model can be used to simulate the vibration response of the human body. A sensitivity analysis was conducted using the Monte Carlo method based on the 5-DOF model. In that paper, primary and secondary PID controllers were applied to the seat system for active vibration control as shown in Figure 1.21. The secondary PID controller produces a desired output control force signal according to the acceleration feedback signal of the mass oscillator. The primary PID controller uses the relative displacement feedback signal and the signal generated from the secondary PID controller as input error signals. Then, the primary PID controller generates a final output control force signal to drive the actuator to provide control to mitigate vibrations of the seat system. The advantages of the PID control from that research are that it is simple and practical, but it also has the disadvantage of poor robustness.

Figure 1.21 Contents page from paper Reduction of low-frequency vibration of a truck driver and seating system through system parameter identification, sensitivity analysis, and active control. *Mech. Syst. Signa l Process.* 2018, *105*, 16–35. Wang, X.; Bi, F.; Du, H.

<Image removed due to copyright restrictions>

Figure 1.21 Block diagram of the proportional-integral-derivative (PID) control system [68].

Another PID control algorithm application for active vibration control of seat systems was proposed [69]. In that study, a 13-DOF biodynamic model was designed for improving comfort and reducing the effects of low-frequency vibration on pregnant women and fetuses. For the controller design, the genetic algorithm was used to optimize the PID coefficients and the performance of the PID controller. Also, the fuzzy PID control algorithm as shown in Figure 1.22 was used to design the controller to improve the robustness of the vibration control of the seat system. The performances of these two different PID controllers were compared through simulation with that of a seating system with a passive suspension. The results proved that the fuzzy PID controller in that study was the best for the low-frequency vibration control of the seat system.

Figure 1.22 Contents page from paper *Vibration Control of an Active Seat Suspension System Integrated Pregnant Woman Body Model* (No. 2019-01-0172). SAE Technical Paper. Ali, S.A., Metered, H., Bassiuny, A.M. and Abdel-Ghany, A.M., 2019.

<Image removed due to copyright restrictions>

Figure 1.22 Fuzzy logic controller block [69].

A feed-forward adaptive controller combined with the FXLMS algorithm as shown in Figure 1.23 and a feedback controller combined with the H-infinity algorithm was proposed to reduce the small-amplitude vibration of a vehicle seat system [70]. The researchers compared three different control methods and found that the FXLMS feed-forward adaptive controller alone could reduce the vibration amplitude of 4.8 dB at 10 Hz when it was turned on compared with the situation when the controller was turned off. The reduction of vibration at 10 Hz is important as the most sensitive low-frequency vibration of the human body is in the range of 1.6-10 Hz which was mentioned before. Therefore, it can be understood that the research work was still focused on reducing the impact of low-frequency vibration on the human body. The feedback controller with the H-infinity algorithm could reduce the vibration amplitude by 3.6 dB. Finally, the hybrid controller combined with the two control methods successfully reduced the vibration amplitude by 11 dB. The possible reason for this may have been that although the feed-forward adaptive FXLMS algorithm has the advantage of taking the less computational time and easy implementation, it relies on the measurable reference signal. Once an unpredictable change of the vibration source occurred, this change would greatly affect the convergence speed of the adaptive feed-forward controller algorithm.

However, the feedback controller based on the H-infinity algorithm has a good and robust performance. Therefore, the hybrid controller combining the advantages of the two algorithms should have the best and most robust performance for seat vibration control.

Figure 1.23 Contents page from paper Application of an active controller for reducing small-amplitude vertical vibration in a vehicle seat. *Journal of Sound and Vibration*, *274*(3-5), pp.939-951. Wu, J.D. and Chen, R.J., 2004.

<Image removed due to copyright restrictions>

Figure 1.23 Schematic of the hybrid controller [70].

A feedback controller based on the H-infinity algorithm was proposed to reduce the vibration transmissibility of a seating system [71]. A 3-DOF mass-spring biological model was introduced to simulate the human body to improve the accuracy of the controller as shown in Figure 1.24. Unlike the traditional H-infinity algorithm controller, the controller in this paper was optimized with a targeted frequency range by using the generalized Kalman–Yakubovich–Popov (KYP) lemma, which was mainly controlled in the sensitive frequency range of the human body (4–8 Hz). According to the ISO 2631 standard, the D-class road profile roughness was simulated as the road surface excitation for the active suspension system. The simulation results showed that the system could significantly reduce vibration in the targeted range (4–8 Hz) which stays within the resonant frequency range of the human body. The vibration in this frequency range most influences the comfort of the driver and passengers.

Figure 1.24 Contents page from paper Vibration control for active seat suspension systems via dynamic output feedback with limited frequency characteristic. *Mechatronics*, *21*(1), pp.250-260. Sun, W., Li, J., Zhao, Y. and Gao, H., 2011.

<Image removed due to copyright restrictions>

Figure 1.24 Three-DOF biodynamic model [71].

An integrated control strategy that combines the driver body biodynamic model and the quarter car model to include active seat suspension and active vehicle suspension vibration controls was developed to enhance ride comforts shown in Figure 1.25 [72]. In the controller design, the state feedback H-infinity controller of model simplification provided good robustness, considering friction as a feedback signal. According to the experiment results, the system can largely reduce the driver’s head acceleration. It was shown that integrated active seat suspension and vehicle suspension controls could improve comfort compared with other separate controls.

Figure 1.25 Contents page from paper
Integrated Seat and Suspension Control for
a Quarter Car With Driver Model. *IEEE
Trans. Veh. Technol.* 2012, *61*, 3893–3908.
Du, H.; Li, W.; Zhang, N.

<Image removed due to copyright restrictions>

Figure 1.25 The model of the integral control strategy [72].

The different control system design details are summarized in Table 1.2.

Table 1.2 Summary of the control system designs

Author	Method	Target Frequency	Vibration Control Performance Criterion	Model	Performance	Pros and Cons
Wang et al. (2018)	PID control	7.51 Hz	Displacement (m)	5-DOF	The peaks of vibration amplitude are reduced to around 5×10^{-10} m	Pros Simple Practical Con Poor robustness
Maciejewski et al. (2014)	Adaptive control Reverse model Proportional-Derivative (PD) control	0.5–4 Hz	Seat Effective Amplitude Transmissibility (SEAT) (dimensionless) Transmissibility (Dimensionless) Acceleration (m/s^2)	1-DOF	The vibrations at about 1.3 Hz are reduced by about 50%	Pros Adaptable Large range of load Con Signal delay

Maciejewski et al. (2010)	Robust control Triple feedback control	0.5–4 Hz	SEAT (Dimensionless) Transmissibility (Dimensionless)		The amplitude at resonance is reduced by about 50%	Pro Can work with a different mass load Con May cause chattering
Wu and Chen (2004)	FXLMS control H-infinity control	10, 20, and 30 Hz	Accelerations in dB ref 1 m/s^2		The active seat system achieves 11 dB vibration attenuation at 10 Hz	Pro Good robustness Con May cause chattering
Ning et al. (2016)	H-infinity control with friction compensation	1–4.5 Hz	Root-mean-square (RMS) acceleration (m/s^2) Frequency-weighted RMS (FW-RMS) acceleration (m/s^2) Vibration Dose Value	1-DOF	Compared with a passive seat system, the RMS is reduced by 57%, the FW-RMS is reduced by 35.5%, the VDV value is reduced by 34.6%, the SEAT value is reduced by 35.6%, and the	Pro Good robustness Con Highly reliant on the accuracy of the model

			(VDV) ($m/s^{1.75}$) SEAT (dimensionless) VDV ratio (dimensionless)		VDV ratio is reduced by 34.6%.	
Sun et al. (2011)	H-infinity control in the finite frequency domain	4–8 Hz	Power Spectral Density (PSD) (m^2/s^3) Acceleration (m/s^2)	3-DOF		Pro Good robustness Con Highly reliant on the accuracy of the model
Gan et al. (2015)	FXLMS control FBLMS control	4–12 Hz	dB ref m/s^2		For single-frequency cancellation, a 26 dB cancellation is achieved on the seat pan at the frequency of 6 Hz. For the multiple harmonic	Pro Adaptable Con Can be affected by noise or disturbance

					cancellations, the average level of vibration reduction is around 20 dB at 4, 6, 8, and 12 Hz.	
Ning et al. (2016)	H-infinity control	2–6 Hz	RMS acceleration (m/s^2) FW-RMS acceleration (m/s^2) VDV ($m/s^{1.75}$) SEAT (Dimensionless) VDV ratio (Dimensionless)	2-DOF	Compared with a passive seat system, the RMS is reduced by 31.96%, the FW-RMS is reduced by 43.42%, the VDV value is reduced by 42.96%, the SEAT value is reduced by 43.41%, and the VDV ratio is reduced by 42.68%.	Pro Good robustness Con Highly reliant on the accuracy of the model
Ning et al. (2018)	Sliding mode control H-infinity control		RMS (m/s^2) FW-RMS (m/s^2) VDV ($m/s^{1.75}$)	2-DOF	Compared with a passive seat system, for vertical acceleration, the RMS is reduced by 41.9%, the FW-RMS is reduced by 32.1%,	Pros Adaptable High robustness

					and the VDV is reduced by 32.8%. For lateral acceleration cancellation, the RMS is reduced by 55.4%, the FW-RMS is reduced by 49.4%, and the VDV is reduced by 52.2%.	Con Highly reliant on the accuracy of the model
Ning et al. (2017)	Disturbance observer Takagi–Sugeno fuzzy control	2–4 Hz	Acceleration (m/s^2) Transmissibility (Dimensionless)	2-DOF	Compared with a well-tuned passive seat system, the active seat system can reduce the RMS by 45.5% and 49.5% with a mass load of 55 and 70 kg, respectively.	Pro Effectively reduce the workload
Du et al. (2012)	H-infinity state feedback control		Head acceleration (m/s^2)	8-DOF		Pro Good robustness Con

						Highly reliant on the accuracy of the model
Ning et al. (2017)	Sliding mode control	1.5 Hz	RMS acceleration (m/s^2) FW-RMS acceleration (m/s^2) VDV ($m/s^{1.75}$) SEAT (Dimensionless) VDV ratio (Dimensionless)	2-DOF	Compared with a passive seat system, the RMS is reduced by 54.6%, the FW-RMS is reduced by 34.1%, the VDV value is reduced by 32.6%, the SEAT value is reduced by 34.1%, and the VDV ratio is reduced by 32.6%.	Pros Adaptable High robustness Con Highly reliant on the accuracy of the model

1.3 Artificial Neural Network Control

Unlike a model-based controller, the ANN controller is data-based. It can be used to identify complex nonlinear objects that are difficult to accurately model and the ANN controller can be used as a controller for adaptive control. Compared with traditional controllers, ANN controllers have many features. They have powerful nonlinear processing capabilities and are well suited for dealing with problems with a large number of input variables, as well as multivariable output. Also, the ANN can learn unknown information autonomously. However, for active vibration control of a seating system, the ANN system has not been widely accepted.

An ANN controller was proposed to control a nonlinear vehicle model having 8-DOF as shown in Figure 1.26 [73]. In this study, the active seat suspension system control was combined with an active vehicle suspension system control. The ANN controller could solve the nonlinear problem caused by the vehicle system under excitation disturbances. The ANN model was trained with errors between actual and expected output results by using backpropagation. The results demonstrated that the ANN controller performs well at controlling seat system vibration.

Figure 1.26 Contents page from paper Neural network control of seat vibrations of a non-linear full vehicle model using PMSM. *Math. Comput. Model.* 2008, *47*, 1356–1371. Guclu, R.; Gulez, K.

<Image removed due to copyright restrictions>

Figure 1.26 An integral controller based on artificial neural networks (ANNs) for

active chassis suspension and active seat suspension system controls [73].

The control system for an active seat suspension combining an ANN module, the active force control (AFC) method, and a PID controller was proposed as shown in Figure 1.27 [74]. In the design of the ANN model, a hidden layer structure of 10 neural units was considered to have the best performance. Reverse learning was used to train the ANN model to estimate the mass of the seat–occupant system. Besides, the PID controller was designed to work with minimal disturbance and at low speed, and the AFC controller was used to improve the robustness and vibration control performance of the system. In this controller, the system error was taken as the input, and the estimated mass was set as the output. The Levenberg–Marquardt algorithm was used to provide numerical solutions for nonlinear minimization. After comparison with the PID controller, it was found that the ANN controller performed better than the other controllers.

Figure 1.27 Contents page from paper Active Off-Road Seat Suspension System Using Intelligent Active Force Control. *J. Low Freq. Noise Vib. Act. Control* 2015, *34*, 475–489. Tahmasebi, M.; Gohari, M.

<Image removed due to copyright restrictions>

Figure 1.27 An intelligent controller via an ANN algorithm [74].

The ANN controllers mentioned here are summarized in Table 1.3.

1.4 Biodynamic Modelling

In the study of the active vibration control of a vehicle seat system, an accurate biodynamic model that aims to predict the dynamic response of a human body is necessary because it can provide more efficient control. In Ref. [68], a 5-DOF seat–occupant model as shown in Figure 1.28, which can be used to simulate the dynamic behavior of the human body, was proposed and the parameter sensitivity was determined based on the model; the relevant data were also used in the design of the active control system. In Ref. [71], a 2-DOF biodynamic model and a 2-DOF seat suspension system model were combined, and a 3-DOF seat–occupant model was established to describe the dynamic response of the human body in space. However, due to the difficulty of measuring actual human body properties and because an accurate biodynamic model may dramatically increase the amount of computation time, a simplified model has been commonly used in research. In Refs. [59, 60], the human body was replaced by a mass, and the amount of calculation time was reduced by ignoring the complex dynamic behavior of the human body itself.

Table 1.3 Summary of ANN controllers

Author	Number of Hidden Layers	Number of Nodes	Training Method		Pros and Cons
Guclu and Gulez (2008)	2	First layer: 9 Second layer:10	Back Propagation	Compared with an uncontrolled system, the maximum displacement of the passenger seat with NN control is reduced from 2.8×10^{-3}	Pro Good on multi-input and multioutput control Con Low

				to 0.2×10^{-3} m.	robustness
Gohari and Tahmasebi (2015)	1	10	Back Propagation		Pro Good on nonlinear problems Con Need large ideal training data

Figure 1.28 Contents page from paperReduction of low-frequency vibration of a truck driver and seating system through system parameter identification, sensitivity analysis, and active control. *Mech. Syst. Signal Process.* 2018, *105*, 16–35. Wang, X.; Bi, F.; Du, H.

<Image removed due to copyright restrictions>

Figure 1.28 A 5-DOF seat–occupant model [68].

1.5 Identified Research Gaps, Research Questions, and New Directions

In previous studies, a lot of innovations were proposed regarding active seat suspension and controllers. A large number of simulation studies and actual experiments of active vehicle seat suspension have been conducted in the laboratory. However, there are still some research areas that need to be done, the research gaps exist and need to be filled.

For the design and development of the active seat suspension structure of a vehicle, the convenience of the linear motor and the reliability of the traditional motor is fully considered. However, the bloated structure is still not practical to be implemented. In a small vehicle cab, a device whose size is larger than the traditional vehicle seat system cannot be accommodated. Therefore, how to reduce the size of the active seat suspension to pack it into a small space in the cab is worth studying.

For the optimization of passive seat structures, system optimization methods will be applied to optimize design parameters and improve vibration isolation performance. It is essential to develop an appropriate optimization method to improve the vibration isolation performance of the active seat suspension system and to reduce the packaging size, because the optimized mechanical structure for vibration isolation may lead to the reduced intervention time and frequency of the active seat suspension system. Due to the particularity of the human body, it is difficult to identify its model parameters from measurement data, on the other hand, an accurate bio-dynamic model that can replay body dynamic characteristics plays a significant role in system optimization and active vibration control. Therefore, a fast and accurate parameter identification method for the human bio-dynamic model will help enhance vibration control performance and increase the application range of the active seat suspension system.

Signal acquisition and analysis in vibration measurement is a complex process that is easily affected by the errors induced by the measurement environment. How to simplify the signal acquisition and analysis process and achieve the measurement of ISO standard acceleration using simple equipment is also a challenge.

Proceeding from the research gaps indicated above, the following research questions are raised:

1. How is the actuator mechanical structure integrated with traditional seat structure to reduce the size of an active seat system and pack it into a vehicle cab for vibration control?

2. How is the influence of system parameters on the vibration isolation performance determined using the optimization method?

3. How is a reliable and accurate biodynamic model developed based on vehicle measurement data?

4. How is the ISO standard acceleration measurement and evaluation simplified via ANN model training?

Due to the load-carrying characteristics of commercial vehicles, the vibration control of the seat for commercial vehicles is more important than that for other types of vehicles. This study will analyse and model the relevant low-frequency vibration around 4Hz which is most sensitive to the human body and develop a simple and convenient method to achieve better vibration control performance of the seat. The motivation of the research is to develop a truck seat with a compact active suspension to improve ride comfort and practicality. The research has designed a novel active truck seat suspension system for a further study of active vibration control of the seating suspension system. The thesis focuses on a study of the parameter identification method of the seating suspension system and design parameter optimisation method for the best vibration isolation performance rather than focuses on the active vibration control research which will be conducted by another Ph.D. student.

1.6 List of publications

Zhao, Y. and Wang, X., 2019. A review of low-frequency active vibration control of seat suspension systems. *Applied Sciences*, *9*(16), p.3326.

Zhao, Y., Alashmori, M., Bi, F. and Wang, X., Parameter identification and robust vibration control of a truck driver's seat system using multi-objective optimization and

genetic algorithm. *Applied Acoustics*, *173*, p.107697.

2 Vibration Comfort Investigation Using a Motion Platform.

2.1 Introduction

Accurate assessing the riding comfort is the basis of designing and developing a seating system. This chapter studies the seat system comfort through evaluating the seating system acceleration according to ISO2631-1997 standard where a full-function truck seat is tested with a dummy driver under excitation of a CAKS motion platform, which can provide 3-DOF dynamic excitations of the vertical, pitch, and roll. Also, the measured acceleration results of the seat system according to ISO2631-1997 standard will be compared with the seat effective amplitude transmissibility (SEAT) results, which is another way to evaluate the riding comfort.

By changing the seat system setting, including adjusting the air cushion inflation pressure and shock absorber position, the SEAT and ISO standard acceleration values under different seat system setting conditions will be obtained. These two values will be compared and discussed to reveal their relationship, and the test results will be applied to validate the two evaluation methods of riding comfort.

Generally, the RMS acceleration, transmissibility ratio, and SEAT values are all commonly used to evaluate the riding comfort and describe the dynamic characteristics of the seat system. Meanwhile, the more rigorous and complex measurements, such as the British standard and ISO standard are also applied to evaluate the ride comfort of the vehicle seat system [75-78].

In this study, the objective is to study how to measure SEAT value and ISO standard acceleration value to evaluate the riding comfort and the vibration mitigation performance of the truck seat system. The comparison of these two values and the identification of their relationship will be the focus of this chapter.

2.2 Experiment design and data collection

As shown in Figure 2.1(a), to replicate the condition where a vehicle seat works in a truck in the laboratory, a real and full-function truck seat system (IVECO A89614-51) is mounted on the motion platform. A 12-Volt power supplier and the air pressure supply pipeline are connected to the truck seat system to provide the power required for the control of the seat positions and air cushion pressures.

CKAS is the leading manufacturer of flight simulation equipment, motion platforms & systems, truck simulators, and enthusiast setups that offer quality workmanship and affordability. CKAS U2s 3-DOF Motion Platform system is a small scale 3-DOF heave-pitch-roll electric motion platform excitation system. CKAS U2s 3-DOF Motion Platform includes the angular motions of pitch around the lateral y-axis and roll around the vertical z-axis in addition to the linear heave motion in the vertical z-direction. Despite using a 3-DOF shaker system, floor and dummy head accelerations are evaluated in the vertical (heave) z-direction in this thesis, as the vertical direction vibration has a major influence on the ride comfort according to the previous literature review. The excited motion platform system (CKAS U2s 3-DOF Motion Platform) is controlled by a computer with the CKAS software to replicate the vibrations of the seat system in a truck. In this experiment, the vibration excitation signal is generated from the recorded truck floor acceleration signals in the field and is played back and amplified by the CAKS motion platform to generate an excitation for the seat system to simulate the seat system vibration conditions of a real truck cockpit.

The dummy driver, as shown in Figure 2.1(b), is used to simulate the human driver's body to simulate the dynamic characteristics of a real human driver's body in the seat system. Its size and weight are those of the average values of an adult. Due to the high risk of testing human beings for the effect of the low-frequency vibration, the dummy can be applied to minimize the risk of potential hazards.

Accelerometers are used to pick up the vibration acceleration signals. According to the

ISO-2631 standard, the seat base and the backrest are the two main test positions where the tri-axis vibration signals should be measured and recorded. Therefore, two tri-axial accelerometers (B & K type 4506) as shown in Figure 2.1(c) contained within two foam pads are placed on the cushion and the backrest to pick up the vibration signals in the three directions of x, y, and z. Two other uni-axial accelerometers (PCB 8346) are used to measure and record the accelerations on the floor and the head of the dummy in the vertical direction. The accelerometers are connected to the printed circuit board (PCB) power supply units, the outputs of which are connected to the National Instrument data acquisition frontend box of NI USB-6259 as shown in Figure 2.1(d). The 8-channel signals are directly recorded by the data acquisition frontend box controlled by a laptop computer and the National Instrument SignalExpress software. The recorded data are saved in the MS-Excel format for post-processing.

Before the actual vibration signal is recorded, each of the data acquisition channels of the accelerometers must be calibrated using the B & K 4294 calibrator, which helps gain the confidence of the measurement data and improve the measurement accuracy of the recorded measurement data.

(a)

(b)

Figure 2.1 The experiment set up and devices for the truck test on the CKAS motion platform: (a) the truck seat, (b) the dummy.

In this study, two variables will affect the vibration mitigation performance of the seating system, namely the seat height setting and the shock absorber setting. The seat height setting can be adjusted through a switch to increase or decrease the seat air cushion inflation pressure, and the shock absorber setting can be adjusted through another switch to turning on or off the shock absorber. As shown in Table 2.1, six seating system conditions are corresponding to six different combinations of the height and shock absorber settings, which are the following:

the high absorber position @low seat cushion inflation pressure - 'HL',

the high absorber position @medium seat cushion inflation pressure - 'HM',

the high absorber position @high seat cushion inflation pressure - 'HH',

the low absorber position @low seat cushion inflation pressure - 'LL',

low absorber position @medium seat cushion inflation pressure - 'LM', and low absorber position @high seat cushion inflation pressure - ‘LH’.

Among the six seating system conditions, the seat air suspension spring is the softest in the ‘HL’ state and the hardest in the ‘LH’ state.

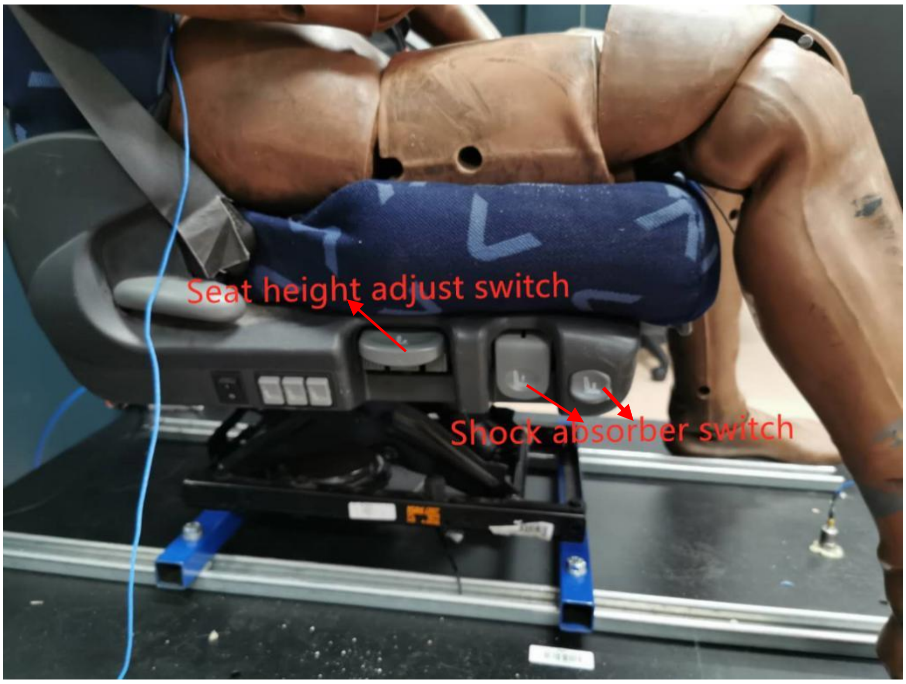

Figure 2.2 The seat height setting and shock absorber setting

Table 2.1 The seating system conditions corresponding to the six different combinations of the height and shock absorber settings.

Shock absorber settings	**Seat air cushion height settings**		
	Low (soft)	**Medium**	**High (hard)**
High (soft)	HL	HM	HH
Low (hard)	LL	LM	LH

2.3 SEAT value

The seat effective amplitude transmissibility (SEAT) value is often used to evaluate the seat comfort and measure the vibration reduction performance of a seat suspension system. The SEAT value is determined by the weighted acceleration amplitudes of the seat base divided by those of the floor. If the SEAT value is greater than 100%, it means that the seat suspension system cannot reduce the vibration transmitted from the floor and even increase the vibration. Oppositely, less than 100% of the SEAT values means that the seat suspension system can reduce the vibration. In this study, the SEAT values are calculated from the seat to head, which can reflect the influence of the seating system on the human body comfort. The SEAT values are calculated by

$$\text{SEAT\%} = \left(\frac{\int G_{head}(f)W_i^2(f)df}{\int G_{seat}(f)W_i^2(f)df}\right)^{\frac{1}{2}} \times 100\% \qquad (2.1)$$

where $G_{head}(f)$ is the auto-power spectrum density of the acceleration at the head, $G_{seat}(f)$ is the auto-power spectral density of the acceleration at the seat base, $W_i(f)$ (or $W_k(f)$) is the frequency weighting function or factor in the vertical direction of z as shown in Figure 2.3. Although the frequency range of Figure 2.3 is from 0.125 to 250 Hz, the scope of the thesis is focused on the low-frequency vibrations around 4 Hz.

2.4 ISO standard acceleration calculation

The ISO acceleration value is a total vibration value calculated according to the ISO-2631 standard for evaluating the ride comfort. In the calculation process of the ISO acceleration value, the vibration values in the three axial directions have been weighted by Eq. (2.2)

$$\begin{cases} a_w = \left[\sum (W_i a_i)^2\right]^{\frac{1}{2}} \\ a_v = \left(k_x^2 a_{wx}^2 + k_y^2 a_{wy}^2 + k_z^2 a_{wz}^2\right)^{\frac{1}{2}} \\ a_t = \left(a_{v1}^2 + a_{v2}^2\right)^{\frac{1}{2}} \end{cases} \qquad (2.2)$$

where a_i is the root mean square (RMS) value for the ith one-third octave band measured acceleration for the corresponding axis, a_w is the frequency-weighted acceleration for each direction, a_v is the vector sum of the frequency-weighted RMS acceleration for each direction, k_x, k_y, and k_z are multiplication factors in the directions of x, y, and z as shown in Table 2.2, a_t is the overall total vibration value, a_{v1} is the vector sum of the frequency-weighted RMS acceleration of the seat base in the directions of x, y and z, and a_{v2} is the vector sum of the frequency-weighted RMS acceleration of the seatback in the directions of x, y, and z.

Table 2.2 The Frequency-Weighting functions or factors and the multiplication factors, from the ISO-2631 Standard

	Accelerometer pad					
	Seat base			**Seatback**		
Axis	x	y	z	x	y	z
Weighting	W_d	W_d	W_k	W_c	W_d	W_d
Multiplication factor *k*	1	1	1	0.8	0.5	0.4

Figure 2.3 Contents page from ISO standard International Organization for Standardization, Mechanical vibration and shock—evaluation of human exposure to whole body vibration—part 1: general requirements, ISO 2631-1:1997, 1997.

<Image removed due to copyright restrictions>

Figure 2.3 Frequency-weighting function curves W_k, W_d, and W_c from the ISO-2631 Standard [104].

2.5 Results and discussion

As variables, the setting adjustment of the seat cushion height and shock absorber can change the seat vibration isolation performance. In this study, the seat cushion height is set to three levels as 'High', 'Medium', and 'Low', and the height adjustment is changed by changing the inflation pressure of the air cushion in the seating system. The setting of the shock absorber is not indicated in the seating system, so the setting is switched to the highest position and the lowest position. When the setting is switched to the highest position, the seat suspension is the softest, and when the setting is switched to the lowest position, the seat suspension becomes the hardest. With different setting combinations, there are six different vibration isolation characteristics for this seating system.

It can be seen from Figure 2.4(a) that when the shock absorber setting is placed at the highest position, the SEAT value is significantly larger than the one when the shock absorber setting is placed at the lowest position. The 'HL' setting has the highest SEAT value of 54.64%, and the lowest SEAT value of 47.27% appears with the 'LH' setting. When the position of the shock absorber setting is 'high', as the seat air cushion height increases, the SEAT value is decreased from 54.64% to 49.18%. Also, when the shock absorber setting is switched to the 'low' position, the SEAT value is reduced from 47.82% to 47.27%, but not significantly as above.

The ISO acceleration value is calculated and shown in Figure 2.4(b). In the ISO acceleration calculation process, the acceleration value of the "high" shock absorber setting position is usually greater than the acceleration value of the "low" shock absorber setting position, unless the seat cushion height is set to "low". Under the same shock absorber position setting, as the seat cushion height increases from "low" to "high", the ISO acceleration values decrease from 0.34 and 0.36 to 0.31 and 0.28, respectively. In the whole chart, as shown in Figure 2.4(b), the same as "LH", the minimum ISO acceleration value is still 0.28. This is because in the low shock absorber position and the high seat cushion position, the seat suspension system is the hardest, resulting in reduced low-frequency vibrations. On the other hand, in the seat system setting a combination of the high shock absorber position and the low seat cushion position "HL", the seat suspension system is the softest, resulting in increased low-frequency vibrations.

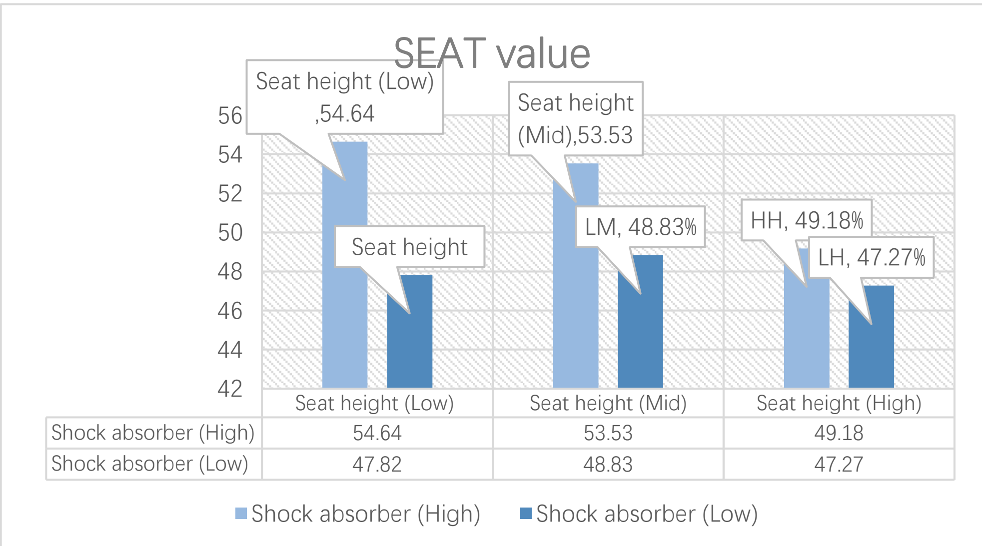

(a)

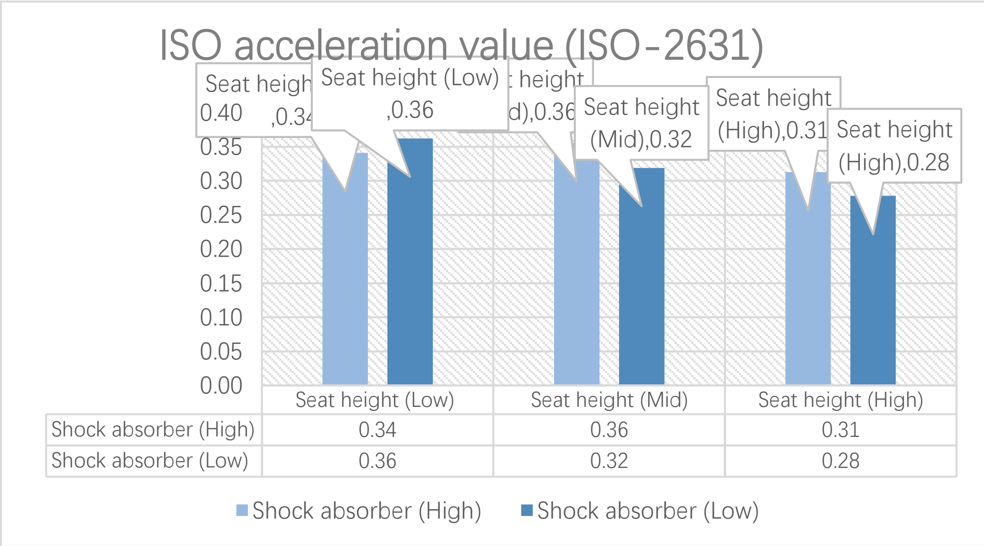

(b)

Figure 2.4 The calculation results of (a) SEAT values and (b) the acceleration values according to the ISO-2631 standard.

By comparing the results of Figures 2.4(a) and 2.4(b), it can be seen that the overall trends of the results, evaluated by the two different methods, are very similar. Under the vibration excitation, as the setting position of the shock absorber changes from the ‘H’ to the ‘L’ or decreases and the seat air cushion height setting position changes from the ‘L’ to the ‘H’ or increases, the seat suspension system changes from the ‘softest’ to the ‘hardest’, the vibration isolation performance of the seat suspension system will be gradually improved. Otherwise, the vibration isolation performance of the seat system will be reduced. Both the two evaluation methods produce the same optimal combination, which is the combination of the highest seat air cushion height setting position and the lowest shock absorber setting position.

2.6 Error analysis

The main measurement errors could be originated from the defection of the seat suspension system and the sensor installation error. Since the accelerometer sensor needs to be connected to the National Instrument data acquisition frontend box and the computer through the signal conditioners or amplifiers certain signal interference induced errors are inevitable during the experiment. The DC signal offset of the data acquisition frontend box also aggravates the errors to a certain extent. Although the errors can be reduced through the channel grounding to earth reset and channel calibrations, they cannot be completely avoided. The sensor installation error is mainly reflected by the directional sensitivity and the way that the accelerometer sensors are mounted. It is very hard to make the measurement direction of the sensor completely coincide with the excitation direction. This is because that there is no rigid connection between the dummy driver body and the seat base, a slight movement could result in inaccurate measurement results and lead to errors.

2.7 Summary

This chapter introduces how ISO acceleration value and SEAT value are measured by using the truck seat and CKAS motion platform. The results show that when the seat is set to low shock absorber setting position and high, the result of the seat is the best Good vibration isolation performance. The results of the two evaluation methods have the same trend, which proves that both methods are reliable and can be used to evaluate the comfort of the seat. However, it is inconsistent with the prediction results in the subsequent optimization study. The reason for this result is mainly because that the signal acquisition range is 0.1-800 Hz, so the calculation of the two values not only includes the seat system's low-frequency vibration but also takes into account the dynamic response of the seat in the mid-to-high frequency range. This makes the results of the RSM model optimized for low-frequency vibrations divergent from the measurement results. However, since the human body is most sensitive to low-frequency vibrations (4Hz), this chapter is mainly used to verify whether the two measurement methods have the same prediction trend.

After the ISO acceleration value and SEAT value are defined and measured from experimental measurement data by using the dummy driver, truck seat, and CKAS motion platform, the driver body and seat system simplified as a 5-DOF mass-spring-dashpot lumped parameter model will be studied, where the parameters of the system will be identified from the field test vibration measurement data using the Generic Algorithm. The sensitivity analysis of the system model parameters will be conducted in the following chapter.

3 5-DOF Bio-Dynamic Model and its Sensitivity Analysis.

3.1 Introduction

As an active research topic, recently, the phenomena and potential dangers associated with long-term exposure to low-frequency vibrations have been systemically investigated. According to recent research, it has been found that long-term exposure to low-frequency vibrations may cause health issues, including musculoskeletal diseases, digestive diseases, visual system diseases, and even an increased risk of cancer [2].

An integrated seated human body system and a quarter car model was developed to verify the performance of the integrated control system based on a static output feedback $H\infty$ control strategy for low-frequency vibration mitigation [80]. Because of the complex dynamic response of the human body exposed to the low-frequency vibration environment, some system parameters of the multiple degrees of freedom (M-DOF) human body model were not measurable in practice, so the overall vibration control performance of the seat system could be accordingly compromised. However, the relevant parameter identification method of the seated human body model has not been systemically studied in previous research.

In the research of seat vibration mitigation, directly using the human body to conduct experiments will bring high risk, so a bio-dynamic model that can replay the dynamic characteristics of the human body plays an important role in the research.

For example, an active multivariable control strategy and a 5-DOF seated human body system model to simulate the vibration mitigation in the vertical and rotational directions were proposed in Ref. [81]. The simulation results show that the system modeling and the controller design based on the pole placement analysis method can be used to reduce Multi-DOF vibration. However, the model parameters in the study were still derived from other relevant literature. A semi-active electro magnetorheological (ER) seat suspension was developed and controlled by a Sliding Mode Controller [54]. In the study, a 6-DOF seat-occupant model was developed for the related simulation and analysis. The results of the experiment proved that the semi-active ER seat suspension was able to reduce the VDV value by 15% and the SEAT value by 10%. However, the model-related parameters in the study were still sourced from other relevant research literature.

In terms of a pneumatic seat suspension, a 3-DOF model combining a pneumatic seat suspension with a car chassis suspension was used in the design of the LQG controller [82]. The feasibility of the controller was proven according to the results of the experiment in this study, but the signals of road excitation used in the experiments were still calculated from the road displacement spectrum defined in the ISO standards or sourced from the laboratory simulation tests. An active seat suspension system to improve the vibration mitigation performance of the vehicle seat system was designed in Ref. [59]. In the research, the calculated reverse mode of the pneumatic spring and the primary controller with the adaptive mass recognizing system were used to enhance the robustness of the control system. However, the control system was still not validated by the field test and measurement results.

For the method of parameter identification, Curve Fitting Toolbox in MATLAB is the most general method used to identify parameters for modeling [2]. In the research [68], a fast parameter identification method based on entropy compromise programming criteria for multi-degree-of-freedom linear and nonlinear biodynamic models was developed. However, the error of the simulation results was around 10% compared with the measurement results.

The research gaps identified from the above literature studies are the identification of the seat system parameters from field test and measurement results to establish a reliable bio-dynamic model. The motivation of this research is to mitigate the low-frequency vibration of the seat system to lower the risks of occupational and safety-related health issues caused by the long-term exposure of the low-frequency vibration in commercial vehicles or trucks.

The major objectives of this research are to develop a 5-DOF high-precision seat-occupant model by identifying its system model parameters using multi-objective optimization Genetic Algorithm from the field test measurement data of four different brands of trucks of the same driver and seat system design to predict the dynamic response of human body under low-frequency vibration excitations. The system parameters will be identified for the driver and seat systems of the four different brands of trucks using a multi-objective optimization Genetic Algorithm where the mass and stiffness coefficients are adjusted until the calculated resonant frequencies coincide with the measured resonant frequencies and the goodness of fit of the simulated and measured resonant frequencies meets with the preset tolerance criteria. The damping coefficients will be adjusted until the calculated frequency domain head response peak values coincide with the measured frequency domain head response peak values and the goodness of fit of the simulated and measured frequency domain head response peak values meets the preset tolerance criteria. With the good tune seat-occupant biodynamic model, the seat effective amplitude transmissibility (SEAT) values will be introduced and the relevant parameter sensitivity analysis will be conducted.

3.2 Analytical simulation model

The main purpose of this chapter is to find out a way to attenuate the vibration of a seating system of trucks or other heavy-duty commercial vehicles. An analytical biodynamic model of the seat-occupant system will be established through the lumped mass-spring-dashpot parameter modeling as shown in Figure 1.28 to simulate the dynamic response of the human body under low-frequency large amplitude vibration conditions. The whole model consists of 5 main mass parts and 6 groups of spring-damper systems. M_1 represents the seat mass fixed to the floor through a scissor structure combining with an air cushion and a shock absorber. K_1 represents the spring stiffness constant of the seat suspension system. C_1 represents the damping coefficient of the seat suspension system. There is a soft foam seat cushion placed between the seat and driver's buttock. Since the cushion is made from a light foam material, the mass of the cushion is ignored. K_{2c} represents the spring stiffness of the cushion and C_{2c} represents the damping coefficient of the cushion. In this study, it is assumed that the driver keeps his body upright and sits on the top of the soft seat cushion. The lumped mass-spring-dashpot parameter model of the driver's body is divided into four parts: pelvis, upper torso, viscera, and head. Based on the linear lumped mass-spring-dashpot parameter system, these four parts are presented as mass M_i, spring stiffness constant K_i and damping coefficient C_i for i =2, 3, 4, and 5. z_i (i =2, 3, 4, 5) is the displacement coordinates of these four parts of driver's body respectively.

One thing needed to note is that only 71 percent of the driver's body weight is supported by the seat system, and the other 29 percent of body weight is withstood by the feet [83]. Thus, in this seat-occupant system model, the pelvis part includes the lumbar and middle thigh, but not includes calves and feet. Besides, z_0 and $\dot{z}_0$ are the displacement and velocity of the floor vibration which was excited by the idle running engine or the rough road surface excitation.

Figure 3.1 Contents page from paperReduction of low-frequency vibration of a truck driver and seating system through system parameter identification, sensitivity analysis, and active control. *Mech. Syst. Signal Process.* 2018, *105*, 16–35. Wang, X.; Bi, F.; Du, H.

<Image removed due to copyright restrictions>

Figure 3.1 Lumped mass-spring-dashpot parameter model of the seat suspension coupled with a human body [68].

The equations of the motion of the 5-DOF seat-occupant system are given by:

$$\begin{cases} M_1 \cdot \ddot{z}_1 + C_1 \cdot (\dot{z}_1 - \dot{z}_0) + K_1 \cdot (z_1 - z_0) + \dfrac{C_2 \cdot C_{2c}}{C_2 + C_{2c}} \cdot (\dot{z}_1 - \dot{z}_2) + \dfrac{K_2 \cdot K_{2c}}{K_2 + K_{2c}} \cdot (z_1 - z_2) = 0 \\ M_2 \cdot \ddot{z}_2 + C_3 \cdot (\dot{z}_2 - \dot{z}_3) + K_3 \cdot (z_2 - z_3) + \dfrac{C_2 \cdot C_{2c}}{C_2 + C_{2c}} \cdot (\dot{z}_2 - \dot{z}_1) + \dfrac{K_2 \cdot K_{2c}}{K_2 + K_{2c}} \cdot (z_2 - z_1) = 0 \\ M_3 \cdot \ddot{z}_3 + C_5 \cdot (\dot{z}_3 - \dot{z}_5) + K_5(z_3 - z_5) + C_3 \cdot (\dot{z}_3 - \dot{z}_2) + K_3(z_3 - z_2) + C_4 \cdot (\dot{z}_3 - \dot{z}_4) + K_4(z_3 - z_4) = 0 \\ M_4 \cdot \ddot{z}_4 + C_4 \cdot (\dot{z}_4 - \dot{z}_3) + K_4(z_4 - z_3) = 0 \\ M_5 \cdot \ddot{z}_5 + C_5 \cdot (\dot{z}_5 - \dot{z}_3) + K_5(z_5 - z_3) = 0 \end{cases} \quad (3.1)$$

where M_1 is the seated mass; M_2 is the driver's pelvis mass; M_3 is the driver's upper torso mass; M_4 is the driver's viscera mass; M_5 is the driver's head mass. K_1 is the stiffness of the seat suspension system; K_2 is the spring stiffness constant of the driver's pelvis; K_{2c} is the stiffness of the seat cushion; K_3 is the stiffness of the upper torso of the diver's body; K_4 is the stiffness of the viscera of the driver's body; K_5 is the stiffness of the combination of the driver's neck and head. C_1 is the damping coefficient of the seat suspension system; C_{2c} is the damping coefficient of the seat cushion; C_2 is the damping coefficient of the driver's pelvis; C_3 is the damping coefficient of the driver's upper torso; C_4 is the damping coefficient of the driver's viscera; C_5 is the damping coefficient of the combination of the driver's neck and head. Since the natural frequencies of the seat-occupant system model need to be calculated in MATLAB, the parameters of the stiffness and mass matrices should be identified by using the multiple objective Genetic Algorithm with the test data measured from real-time truck field tests, which will be shown below.

From Equation (3.1), the mass and stiffness matrices of [M] and [K] are:

$$[M] = \begin{bmatrix} & M_1 & 0 & 0 & 0 & 0 \\ & 0 & M_2 & 0 & 0 & 0 \\ 0 & 0 & 0 & M_3 & 0 & 0 \\ & 0 & 0 & 0 & M_4 & 0 \\ & 0 & 0 & 0 & 0 & M_5 \end{bmatrix} \tag{3.2}$$

and

$$[K] = \begin{bmatrix} & K_1 + \dfrac{K_2 \cdot K_{2c}}{K_2 + K_{2c}} & -\dfrac{K_2 \cdot K_{2c}}{K_2 + K_{2c}} & 0 & 0 & 0 \\ 0 & -\dfrac{K_2 \cdot K_{2c}}{K_2 + K_{2c}} & K_3 + \dfrac{K_2 \cdot K_{2c}}{K_2 + K_{2c}} & -K_3 & 0 & 0 \\ & 0 & -K_3 & K_3 + K_4 + K_5 & -K_4 & -K_5 \\ & 0 & 0 & -K_4 & K_4 & 0 \\ & 0 & 0 & -K_5 & 0 & K_5 \end{bmatrix} \tag{3.3}$$

and damping coefficient matrix is:

$$[C]=\begin{bmatrix} C_1+\dfrac{C_2\cdot C_{2c}}{C_2+C_{2c}} & -\dfrac{C_2\cdot C_{2c}}{C_2+C_{2c}} & 0 & 0 & 0 \\ -\dfrac{C_2\cdot C_{2c}}{C_2+C_{2c}} & C_3+\dfrac{C_2\cdot C_{2c}}{C_2+C_{2c}} & -C_3 & 0 & 0 \\ 0 & -C_3 & C_3+C_4+C_5 & -C_4 & -C_5 \\ 0 & 0 & -C_4 & C_4 & 0 \\ 0 & 0 & -C_5 & 0 & C_5 \end{bmatrix} \tag{3.4}$$

Equation (3.1) can be then written in the form of

$$[M]\{\ddot{z}\} + [C]\{\dot{z}\} + [K]\{z\} = \{F(t)\} \tag{3.5}$$

where $\{z\}^{\mathrm{T}}$ is the transpose of the displacement vector $\{z\}$ and is given by $\{z\}^{\mathrm{T}} = \{z_1, z_2, z_3, z_4, z_5\}$; $\{F(t)\}^{\mathrm{T}}$ is the transpose of the excitation force vector $\{F(t)\}$ and is given by $\{F(t)\}^{\mathrm{T}} = \{C_1\cdot\dot{z}_0 + K_1\cdot z_0, 0,0,0,0\}$. The modal natural resonant frequencies are calculated from the mass and stiffness matrices using the Eigen analysis method through a MATLAB program. The mass and stiffness values are adjusted and optimized through the multiple objective optimization Genetic Algorithm (GA). A genetic algorithm is a search heuristic that is inspired by Charles Darwin's theory of natural evolution. This algorithm reflects the process of natural selection where the fittest individuals are selected for reproduction to produce offspring of the next generation. Genetic Algorithm (GA) can be applied for multiple objective optimizations. In other words, the calculated modal resonant frequencies of the lumped mass-spring-dashpot parameter model have to be close to the experimentally measured modal resonant frequencies through the optimization. After the process of the optimization completed, the goodness of fit will meet the preset tolerance criteria and the robustness and accuracy of the identified parameters of the model will be enhanced by averaging the identified parameters from the four different truck groups with the same test driver and the seating systems of the same design.

To calculate the frequency response functions of the seated mass, driver’s pelvis mass, driver’s upper torso mass, driver’s viscera mass, and driver’s head mass concerning the base excitation, the Laplace transform is applied to Equation (3.1), which produces the following matrix equations

$$\begin{Bmatrix} \frac{z_1}{z_0} \\ \frac{z_2}{z_0} \\ \frac{z_3}{z_0} \\ \frac{z_4}{z_0} \\ \frac{z_5}{z_0} \end{Bmatrix} =$$

$$\begin{bmatrix} M_1 \cdot s^2 + (C_1 + \frac{C_2 \cdot C_{2c}}{C_2 + C_{2c}}) \cdot s + K_1 + \frac{K_2 \cdot K_{2c}}{K_2 + K_{2c}} & -\left(\frac{C_2 \cdot C_{2c}}{C_2 + C_{2c}} \cdot s + \frac{K_2 \cdot K_{2c}}{K_2 + K_{2c}}\right) & 0 & 0 & 0 \\ -\left(\frac{C_2 \cdot C_{2c}}{C_2 + C_{2c}} \cdot s + \frac{K_2 \cdot K_{2c}}{K_2 + K_{2c}}\right) & M_2 \cdot s^2 + (C_3 + \frac{C_2 \cdot C_{2c}}{C_2 + C_{2c}}) \cdot s + K_3 + \frac{K_2 \cdot K_{2c}}{K_2 + K_{2c}} & -(C_3 \cdot s + K_3) & 0 & 0 \\ 0 & -(C_3 \cdot s + K_3) & M_3 \cdot s^2 + (C_3 + C_4 + C_5) \cdot s + K_3 + K_4 + K_5 & -(C_4 \cdot s + K_4) & -(C_5 \cdot s + K_5) \\ 0 & 0 & -(C_4 \cdot s + K_4) & M_4 \cdot s^2 + C_4 \cdot s + K_4 & 0 \\ 0 & 0 & -(C_5 \cdot s + K_5) & 0 & M_5 \cdot s^2 + C_5 \cdot s + K_5 \end{bmatrix}^{-1}$$

$$\cdot \begin{Bmatrix} C_1 \cdot s + K_1 \\ 0 \\ 0 \\ 0 \\ 0 \end{Bmatrix} \qquad (3.6)$$

When $s=i\omega$, the Laplace transform becomes the Fourier transform. Equation (3.6) is expressed in the frequency domain as the results of the Fourier transform. The displacement transmissibility ratios of the five parts in the model (z_1/z_0, z_2/z_0, z_3/z_0, z_4/z_0, and z_5/z_0) can be calculated through Equation (3.6). And then, Equation (3.1) can be solved in the frequency domain using the Fourier transform when the values of the mass, stiffness constant, and damping coefficients of the lumped mass-spring-dashpot seat-occupant system model in Equation (3.6) are identified by the multiple objective optimization GA methods. The identification process will be presented below.

3.3 Experiment measurement

3.3.1 Test vehicle and instrumentation

Vehicle tests and vibration measurements were conducted on four different brands of trucks running at idle without air conditioners being turned on where experimental test data was collected.

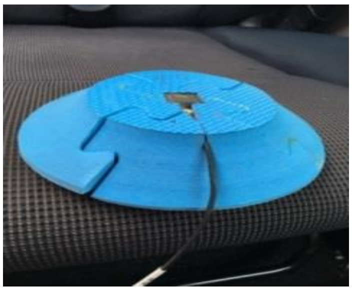

(a) **(b)**

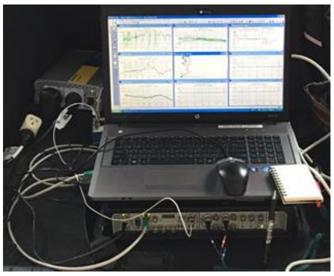

(c) **(d)**

Figure 3.2 Test set up; (a) a tri-accelerometer installed in a foam cushion pad; (b)

headband strap or bandage of holding the tri-accelerometer onto the head; (c) truck cabin installed with a driver's seat (d) the data acquisition frontend system.

A foam cushion pad as shown in Figure 3.2(a) was used to mount the tri-axial accelerometer on the seat base and seat back respectively, thus, the tested driver would not feel any uncomfortable on his back and buttock during the measurement and the sensor could pick up the vibration signals on the seat base and back in three directions of x, y, and z. A headband strap as shown in Figure 3.2(b) was used to hold the tri-axial accelerometer onto the tested driver's head to make sure that the head vibration signals in the directions of x, y, and z could be recorded.

In Figure 3.2(c), the truck cabin with the well-performed tuning seat system is displayed. A uniaxial accelerometer used to record the seat track vibration signal inboard on the floor in the vertical direction was fixed onto the cabin floor by hot glue gun adhesive. A tri-axial accelerometer was used to record the vibration signals from the seat base, seat back, and tested driver's head.

3.3.2 Data acquisition and recording

The uniaxial and the tri-axial accelerometers were connected to the Bruel & Kjaer Pulse frontend through four channels. The Bruel & Kjaer Pulse Frontend as shown in Figure 3.2(d) was used as a signal conditioner, amplifier, and recorder. An Ethernet data cable (AO-1450) was used to connect the frontend and the laptop computer which was installed with the Bruel & Kjaer Pulse Labshop software. 'Time Recorder', the data recording module of the software, was used to record the vibration signals for 10 seconds in the frequency range from 0 to 20 kHz. The 'Playback' function of the software was used to conduct FFT analysis and the frequency range from 0 to 50 Hz was used for the output spectrum calculation. In addition, 400 FFT lines and 5 second average time were used to calculate auto-power spectra, frequency response functions, and coherence functions.

3.3.3 Test process

The uniaxial accelerometer on the floor and the tri-axial accelerometer on the seat base, seat back, and the driver's head orderly measured the vibration signals and the Bruel & Kjaer Pulse software system recorded them by four channels of the frontend system through the cable connections. Because the frontend system only has four input channels, so the vibration signals of the seat base in the directions of x, y, and z, the vibration signals of the seatback in the directions of x, y, and z, and the vibration signals of the tested driver's head in the directions of x, y and z were respectively recorded together with the vibration signal of the floor in the vertical direction in three individual measurements. Due to each of the three individual measurements being repeated three times for a truck test condition, so there are nine measurements in total for the truck test condition.

3.4 Identification and Optimization of System Parameters

Genetic algorithm (GA) is a method that can be used to solve both the constrained and unconstrained optimization problems. GA is based on a natural selection process that could modify biological evolution. It integrates numerical analysis, matrix computation, and graphics in a user-friendly environment [84]. In this paper, the genetic algorithm is used to identify the stiffness, damping, and mass of the seat-occupant model through multiple objective optimizations. The process of the multiple objective optimization genetic algorithm can be described according to the following steps:

1. The initial population is given by the program or a random initial population is generated by itself. This population will be recorded as population zero.

2. Individuals in the population zero will be assessed and the individuals with the high fitness will be selected and combined into the parent population.

3. A child population is then generated by the program using selection, crossover, and mutation.

4. The parent population (the last generation) and child population will be combined by the program to generate a new population.

5. The new non-dominated population will be sorted by the program and the new front is generated.

6. The optimal population will be picked up by the program based on the crowded distance sorting to calculate the new generation.

If the present tolerance of the fitness function is less than the preset tolerance of the fitness function of the optimal population, the output result should be produced. Otherwise, repeat Steps 3 to 5.

In this study, according to the experimental results obtained from the field tests of 4 Trucks, the parameters (element values of the matrixes [K], [M] and [C]) of the 5-DOF lumped mass-spring-dashpot seat-occupant system model can be identified and optimized by using the multiple objective optimization Genetic Algorithm method (GA).

The procedure of the parameter identification of the elements of matrices [K], [M], and [C] is divided into two steps which are:

1$^{st.}$ Determination of the element values of [K] and [M] matrices

2$^{nd.}$ Determination of the element values of [C] matrix

3.4.1 Bound for the identified parameters

Appropriate parameter bound setting for the GA process or definition of reasonable ranges of the parameters for the lumped mass-spring-dashpot parameter model can reduce computation time. However, in the experiment, the parameters of the mass, stiffness, and damping coefficients of the seat-occupant system models are difficult to measure, because the parameters might be influenced by posture variations of the tested driver, and it is not feasible to measure the mass, stiffness and damping coefficients of the human body parts, so the bound setting in this study is assumed to make the system parameters be located in reasonable ranges. The bound setting of the lumped mass-spring-dashpot parameters is shown in Table 3.1. According to the bound setting in Table 3.1, the simulated resonant frequencies of the lumped-parameter model in Table 3.2 are calculated using the Genetic Algorithm method and shown to be very close to the measured resonant frequencies, proving that the bound setting in Table 3.1 is feasible and reasonable.

Table 3.1 The parameter bound setting for the GA parameter identification process

Mass			**Stiffness Constant**			**Damping Coefficient**		
	Lower	Upper		Low	Upper		Lower	Upper
$\boldsymbol{M_1}$	13		K_1	100	50000	C_1	100	10000
$\boldsymbol{M_2}$	10	30	K_2	100	300000	C_2	100	10000
$\boldsymbol{M_3}$	15	30	K_{2c}	100	50000	C_{2c}	100	10000
$\boldsymbol{M_4}$	3	10	K_3	100	300000	C_3	0.1	1000
$\boldsymbol{M_5}$	3	10	K_4	100	300000	C_4	0.1	1000
			K_5	100	300000	C_5	0.1	1000

3.4.2 Fitness function

At the first step, for the parameter identification of [K] and [M] matrix elements with the GA method, an appropriate fitness function is formulated through a comparison between the calculated and measured natural resonant frequencies of the seat-occupant system. The natural resonant frequencies of the seat-occupant model were calculated by the equation

$$\left\{[K]-\omega^2[\mathrm{M}]\right\}\left\{u\right\}=0 \tag{3.7}$$

where ω is the natural resonant frequency of the lumped mass-spring-dashpot parameter model, {u} is the mode shape, and [M] and [K] are the mass and stiffness matrices which have already been defined in Equations (3.2) and (3.3). The natural resonant frequencies of the seat-occupant system can be identified/measured from the peak frequencies of the measured auto-power spectrum density or the measured transmissibility ratio data (frequency response functions) using the Brule & Kjaer Pulse data acquisition system and Labshop software system as shown in Figure 3.3. With the identified/measured natural resonant frequencies shown in Table 3.2, the fitness function for identification of the element values of the [K] and [M] matrixes are given by

$$error=\sum_{n=1}^{N}\left|f_n^{measured}-f_n^{calculated}\right|^2 \tag{3.8}$$

where $f_n^{measured}$ and $f_n^{calauted}$ (n=1,2,3,4,5) are the measured and calculated first five natural resonant frequencies of the lumped mass-spring-dashpot seat-occupant system parameter model respectively.

In this step, since the element values of the [K] and [M] matrixes $(M_1, M_2, M_3, M_4, M_5, K_1, K_2, K_{2c}, K_3, K_4, K_5)$ need to be identified, so all of them are presented as eleven unknown parameters $x_1, x_2 \dots, x_{11}$. And then, with the parameter bounds defined in Table 3.1, in Equation (3.8), minimizing the mean square error or the GA fitness function can solve these eleven unknowns, which means these element values of [K] and [M] matrixes can be identified and optimized.

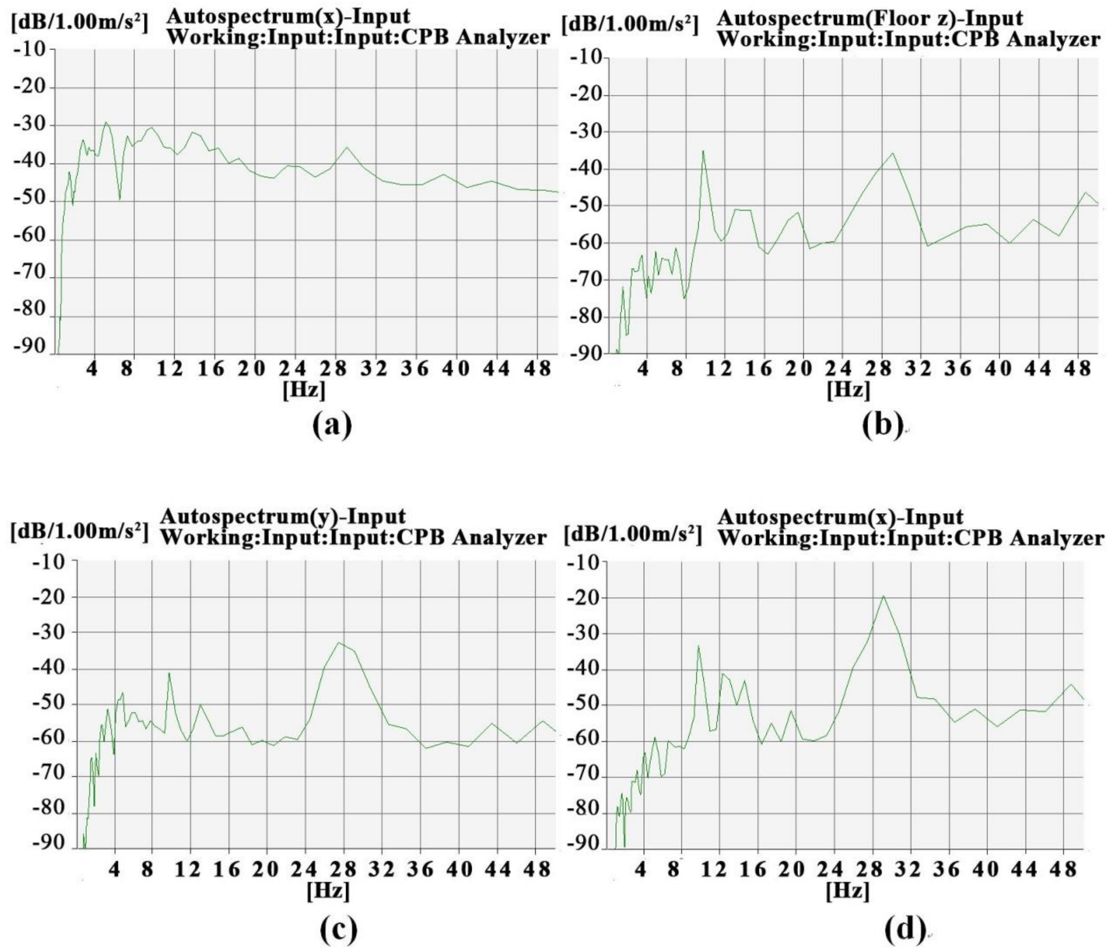

Figure 3.3 The amplitude curves of the acceleration auto-spectrum in the vertical direction; (a) at the human head; (b) at the inboard seat track on the floor; (c) at the seat base; (d) at the seat back for Truck 2.

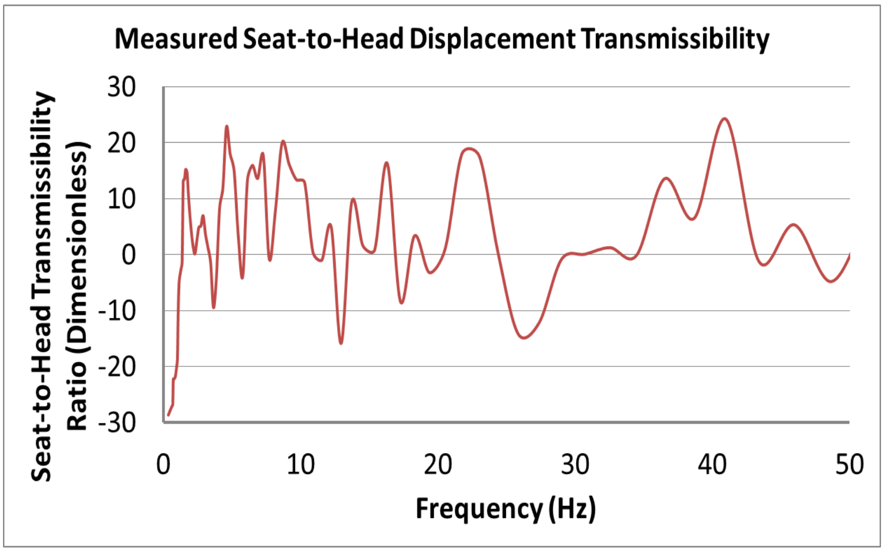

(a)

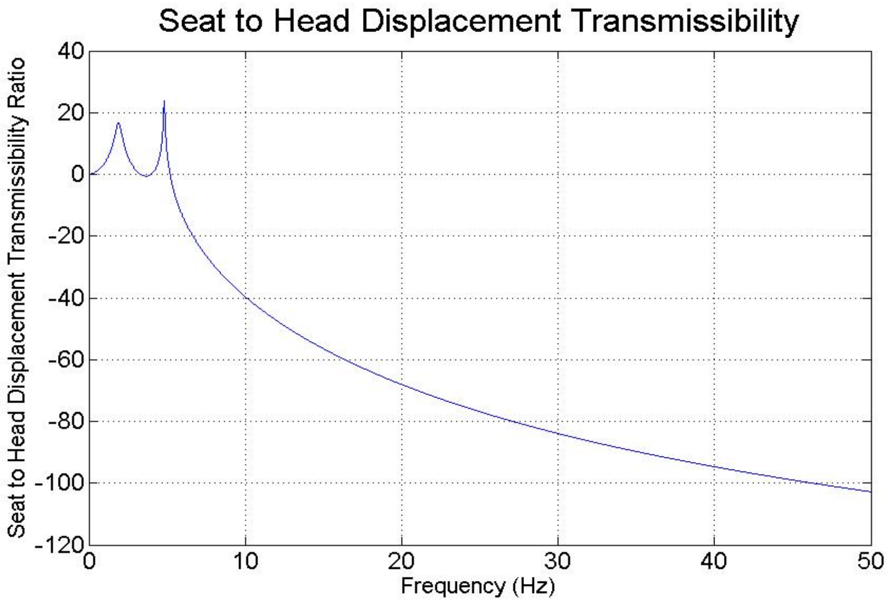

(b)

Figure 3.4 Transmissibility ratios from the seat base to the driver's head in the vertical direction (dimensionless); (a) the measured transmissibility ratio; (b) the simulated transmissibility ratio for Truck 2.

Secondly, to identify the element values of [C] matrix, the fitness function of the GA method is formulated by comparing the calculated and the measured peak values of the seat to head displacement transmissibility ratios of the seat-occupant systems in the peak frequency of about 4 Hz.

The reason for choosing the peak frequency of 4 Hz is that the frequency peak which is outstanding in the measured seat to head displacement transmissibility ratios may mainly cause discomfort of the driver. This is because the peak frequency of 4 Hz corresponds to the vertical vibration resonant mode of the driver seat system and stays in the resonant frequency range of human body vibration.

The measured peak values of the seat to head displacement transmissibility ratios at about 4 Hz were obtained from the Fourier transform of the field vibration measurement data using the Brule & Kjaer Pules Labshop software system as shown in Figure 3.4(a). In Figure 3.4(b), for the lumped mass-spring-dashpot parameter model, the seat to head displacement transmissibility ratio (z_5/z_1) and its peak value at about 4 Hz is calculated through Equation (3.6). With the parameters defined in Table 3.3, the fitness function for identification of the element values of [C] is given by

$$\text{squared error} = (R_{measured} - R_{calculated})^2 \tag{3.9}$$

where $R_{measured}$ and $R_{calculated}$ are the measured and calculated peak values of the seat to head transmissibility ratios of the seat-occupant systems at around 4 Hz respectively. Same as above, the element values of [C] matrix ($C_1, C_2, C_{2C}, C_3, C_4, C_5$) are presented as six unknowns x_i' ($i = 1,2, \dots, 5$) or ($x_1', x_2' \dots, x_6'$). With the parameter bounds defined in Table 3.1, in Equation (3.9), the minimum mean square error of the peak values at about 4 Hz means the calculated peak transmissibility ratio of the lumped mass-spring-dashpot parameter model is close to the measured peak transmissibility ratio of the real seat-occupant system at the same natural resonant frequency of about 4 Hz.

3.5 The parameter identification results through the multiple objective optimization GA

The simulated natural resonant frequencies of these 4 models are compared with the measured natural resonant frequencies of these 4 models as shown in Table 3.2. The largest error value (22%) appears between the simulated and measured fourth natural resonant frequencies. However, in this study, our main focus is the first three natural resonant frequencies where large vibration could be produced in the low-frequency range, and the errors between the simulated and measured first three natural resonant frequencies are very small, lowering to around 4%.

The identified parameters of the mass and stiffness of the lumped mass-spring-dashpot models of the four trucks are listed in Table 3.3. It is seen from Table 3.3 that the ranges of each group of corresponding mass and stiffness of the lumped-parameter model are very close to one another for the four tested trucks. The similar mass and stiffness parameters identified from the seat-occupant system of the four trucks have validated the GA parameter identification method and illustrated the robustness of the identified parameters as the same driver and same seat system design was used in the four different brands of trucks. To further enhance the robustness of the seat-occupant system model, the identified parameters of the mass and stiffness of the lumped mass-spring-dashpot models of the four trucks are averaged and listed in the last column of Table 3.3.

Table 3.2 Measured and simulated natural resonant frequencies of the driver and seat systems of four different brands of trucks

Truck Brands	Measured Resonant Frequencies (Hz)	Simulated Resonant Frequencies, (Hz)
Truck 1	1.42, 3.47, 4.1, 10.79, 36.7	1.43, 3.5, 4.17, 8.4, 37.3

Truck 2	1.45, 3.45, 4.87, 9.5, 37.5	1.44, 3.47, 4.86, 8.4, 37.47
Truck 3	1.73, 3.26, 4.1, 9.173, 36.52	1.42, 3.336, 4.01, 8.5, 36.56
Truck 4	1.45, 3.45, 5.158, 9.72, 38.68	1.46, 3.62, 5.08, 8.51, 38.69

Table 3.3 The identified parameters and their average values of the driver and seat system models of the four different brands of trucks

Parameters	Units	Truck 1	Truck 2	Truck 3	Truck 4	Average
M_1	kg	13	13	13	13	13.00
M_2	kg	25.101	25.37	25.10	25.01	25.15
M_3	kg	23.185	19.33	21.07	20.08	20.92
M_4	kg	3.113	3.076	3.73	3.29	3.30
M_5	kg	4.171	4.70	4.75	4.70	4.58
K_1	N/m	24936.13	24784.75	24950.34	24746.02	24854.31
K_2	N/m	29768.49	28098.38	28546.57	28479.32	28723.19
K_{2c}	N/m	14320.91	14996.05	14972.64	14887.21	14794.20
K_3	N/m	4980.08	4253.84	4901.48	4214.34	4587.43
K_4	N/m	157505.87	146948.35	166927.41	166770.10	159537.93
K_5	N/m	2104.38	3414.98	2016.96	3892.20	2857.13

In Table 3.4, the measured and simulated maximum peak values of the transmissibility ratios from the seat base to head were compared for all the four test trucks where the damping coefficients or element values of [C] are identified by matching the maximum peak values of the measured and simulated transmissibility ratios using the GA method as illustrated before.

Table 3.4 Comparison of the maximum peak values of the measured and simulated transmissibility ratios from the base to head for all the four test trucks

Test trucks	Measured transmissibility from the Base to Head (Dimensionless)	Simulated transmissibility from the Base to Head (Dimensionless)
	Maximum	Maximum
Truck 1	19.36	19.41
Truck 2	24.25	23.86
Truck 3	20.05	20.16
Truck 4	17.18	17.0

Table 3.5 lists the identified damping coefficient parameters of the lumped mass-spring-dashpot seat-occupant system models of the four trucks. It is seen from Table 3.5 that the difference of the damping coefficients of the models of the four trucks is significant, as the damping coefficients are sensitive to the variations of the driver's posture and seat system mounting. The identified damping coefficient parameters of the lumped mass-spring-dashpot seat-occupant system models of the four trucks are averaged and listed in the last column of Table 3.5. The averaged identified mass, stiffness, and damping coefficient parameters of seat-occupant system models of the four trucks can better describe and simulate the dynamic response characteristic of the model as shown in Figure 3.4(b). All results shown above have confirmed that the

parameters optimized and identified by the GA method for the 5-DOF lumped mass-spring-dashpot seat-occupant system model are reliable and meet the criteria, which means that with these parameters, the 5-DOF model can be used to precisely simulate and analyze the dynamic response performance of the truck seat-occupant system.

Table 3.5 The identified damping coefficients and their average values for the driver's seat systems of all the four trucks

Test trucks	C_1 (Ns/m)	C_2 (Ns/m)	C_{2c} (Ns/m)	C_3 (Ns/m)	C_4 (Ns/m)	C_5 (Ns/m)
Truck 1	6776	4438	430	667	649	0.2
Truck 2	7881	4462	4966	18.7	991	0.3
Truck 3	7846	2980	286	30	450	2.5
Truck 4	9663	3515	2415	66	944	0.2
Average Truck 1-4	8041.5	3848.75	2024.25	195.425	758.5	0.8

3.6 The parameter sensitivity analysis of the seat-occupant system for the SEAT values

The seat effective amplitude transmissibility (SEAT) value is often used to be an important indicator for evaluating seat comfort in the study of vibration control of a seating system and to measure the performance of the seat suspension system. The SEAT value is determined by comparing the difference between the weighted acceleration amplitudes at the floor and the seat base. If the SEAT value is greater than 100%, means the seat suspension system cannot reduce the vibration transmitted from the floor and even increase the vibration. Oppositely, less than 100% of the SEAT values mean that the seat suspension system can reduce the vibration. Generally, the SEAT values are calculated from the floor to the seat, but in this research, the SEAT values were calculated from the seat base to the head, which can reflect the influence of the comfort of the seat system to the human body.

After establishing the analytical seat-occupant model, the parameter sensitivity analysis can be conducted by changing the parameters accordingly, which provides a theoretical basis for further optimizing the seat suspension system. The analytical seat-occupant model will also provide information and data to the active vibration controller design. The developed biodynamic model can also predict the SEAT value more accurately.

By increasing all parameters by 10%, it is seen from the data in Table 3.1 that in the stiffness matrix of the seat-occupant model, K_5 representing the stiffness of the neck is the most sensitive parameter most affecting on the SEAT values from the seat to the head. Decreasing the stiffness of the neck will decrease the SEAT value.

In the mass matrix, M_5, which represents the driver's head mass, has the second-highest influence on the SEAT values. Increasing the mass of the driver's head will decrease the SEAT value.

In the damping matrix, seat damping coefficient, C_1, has the highest sensitivity on the SEAT values. Besides, in the 5-DOF seat-occupant biodynamic model, the parameter changes in the stiffness, mass, and damping coefficient of the upper torso also have a great influence on the SEAT value. For example, increasing the stiffness of the upper torso K_3 by 10% would add the SEAT value (from the seat to the head) by 4.7%, respectively. However, if the mass of the torso M_3 is increased by 10%, the SEAT value will be reduced by 5.8% correspondingly. Increasing the mass of the torso will decrease the SEAT value.

Since the SEAT value is a value, which is difficult to be visually illustrated by a chart or a figure. Therefore, the reliability of the parameter sensitivity analysis of the SEAT values can be verified by comparing the transmissibility ratio variation tendency and the SEAT value variation tendency after adjusting the corresponding parameters. It can be seen from Figure 3.5 (a) that the transmissibility ratio from the base to the head with a 10% change of K_5 has been significantly increased compared with the original value. This trend is the same as the changing trend of the SEAT values as shown in Table 3.6. It is seen from Fig. 5 (b) that the red curve that represents the transmissibility ratio from the base to the head with a 10% parameter increase of M_5 is lower than the blue curve. This trend of the transmissibility ratio is also the same as that of the related SEAT value. Therefore, the transmissibility ratio (seat to head) and the SEAT values (seat to head) have the same trend as the parameters increase, which indicates that the parameter sensitivity analysis of the SEAT values is reliable.

Table 3.6 The SEAT Value (seat to head) with and without the 10% increase of all the parameters

K Value	Original	110% K_1	110% K_2	110% K_{2c}	110% K_3	110% K_4	110% K_5
SEAT Value (%)	1.2296	1.2307	1.2343	1.239	1.2876	1.2299	1.3247
Tendency & Error		⬆ 0.1%	⬆ 0.4%	⬆ 0.8%	⬆ 4.7%	⬆ 0.02%	⬆ 32.1%
M value		110% M_1	110% M_2	110% M_3	110% M_4	110% M_5	
SEAT Value (%)		1.2516	1.2139	1.1577	1.2176	1.0279	

Tendency & Error		1.8%	-1.3%	-5.8%	-1%	-16.4%	
C Value		110% C_1	110% C_2	110% C_{2c}	110% C_3	110% C_4	110% C_5
SEAT Value (%)		1.2015	1.239	1.2478	1.2393	1.2296	1.225
Tendency & Error		-2.3%	0.8%	1.5%	0.8%	0	-0.4%

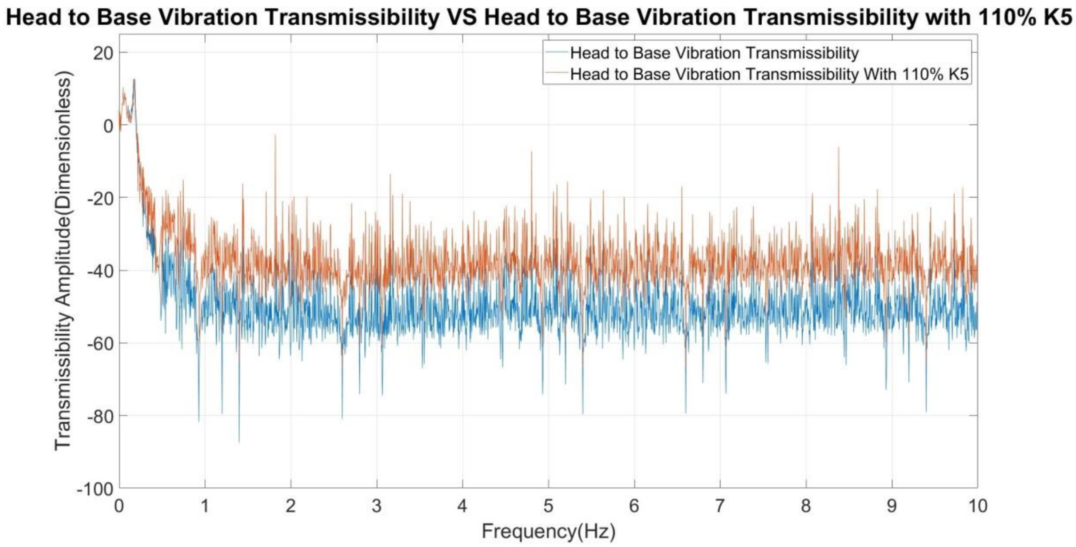

(a)

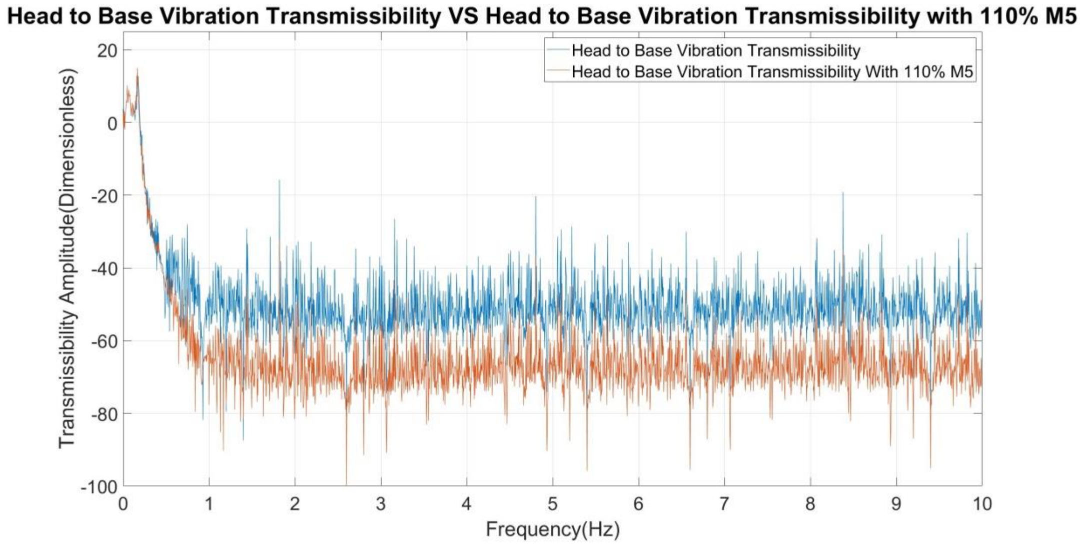

(b)

Figure 3.5 (a) The base to head transmissibility ratio with and without a 10% increase of the driver's neck stiffness K5; (b) The base to head transmissibility ratio with and without a 10% increase of the driver's head mass M5

By analysing the sensitivity of the parameters for the SEAT values, the SEAT values are increased by 0.1% and 0.8% respectively when the seat stiffness K_1 and the seat cushion stiffness K_{2c} of the seat cushion are increased by 10%. These increases in SEAT values will slightly reduce the comfort of the seat system. When the seat mass M_1 is increased by 10%, the SEAT value is increased by 1.8%, which means that the seat comfort is reduced. Finally, increasing the seat damping coefficient C_1 and the cushion damping coefficient C_{2c} has shown an opposite result that the SEAT value is decreased by 2.3% and increased by 1.5% respectively, which means that the increased seat damping coefficient will enhance the comfort level, but the increased seat cushion damping will degrade the comfort.

3.7 Conclusions

This chapter adopts a five-degree of freedom (5-DOF) lumped mass-spring-dashpot system to model a truck driver seat system where the four degrees of freedom lumped mass-spring-dashpot human body system is connected to a single degree of freedom (S-DOF) lumped mass-spring-dashpot seat suspension system at the seat base through a soft foam seat cushion. The vibration accelerations of the driver's head, seat back, seat base, and the inboard driver's seat track on the floors of four different brands of trucks were measured in field tests where the trucks were tested at idle in a park with air conditioner being turned off. The measurement results have been used to identify the mass, stiffness, and damping coefficients of the 5-DOF lumped mass-spring-dashpot system models. The following conclusions are made:

1. This research has developed a new method to identify system parameters of a driver seat system model from the field vibration measurement results.
2. The experimental results have verified the simulation results, which have validated the parameter identification method and the simulation model of the driver seat suspension system.
3. The parameter sensitivity analysis showed that the stiffness coefficients of the seat and seat cushion have a smaller influence on the seat comfort or the SEAT value than the damping coefficients of the seat and seat cushion.
4. The stiffness of the neck is the most sensitive parameter to the SEAT value from the seat to the head and has the largest influence on the SEAT value. Decreasing the stiffness of the neck will improve comfort.
5. Increasing the mass of the seat base degrades the comfort. Increasing the mass of the driver's head or the torso will improve comfort.
6. Increasing the damping coefficient of seat and seat cushion will enhance and degrade the seat comfort respectively.

After the 5-DOF mass-spring-dashpot lumped parameter model is established, its parameters have been identified from the field test vibration measurement data, the validated model has been studied for the parameter sensitivity analysis. To study the parameter effects of the nonlinearity and interactions of the model parameters, the response surface method will be employed to predict the vibration isolation performance or the transmissibility ratio from design parameters. The design parameters will be optimized within the specified range for the best vibration isolation performance or the minimum transmissibility ratio. This will be illustrated in the next chapter.

4 5-DOF Bio-dynamic model sensitivity analysis and optimization through response surface method

4.1 Introduction

As a vibration mitigation device, vehicle seats can protect people from low-frequency vibrations generated by road excitation. According to the papers [1,2], long-term exposure to a low-frequency vibration environment may cause various injuries or even some chronic diseases, including spine injury, myopathies, digestive system diseases, reproductive system injury, and even cancer. Therefore, how to improve the low-frequency vibration isolation performance of the seat system for a commercial vehicle has become a hot topic. People have been developing innovative active, semi-active, or passive seat suspension systems that can mitigate the low-frequency vibration more efficiently. For example, the active seat suspension generally uses a traditional rotation motor or a new type of linear motor as a force actuator where the resistive torque or force is generated to reduce vibration [20,63], while the semi-active seat suspension usually uses magnetorheological fluid or elastomer of variable stiffness and damping coefficients as materials of shock absorber to reduce the low-frequency vibration [35,76]. Although active and semi-active seat suspensions have good vibration control performance, they also have some disadvantages such as high energy consumption, complicated control algorithms, and high costs.

Compared with the expensive active/semi-active seat suspension systems, the new system optimization method can be widely applied to existing passive seat suspension systems to improve commercial vehicle riding comfort. The new system optimization method applies to both vehicle and seat suspension systems where their results can be integrated.

In Ref. [85], a rigid-flexible coupling model of a car was established by using multi-body system dynamics method and component mode synthesis technology where the flexibility of the car body, twist beam of the rear suspension, and stabilizer rod was considered and the assemblies such as front/rear suspension, steering system, body, and powertrain were treated as rigid bodies. The ride comfort was optimized by using the design of the experiment method. However, the explicit relationship between the input design parameters and ride comfort target was not derived in this paper. The optimization validity was restricted by the specified number of experiments/simulations through the design of the experiment method.

Similarly, in Ref. [86], the Artificial bee colony algorithm and a 9-DOF chassis-seat-occupant dynamic model was used to investigate the ride comfort of passive and active suspension systems using a half vehicle model and to optimize the design parameters of suspension spring stiffness coefficients, suspension shaker absorber damping coefficients and tire stiffness coefficients for improving the ride comfort of the vehicle. In Ref. [87], a global optimization technique of the DIRECT method was developed for optimizing suspension systems to improve the ride comfort of the cab with passive and semi-active suspensions where the comfort objective parameters were used by the norms. For the seat vibration isolation optimization, modeling using the DIRECT method was significant with the required accuracy. In Ref. [88], two different seat models consisting of the Bouc-Wen model which is multiple degree-of-freedom non-linear, and the lumped parameter model presenting the dynamic responses of individual seat components were established and compared. In Ref. [89], the multi-objective optimization method was applied to optimize the vehicle seat system based on three different models, namely the 1-DOF model, 1.5-DOF model, and 2.5-DOF model. While in Refs. [90,91], the 4-DOF integrated model considering the seat-occupant dynamic characteristics, minimum chassis suspension deflection, and tire deformation was built to identify the optimal parameter settings to achieve the best vibration isolation performance. In the research [92], another 4-DOF seat-human body model was established for the seat system optimization design. The quasi-Newton method was applied to optimize the seat system parameters of the seat mass, stiffness, and damping coefficients to improve seat vibration isolation performance under the 50 mm amplitude harmonic excitation where the reliability and accuracy of modeling were confirmed. However, only the ideal seat system parameters were considered and real vehicle experimental measurement data was not applied to the parameter identification. It can be seen from the previous literature that most of the current analytical and simulation models of the seat suspension system cannot present an explicit relationship between the vibration isolation performance target and design parameters, which makes the design optimization process time consuming and ineffective.

However, if a regression prediction model can be developed from the known input parameters with specified ranges and response targets which can either be measured from experiments or calculated from simulations, the optimization process can be quickly and easily implemented through the multiple objective Generic Algorithm optimization. Since experiments are time and consuming, the regression model development experiments can sometimes be replaced by regression model development simulations based on CAE software models or complex mathematical models that are validated by experiments.

Various regression methods were applied for modeling and optimization, among which, RSM has been successfully applied to vehicle suspension design optimization for riding comfort improvement. In Refs. [93-95], the RSM was used to model the vehicle chassis vibration isolation performance and optimize design parameters for the best vibration isolation performance. To develop a vehicle seat suspension system model, the RSM method was applied to model and optimize the seat system based on an integrated vehicle-seat model [96] where the effect of the seat cushion on vibration isolation performance was separately considered. For real truck tests in Ref. [68], a system parameter identification method was developed from field test measurement data of one truck where the measured and simulated values of the natural resonant frequencies and the peak vibration amplitude values at the resonant frequency of the vertical mode were matched using a trial-and-error method. The parameter identification method was time-consuming and based on only one truck where the robustness of the parameter identification is questionable.

Therefore, a new system design optimization method that has strong robustness is needed to improve seat vibration isolation performance. The new method should be able to enhance the vibration isolation performance of the existing vehicle seat suspension system with reduced cost and without additional parts and energy consumption. The new design method should make the design change and optimization of a seat suspension system relatively simple, easy to be implemented. Therefore, a suitable regression modeling method has become a major concern of system optimization.

Previous researches on the vehicle seat suspension system were only focused on studying the effects of individual design parameters on vibration isolation performance. The interaction effects of the design parameters on the vibration isolation performance have not been disclosed so far. The machine learning approach such as a combination of response surface method (or linear regression method) with the Generic Algorithm has not been applied in the design and optimisation of seat suspension system for vibration isolation by so far.

Therefore, three main parts of this research will be presented in this chapter: (1) Establish the relationship between the vibration transmissibility ratio (from head to seat base) and the seat design parameters using the RSM method based on the 5-DOF model. (2) Analyze the sensitivity of the design parameters and their interaction effects. (3) Optimize the design parameters for the best vibration isolation performance.

4.2 Response surface modeling of design parameters of the seat suspension system

4.2.1 Theoretical background of response surface method modeling

The response surface method (RSM) is a comprehensive regression analysis tool that is generally used for the optimization process. It is not only able to produce a continuous variable surface mode but also can establish a response surface, which can estimate the interaction between the factors that can affect the process. RSM method overcomes the shortcomings of traditional univariate optimization experiments. It can establish a nonlinear quadratic relationship between the input variables and the output target. The process of RSM includes the central composite experimental design (CCD), response surface modeling, sensitivity analysis, validation, and optimization. Based on the CCD design and response surface modeling, a second-order polynomial regression model can be developed to predict the performance of any process or system over the input control variables in a specified variation range. The RSM model can be applied to conduct the sensitivity analysis of the target to the input variables and their interactions. The RSM model can be used to predict any target value from any input variables within their specified range. The RSM model can also be used to predict the maximum and minimum target values and corresponding input variables in the specified range using Monte Carlo or GA method. The ANVOA analysis can be applied to validate the RSM model.

In the response surface modeling, input variables z_i will be coded into the dimensionless variables x_i by the following relationship

$$
\begin{cases}
z_0 = \dfrac{z_{\max} + z_{\min}}{2} \\
\Delta z = \dfrac{z_{\max} - z_{\min}}{2} \\
x_i = \dfrac{z_i - z_0}{\Delta z} \quad i=1, 2, 3, 4.....
\end{cases}
\tag{4.1}
$$

where z_0 is the mean value; $z_{\max}$ is the maximum value of the input variables z_i; $z_{\min}$ is the minimum value of the input variables z_i. The dimensionless coding variables x_i is ranged from the minimum level to the maximum level which corresponds to the minimum and maximum values of the input variables z_i, while in the CCD, the range of the dimensionless coding variables x_i is set from -1.414 to +1,414. The relationship between the input variables and target response can be approximated in a nonlinear quadratic equation and given by

$$\tilde{Y} = \beta_0 + \sum \beta_i x_i + \sum \beta_{ii} x_i^2 + \sum \beta_{ij} x_i x_j + \varepsilon$$

(4.2)

where $\tilde{Y}$ represents the predicted response or target, x_i and x_j ($j=i+1, \ldots k$) represent the coded input variables or normalised dimensionless input variables through Equation (4.1). β_0, β_i, β_{ii} and β_{ij} are the regression coefficients including the offset term β_0, primary β_i, quadratic β_{ii} and interactive β_{ij} response coefficients, and ε is the prediction error.

The RSM model coefficients for the response are computed by the multiple variable linear regression method and given by

$$\{\beta\} = ([X]^T[X])^{-1}[X]^T\{Y\} \tag{4.3}$$

where $\{\beta\}$ is a vector of ($u\times1$) regression coefficients, $[X]$ is the matrix ($N\times u$) of encoded dimensionless input variables, u is the number of the regression coefficients; $\{Y\}$ is a vector of ($N\times1$) formed by the response values of the N experiments/simulations where its element Y is the predicted response value presented in Equation (4.2). According to this method, the $\{\beta\}$ coefficients are determined by the least square fittings. In other words, the $\{\beta\}$ values are chosen to minimize the sum of squared residuals.

4.2.2 Predictive RSM modeling

In the RSM modeling, the central composite experimental design (CCD) has been applied to arrange the coded input variables. In the seat suspension system dynamic model is shown in Figure 3.1, four design parameters of the stiffness of the overall seat structure (K_1), the damping coefficient of the seat (C_1), the stiffness of the seat cushion (K_{2c}), and the damping coefficient of the seat cushion (C_{2c}) are used as the four input independent variables in the RSM modeling. The variation ranges or bounds of these input design variables or parameters are defined and specified in Table 4.1.

Table 4.1 Bound setting for the input parameters of RSM modeling

Factors	Max	Min
K_1 (N/m)	58200	1800
C_1 (Ns/m)	11025	3975
K_{2c} (N/m)	58200	1800
C_{2c} (Ns/m)	11025	3975

where x_i (i=1,2,3,4) is set from -1.41 to 1.41 in the CCD which corresponds to that the seat stiffness K_1 changes from 1800 N/m to 58200 N/m; the seat damping coefficient C_1 changes from 3975 Ns/m to 11025 Ns/m; the seat cushion stiffness K_{2c} changes from 1800 N/m to 58200 N/m; the seat cushion damping coefficient C_{2c} changes from 3975 Ns/m to 11025 Ns/m. The response target is the peak transmissibility ratio from the seat to head which can be calculated from the frequency response analysis of Equation (3.1) through Fourier transformation. The coded dimensionless and original dimensional input design variables and predicted response peak transmissibility ratio obtained from simulation via 5-DOF dynamic model are arranged according to the central composite experimental design and presented in Table 4.2. It can be seen from Table 4.2 that the coded or dimensionless input design variables and corresponding dimensional input design parameters of the seat-occupant dynamic model are converted into each other according to Equation (4.1). Based on these input parameters, the response performance index vector $\{Y\}$ can be calculated from Equation (3.1) for the seat suspension system dynamic model as shown in Figure 3.1. Equation (3.1) is converted from the time domain to the frequency domain where the transmissibility ratio from the seat base to the driver's head is solved. MATLAB code is used to calculate the transmissibility ratio with the input system model parameters including the stiffness and damping coefficients of the seat and seat cushion where the peak transmissibility ratio can be identified. The simulated peak transmissibility ratio for each run is given in the last column of Table 4.2.

Table 4.2 Central composite design (CCD) of input design variables and simulated response peak vibration transmissibility ratio for the dynamic system model as shown in Figure 3.1.

Run	**Factors (input variables)**								**Response factors**
	Seat stiffness		**Seat damping coefficient**		**Cushion stiffness**		**Cushion damping coefficient**		
	x_1	K_1 (N/m)	x_2	C_1 (Ns/m)	x_3	K_{2c} (N/m)	x_4	C_{2c} (Ns/m)	Y (Transmissibility)

1	1	50000	1	10000	1	50000	1	10000	14.01
2	-1	10000	1	10000	1	50000	1	10000	13.88
3	1	50000	-1	5000	1	50000	1	10000	14.14
4	-1	10000	-1	5000	1	50000	1	10000	13.64
5	1	50000	1	10000	-1	10000	1	10000	13.70
6	-1	10000	1	10000	-1	10000	1	10000	13.57
7	1	50000	-1	5000	-1	10000	1	10000	13.83
8	-1	10000	-1	5000	-1	10000	1	10000	13.34
9	1	50000	1	10000	1	50000	-1	5000	14.07
10	-1	10000	1	10000	1	50000	-1	5000	13.94
11	1	50000	-1	5000	1	50000	-1	5000	14.17
12	-1	10000	-1	5000	1	50000	-1	5000	13.66
13	1	50000	1	10000	-1	10000	-1	5000	13.57
14	-1	10000	1	10000	-1	10000	-1	5000	13.44
15	1	50000	-1	5000	-1	10000	-1	5000	13.67
16	-1	10000	-1	5000	-1	10000	-1	5000	13.19
17	1.41	58200	0	7500	0	30000	0	7500	13.97
18	-1.41	1800	0	7500	0	30000	0	7500	13.65
19	0	30000	1.41	11025	0	30000	0	7500	13.85
20	0	30000	-1.41	3975	0	30000	0	7500	13.78
21	0	30000	0	7500	1.41	58200	0	7500	13.96

22	0	30000	0	7500	-1.41	1800	0	7500	13.38
23	0	30000	0	7500	0	30000	1.41	11025	13.81
24	0	30000	0	7500	0	30000	-1.41	3975	13.82
25	0	30000	0	7500	0	30000	0	7500	13.81
26	0	30000	0	7500	0	30000	0	7500	13.81

Based on Table 4.2, the elements of the matrix [*X*] are arranged in Table 4.3.

Table 4.3 The arrangement of the elements of matrix [X]

x_0	x_1	x_2	x_3	x_4	x_1x_1	x_2x_2	x_3x_3	x_4x_4	x_1x_2	x_1x_3	x_1x_4	x_2x_3	x_2x_4	x_3x_4
1	1	1	1	1	1	1	1	1	1	1	1	1	1	1
1	-1	1	1	1	1	1	1	1	-1	-1	-1	1	1	1
1	1	-1	1	1	1	1	1	1	-1	1	1	-1	-1	1
1	-1	-1	1	1	1	1	1	1	1	-1	-1	-1	-1	1
1	1	1	-1	1	1	1	1	1	1	-1	1	-1	1	-1
1	-1	1	-1	1	1	1	1	1	-1	1	-1	-1	1	-1
1	1	-1	-1	1	1	1	1	1	-1	-1	1	1	-1	-1
1	-1	-1	-1	1	1	1	1	1	1	1	-1	1	-1	-1
1	1	1	1	-1	1	1	1	1	1	1	-1	1	-1	-1
1	-1	1	1	-1	1	1	1	1	-1	-1	1	1	-1	-1
1	1	-1	1	-1	1	1	1	1	-1	1	-1	-1	1	-1
1	-1	-1	1	-1	1	1	1	1	1	-1	1	-1	1	-1

1	1	1	-1	-1	1	1	1	1	1	-1	-1	-1	-1	1
1	-1	1	-1	-1	1	1	1	1	-1	1	1	-1	-1	1
1	1	-1	-1	-1	1	1	1	1	-1	-1	-1	1	1	1
1	-1	-1	-1	-1	1	1	1	1	1	1	1	1	1	1
1	1.41	0	0	0	1.9881	0	0	0	0	0	0	0	0	0
1	-1.41	0	0	0	1.9881	0	0	0	0	0	0	0	0	0
1	0	1.41	0	0	0	1.9881	0	0	0	0	0	0	0	0
1	0	-1.4	0	0	0	1.9881	0	0	0	0	0	0	0	0
1	0	0	1.41	0	0	0	1.9881	0	0	0	0	0	0	0
1	0	0	-1.41	0	0	0	1.9881	0	0	0	0	0	0	0
1	0	0	0	1.41	0	0	0	1.9881	0	0	0	0	0	0
1	0	0	0	-1.41	0	0	0	1.9881	0	0	0	0	0	0
1	0	0	0	0	0	0	0	0	0	0	0	0	0	0
1	0	0	0	0	0	0	0	0	0	0	0	0	0	0

$\{\beta\}$ is calculated from Equation (4.3). With the regression coefficient $\{\beta\}$, the second-order regression relationship between the four coded variables or dimensionless input design parameters and the response target or the peak transmissibility ratio can be given by

$$\tilde{Y} = 13.8111 + 0.149x_1 + 0.0317x_2 + 0.2012x_3 + 0.0192x_4 - 0.0032x_1^2 + 0.0018x_2^2 - 0.0729x_3^2 + 0.0017x_4^2 - 0.092x_1x_2 + 0.0025x_1x_3 + 0.0013x_1x + 0.0023x_2x_3 - 0.0094x_2x_4 - 0.00457x_3x_4 \quad (4.4)$$

It is seen from Equation (4.4) that the seat cushion stiffness (x_3) has the largest influence on the response target or the peak transmissibility ratio; the seat structure stiffness (x_1) has the second-largest influence on the response target or the peak transmissibility ratio; the seat cushion damping coefficient (x_4) has the least influence on the response target or the peak transmissibility ratio. The coupling effect of the stiffness (x_1) and the damping coefficients (x_2) of the seat structure is larger than the individual effect of the damping coefficients of the seat structure and seat cushion. The coefficient of the squared term of (x_3) is seen to have a larger impact on the response target than the coefficients of the other quadratic terms, and the damping coefficients of the seat structure and seat cushion.

It is seen from Equation (4.4) that when the seat cushion stiffness (x_3), the seat structure stiffness (x_1) the seat structure damping coefficient (x_1), and the seat cushion damping coefficient (x_4) decrease, the peak transmissibility ratio decreases.

4.2.3 Analysis of variance of the RSM model

To validate the RSM model, analysis of variance (ANOVA) was conducted. In the ANOVA analysis, the *F*-value is used as a measure for comparing the source's mean square to the residual mean square. The *P*-value is calculated with the *F*-value and the degrees of freedom (*df*). To validate any regression model from a statistical perspective, the *F*-value must be as high as possible, and the *P*-value should be as low as possible. If the *P*-value is less than 0.05, it means that the model is statistically significant and is validated for prediction.

The ANOVA analysis results of the RSM model are listed in Table 4.4 where the commonly used statistical metrics of the Sum of Squares, degrees of freedom, Mean Square, *F*-value, *P*-value, and the value of the Fit Statistics are included. In Table 4.4, the *F*-value is high to 136.11 and the *P*-value is less than 10^{-4}. Meanwhile, the R^2 value is about 0.9943, which is close to 1. In addition, R^2 is closed to the adjusted R^2. All statistical metrics indicate that the developed RSM model is valid from a statistical standpoint, and the developed RSM model works well for the prediction of the peak vibration transmissibility ratio of the seat suspension system.

Also, in the multiple variable regression analysis, the F-values on x_1 and x_3 are higher than those on the other variables, which are 565.24 and 1030.04 respectively, and the P-values are all less than 10^{-4}. These results show that for the RSM model, these two variables of x_1 and x_3 have a significant impact on the prediction performance of the model, x_3 has a larger effect on the prediction target than x_1. The F-values of x_2 and x_4 are 25.53 and 9.4, which are lower than those of these two variables of x_1 and x_3, while the P-values of x_2 and x_4 are 0.0004 and 0.0107 which are less than the threshold of 0.05. This means that those two variables of x_2 and x_4 are statistically significant in the RSM model, but they have a small effect on the prediction, x_2 has a larger effect on the prediction target than x_4. The ANOVA analysis results of the RSM model have also validated the sensitivity analysis of the input design variables and their interactions from the regression coefficients $\{\beta\}$ of Equation (4.4) as illustrated above where the regression coefficients of x_1 and x_3 are 0.149 and 0.2012 are larger than the regression coefficients of x_2 and x_4 which are 0.0317 and 0.0192 respectively. Therefore, the input design variables x_1 and x_3 have greater impacts on the prediction value $\tilde{Y}$ than the input design variables x_2 and x_4; x_3 has a larger effect on the prediction target than x_1, and x_2 has a larger effect on the prediction target than x_4. In the analysis of the interaction between variables, it can be seen that the F-value of the terms x_1x_2 (172.59) and x_3x_4 (42.49) are larger than those of the other interaction terms, and the P-values of all the interaction terms are less than 0.05, so they are statistically significant. Therefore, the coupling effect between x_1 and x_2 and the coupling effect between x_3 and x_4 will have a large impact on the final prediction, the coupling effect between x_1 and x_2 (172.59) has a larger impact on the final prediction than the coupling effect between x_3 and x_4 (42.49); but the other variable combinations and coupling effects are not statistically significant in the analysis. In other words, the relative changes between the other variable combinations have fewer effects on the model prediction performance. In the seat suspension system, this means that increasing or decreasing the stiffness of the seat structure will more prominently increase or decrease the damping coefficient of the seat structure, as will increasing or decreasing the stiffness of the cushion also increase or decrease the damping coefficient of the cushion. The ANOVA analysis results have validated the RSM model. In the quadratic analysis, the F-value of 57.12 and P-value of < 0.0001 on the squared stiffness of the seat cushion x_3^2 has statistical significance. This means the nonlinear change of the seat cushion stiffness may have a large impact on the prediction of the peak vibration transmissibility ratio.

Table 4.4 ANOVA analysis results for the RSM Model

Source	Sum of Squares	df	Mean Square	F-value	P-value	R^2	Adjusted R^2
Model	1.5	14	0.1069	136.11	< 0.0001	0.9943	0.987
$X_1(K_1)$	0.4438	1	0.4438	565.24	< 0.0001		
$X_2(C_1)$	0.02	1	0.02	25.53	0.0004		
$X_3(K_{2c})$	0.8087	1	0.8087	1030.04	< 0.0001		
$X_4(C_{2c})$	0.0074	1	0.0074	9.4	0.0107		
X_1X_2	0.1355	1	0.1355	172.59	< 0.0001		
X_1X_3	0.0001	1	0.0001	0.1287	0.7266		
X_1X_4	0	1	0	0.0338	0.8575		
X_2X_3	0.0001	1	0.0001	0.1125	0.7436		

X_2X_4	0.0014	1	0.0014	1.82	0.2044
X_3X_4	0.0334	1	0.0334	42.49	< 0.0001
X_1^2	0.0001	1	0.0001	0.1071	0.7497
X_2^2	0	1	0	0.0337	0.8577
X_3^2	0.0448	1	0.0448	57.12	< 0.0001
X_4^2	0	1	0	0.0327	0.8597
Residual	0.0086	11	0.0008		
Lack of Fit	0.0086	10	0.0009		
Pure Error	0	1	0		
Cor Total	1.5	25			

4.3 Prediction of the optimal input design variable combination and the minimum response target

In the specified range of the input design parameters, Equation (4.4) can be treated as the fitness function of the GA to search for the best parameter combination for the minimum peak transmissibility ratio. The bound of all the coded parameters were set from -1.41 to 1.41. MATLAB genetic algorithm (GA) APP was applied to calculate the minimum value of Equation (4.4) and the best parameter combination for the minimum value or the minimum peak transmissibility ratio. Table 4.5 shows that the optimal input variable combination is (-1.41, -1.41, -1.41, -1.41) and the minimum peak transmissibility ratio is 12.9.

Table 4.5 The comparison of the GA optimization results of RSM and linear regression models

Model	x_1	x_2	x_3	x_4	Y
RSM	-1.41	-1.41	-1.41	-1.41	12.9
Linear Regression	-1.41	-1.41	-1.41	-1.409	13.2
	K_1 (N/m)	C_1 (Ns/m)	K_{2c} (N/m)	C_{2c} (Ns/m)	
	1800	3975	1800	3975	

Table 4.5 displays the result that the optimal input variable combination is (-1.41, -1.41, -1.41, -1.41) where the results of the linear regression method are obtained from Chapter 5 which will be illustrated later on. The minimum transmissibility ratio is 13.2 for the linear regression method (LRM) model, which is very close to 12.9 for the RSM model. It is seen from Table 4.5 that the LRM and RSM models have the same optimal combination of the stiffness and damping coefficient of the seat and seat cushion. The optimal results of the LRM and RSM models have been verified with each other. Therefore, the RSM model has been validated by the LRM model.

4.4. Conclusions

This chapter studies the design optimization of a passive truck seat suspension system. To optimize the design of the seat-occupant system for the reduction of seat suspension system vibration, an explicit relationship between the input design parameters/variables and the peak transmissibility ratio has been developed using the response surface modeling. From the RSM model, the peak vibration transmissibility ratio of the seat suspension system can be predicted from any input design parameters within their specified range and the sensitivities of the peak transmissibility ratio to the design parameters such as the stiffness and damping coefficients of the seat structure and cushion are disclosed. The RSM model shows that the peak transmissibility ratio is most sensitive to the seat cushion stiffness, secondly most sensitive to the seat structure stiffness. The interaction effect of the stiffness and damping coefficient of the seat cushion and the interaction effect of the stiffness and damping coefficients of the seat structure on the predicted peak vibration transmissibility ratio is found to be large. The interaction effect of the stiffness and damping coefficient of the seat structure on the predicted peak vibration transmissibility ratio is larger than that of the seat cushion. The seat cushion stiffness may have a large nonlinear impact on the peak vibration transmissibility ratio.

The RSM model has been validated by the ANOVA analysis. It can be concluded that under the low-frequency vibration excitation, reducing the cushion stiffness and damping coefficient and reducing the stiffness and damping coefficient of the seat structure can improve the vibration isolation performance of the truck seat system. It has proved that the new system design optimization method through combining the RSM modeling with Generic Algorithm is effective for design optimization of the seat suspension system.

In order to validate the RSM model, a linear regression model will be developed where the same simulation data is used for both the RSM and linear regression model, which will be illustrated in the next chapter.

5 Development of a Linear Regression Model for Sensitivity Analysis and Design Optimization

5.1 Introduction

Linear regression method (LRM) is a powerful tool that can be used to establish a relationship between the independent variables {x} and the dependent variable Y. The advantages of LRM are easy to use, fast modeling, and simple calculation. Therefore, with the highly developed machine learning algorithm, linear regression is still widely applied in engineering, economics, and business fields.

In the field of vibration, linear regression analysis is widely used in establishing mathematical relationships, predicting results, and verifying model accuracy. In Ref. [97], linear regression analysis was used to evaluate the accuracy of the model output compared with the actual spine signal value. In Ref. [98], to study the influence of body characteristics on whole-body vibration (WBV), a linear regression model was established to predict the relationship between the VDV and the corresponding body characteristics (mass, height, age, and driving experience). Although linear regression has been widely used in the field of vibration control, the linear regression analysis combined with a 5-DOF biodynamic model has not been reported.

Since the model is a linear system, the use of linear regression to establish the mathematical relationship between the input and the output has higher reliability in this study. At the same time, the establishment of a linear regression model can also be used to verify the accuracy of the RSM model.

This chapter aims to establish a linear regression equation between the design parameters of the seat suspension system and the peak vibration transmissibility ratio, and this equation will be applied to optimize the seat suspension system and analyze the parameter sensitivity. Also, the results of the linear regression method (LRM) modeling will be used to verify those of the RSM model.

5.2 Linear regression method modeling of design parameters of the seat suspension system.

5.2.1 Theoretical background of linear regression modeling

The linear regression method (LRM) is a method to establish a linear relationship between the input variables and the output design target. To compare the results of LRM with those of RSM, the steps of LRM are set to be the same as those of RSM including the central composite design of experiments (CCD), linear regression method modeling, sensitivity analysis, ANOVA analysis validation, and optimization. Based on the CCD and linear regression method modeling, a linear parameter model can be developed to predict the performance of any process or system over the input control variables in their specified variation ranges. The LRM model can be applied to conduct the sensitivity analysis of the target to the input variables. The LRM model can also be used to predict the maximum and minimum target values and corresponding input variable combinations in the specified range using Monte Carlo or GA method. However, the LRM model cannot predict the interaction effects of the input variables.

In the linear regression modeling, input variables z_i will be coded into the dimensionless variables x_i according to Equation (4.1).

The dimensionless coded variable x_i is ranged from the minimum level (-1.41) to the maximum level (+1.41) according to the rule of the CCD where the star value is 1.41 for four-parameter variable inputs. The predicted response vector $\{Y\}$ ($N\times1$) can be formed by the response of the N experiments/simulations and given by

$$\{Y\}=[X]\cdot\{\beta\}+\{\varepsilon\} \tag{5.1}$$

where $\{\beta\}$ is a vector of ($u\times1$) regression coefficients, $[X]$ is the matrix ($N\times u$) of encoded dimensionless input variables. [X], $\{\beta\}$ and $\{Y\}$ are given by

$$[X]=\begin{bmatrix}1 & x_{11} & . & . & . & x_{1u}\\ 1 & x_{12} & . & . & . & x_{2u}\\ . & . & . & . & . & .\\ . & . & . & . & . & .\\ . & . & . & . & . & .\\ 1 & x_{n1} & . & . & . & x_{nu}\end{bmatrix}\quad \{\beta\}=\begin{Bmatrix}\beta_0\\ \beta_1\\ \beta_2\\ .\\ .\\ .\\ \beta_u\end{Bmatrix}\quad \{Y\}=\begin{Bmatrix}Y_1\\ Y_2\\ .\\ .\\ .\\ Y_N\end{Bmatrix} \tag{5.2}$$

where Y_i represents the predicted response or target of the i^{th} test (i=1, …N), x_{ij} (j=1, …u) represents the coded input variables or normalised dimensionless input variables of the i^{th} test (i=1, …N) through Equation (4.1). β_0, β_j (j=1, …u) is the linear regression coefficients including the offset terms β_0, primary β_j, variable coefficients, and ε_i (i=1, …N) is the prediction error of the i^{th} test (i=1, …N).

The LRM model coefficients for the variables are computed by the least square error method through Equation (4.3). According to this method, coefficients $\{\beta\}$ are determined by the least square fitting. In other words, $\{\beta\}$values are chosen to minimize the sum of squared residuals.

5.2.2 Predictive linear regression method modeling

In the seat suspension system dynamic model as shown in Figure 3.1, the variables of the stiffness of the overall seat structure (K_1), the damping coefficient of the seat (C_1), the stiffness of the seat cushion (K_{2c}), and the damping coefficient of the seat cushion (C_{2c}) are used as 4 input variables or parameters in the linear regression modeling which are the same as those in the RSM modeling or simulation. The same variation ranges or bounds of these input design variables or parameters are used and specified in Table 4.1. Based on Table 4.2, the elements of the matrix [X] are arranged in Table 5.1.

Table 5.1 The arrangement of the elements of matrix [X]

x_0	x_1	x_2	x_3	x_4
1	1	1	1	1
1	-1	1	1	1
1	1	-1	1	1
1	-1	-1	1	1
1	1	1	-1	1
1	-1	1	-1	1
1	1	-1	-1	1
1	-1	-1	-1	1
1	1	1	1	-1
1	-1	1	1	-1
1	1	-1	1	-1
1	-1	-1	1	-1
1	1	1	-1	-1
1	-1	1	-1	-1
1	1	-1	-1	-1
1	-1	-1	-1	-1
1	1.41	0	0	0
1	-1.41	0	0	0
1	0	1.41	0	0
1	0	-1.41	0	0
1	0	0	1.41	0
1	0	0	-1.41	0

1	0	0	0	1.41
1	0	0	0	-1.41
1	0	0	0	0
1	0	0	0	0

From $[X]$ in Table 5.1 and $\{Y\}$ from the last column of Table 4.2, the regression coefficient $\{\beta\}$ is calculated from Equation (4.3). With the regression coefficient $\{\beta\}$, the linear regression relationship between the four coded or dimensionless input design parameters and response target or peak transmissibility ratio can be given by

$$\tilde{Y} = 13.7553 + 0.149X_1 + 0.0317X_2 + 0.2012X_3 + 0.0192X_4 \quad (5.3)$$

It can be seen from Equation (5.3) that the seat cushion stiffness (x_3) has the largest influence on the response target or the peak transmissibility ratio; the seat structure stiffness (x_1) has the second-largest influence on the response target or the peak transmissibility ratio; the seat cushion damping coefficient (x_4) has the least influence on the response target or the peak transmissibility ratio. It can be seen from Equation (5.3) that when the seat cushion stiffness (x_3), the seat structure stiffness (x_1), the seat structure damping coefficient (x_1), and the seat cushion damping coefficient (x_4) decrease, the peak transmissibility ratio decreases. The sensitivity trend of the LRM model is shown to be the same as that of the RSM model. In other words, these conclusions concerning the parameter sensitivity are the same as those from the RSM modeling and coincide with those in the previous literature [68].

5.2.3 ANOVA analysis and student-t test of the LRM model

To validate the LRM model, the ANOVA analysis and student-t test were conducted. The ANOVA analysis and student-t test results of the LRM model are listed in Table 5.2 where the *F*-value of the whole LRM model is 29.90; the *Significance F* (*P*-value) of the whole LRM model is 2.12×10^{-8} which is much less than 0.05. Multiple R is 0.92, meanwhile, the R^2 value is about 0.85, and the adjusted R^2 is 0.82. All statistical metrics indicate that the developed LRM model is valid from a statistical standpoint, but not as good as the developed RSM model for the prediction of the peak vibration transmissibility ratio of the seat suspension system.

Table 5.2 The ANOVA analysis and student-t test results for the LRM Model

Regression Statistics			*Coefficients*	*t Stat*	*P-value*
Multiple R	0.92	Intercept	13.76	678.02	0.00
R Square	0.85	X Variable 1	0.15	6.44	0.00
Adjusted R Square	0.82	X Variable 2	0.03	1.37	0.19
Standard Error	0.10	X Variable 3	0.20	8.69	0.00
Observations	26	X Variable 4	0.02	0.83	0.42
	df	***SS***	***MS***	***F***	***Significance F***
Regression	4	1.28	0.32	29.90	2.11991E-08
Residual	21	0.22	0.01		
Total	25	1.50			

In addition, in the multiple variable regression analysis, the *t Stat* values of x_1 and x_3 are 6.44 and 8.69 respectively, are higher than those of the other variables, and the P-values of x_1 and x_3 are nearly zero. These results show that for the LRM model, x_1 and x_3 have a significant impact on the prediction performance of the model, x_3 has a larger effect on the prediction target than x_1. The *t Stat* values of x_2 and x_4 are 1.37 and 0.83, which are lower than those of x_1 and x_3, while the P-values of x_2 and x_4 are 0.19 and

0.42. This means that x_2 and x_4 are statistically less significant than x_1 and x_3 in the LRM model. x_2 and x_4 have a small effect on the prediction performance of the model, x_2 has a larger effect on the prediction target than x_4. The student-t test results of the LRM model have also validated the sensitivity analysis of the input design variables from the regression coefficients $\{\beta\}$ of Equation (5.3) as illustrated above where the regression coefficients of x_1 and x_3 are 0.149 and 0.2012, which are larger than the regression coefficients of x_2 and x_4 which are 0.0317 and 0.0192, respectively. Therefore, the input design variables x_1 and x_3 have greater impacts on the prediction value $\tilde{Y}$ than the input design variables x_2 and x_4; x_3 has a larger effect on the prediction target than x_1, x_2 has a larger effect on the prediction target than x_4. Therefore, the ANOVA analysis and student-t test results have validated the linear regression model. The ANOVA analysis and student-t results of the LRM model have the same trend as the ANOVA analysis results of the RSM model.

5.2.4 Prediction of the optimal combination of the stiffness and damping coefficient of the seat and seat cushion for the minimum peak transmissibility ratio

In the specified range of the input design parameters, as shown in Table 4.1, Equation (5.3) can be treated as the fitness function of the GA to search for the best parameter combination for the minimum peak transmissibility ratio. The bound of all the coded parameters were set from -1.41 to 1.41 in the CCD. MATLAB genetic algorithm (GA) optimisation APP was applied to calculate the minimum value of Equation (5.3) and the best parameter combination for the minimum peak transmissibility ratio. Table 4.4 displays the result that the optimal input variable combination is (-1.41, -1.41, -1.41, -1.41). The minimum transmissibility ratio is 13.2 for the LRM model, which is very close to 12.9 for the RSM model showed in Chapter Four. It is seen from Table 4.4 that the LRM and RSM models have the same optimal combination of the stiffness and damping coefficient of the seat and seat cushion. The optimal results of the LRM and

RSM models have verified each other. Therefore, the LRM model has been validated by the RSM model.

5.3 Conclusions

Same as the RSM results, the LRM model prediction results show that reducing the seat suspension system stiffness and damping coefficient, meanwhile also reducing the seat cushion stiffness and damping coefficient can reduce vibration transmissibility ratio of the seat suspension system and improve the ride comfort at the sensitive frequency of about 4 Hz.

The LRM model has been validated by the results of the student-t test. The student-t test results of the LRM model have verified the parameter sensitivity analysis results of the LRM model. The input design parameters have been optimized for the minimum peak vibration transmissibility ratio through the LRM models using the GA algorithm. Both the RSM and LRM models produce the same optimal design parameter combination. The minimum peak vibration transmissibility ratios predicted by the two models are very close. The LRM model is validated by the RSM model. From the student t-test results of the LRM model and ANOVA analysis results of the RSM model, the LRM model is not as good as the RSM model for the prediction of the peak transmissibility ratio from the input design parameters.

The experimental results further verified the conclusions from the RSM and LRM models. In the experiment, in the low-frequency vibration range of 3 to 7Hz, the seat suspension system setting of a low stiffness or low damping would reduce the vibration transmissibility ratio and improve the ride comfort.

6 Artificial Neural Network Modelling of 5-DOF Bio-Dynamic Driver and Seating Suspension System

6.1 Introduction

Artificial neural network (ANN) algorithms have emerged since the 1980s. After continuous development, they have been used in various research fields to model and analyze complex problems. The artificial neural network is composed of processing units or neurons. Each neuron represents a specific activation function, and the connection between neurons belongs to a weighting function. Through different network connection methods, activation functions, and weighted values, the neural network algorithm performs similar adaptive processing on complex nonlinear problems by simulating the way the brain operates. The artificial neural network algorithm has the characteristics of non-linearity, non-limitation, very qualitative, and non-convex. Its essence is to obtain a parallel and distributed information processing capability through the transformation of the network and the change of the excitation function. Therefore, when dealing with complex nonlinear problems, neural networks show the advantages of more efficient and accurate than other mathematical models.

In the research of vehicle vibration control, the ANN algorithm is widely used in the design of the controller system. Due to its good nonlinear fitting ability, the nonlinear system can be efficiently and accurately modeled and predicted. In Refs. [73,98], the ANN model used 16 groups of variables as inputs to predict the dynamic characteristics of the 8-DOF vehicle model with active suspension and used the same algorithm structure to design the control system to control the active suspension system. Experiments showed that the control system based on the ANN algorithm can well work on the nonlinear dynamic characteristics presented by the damper and produce accurate control output. In another study [99], the ANN algorithm was applied to a fuzzy controller, which was controlled by a semi-active pneumatic seat suspension to mitigate vertical vibrations caused by rough road surface excitation. Five fuzzy controllers were optimized to deal with different road roughness situations, while the ANN model was used to predict the road conditions and to decide which specific controller to be activated. The final result showed that the system can reduce the vibration generated by the road roughness better. In other active vibration control studies [74], the ANN model was used in the control system to predict the mass of the seat and human body, to ensure that the control system can accurately output the control rate. The experimental results also showed that this control system using the neural network algorithm can effectively control the vibration under different road roughness conditions, and the robustness of the system was greatly improved. In Ref. [100], an online fast interval type 2 fuzzy neural network system was used to establish the model and to control the vibration of the semi-active seat suspension in combination with the sliding mode controller. The experimental results showed that this compound controller has better performance than the proportional integral derivative (PID) controller.

In the research of vibration control of vehicle seat system, how to model the seat-occupant system to accurately predict the dynamic characteristics of the human body or seating suspension system is usually a complicated nonlinear problem. The introduction of the neural network algorithms allows people to accurately fit a nonlinear problem. In Ref. [101], through training, the neural network model could well predict the dynamic characteristics of the 7-DOF vehicle chassis suspension model, and thus improved the accuracy of the control system. In Ref. [102], the neural network algorithm was used to build a human model, to simulate the dynamic characteristics of the human body, and finally to predict the head acceleration based on the vibration characteristics of the hand and seat. The average error between this prediction and the measurement was about 3.5%. In Ref. [103], the neural network algorithm was used to predict the synchronous acceleration based on the vibration of the pelvis. This application was used to build a human body dynamics model and evaluate the comfort of the seat based on this model. The experimental results also showed that the ANN algorithm has higher accuracy than other control algorithms in this study. In addition to the dynamic analysis of the human body and vehicles, neural network algorithms are also used to identify the roughness of the road surface. In Ref. [105], the neural network model was trained to recognize the roughness of the road through the vehicle dynamic signal recognition and parameter setting. This research allows control systems to have more and better decision-making capabilities.

The application of an artificial neural network algorithm greatly enriches the approach of seat vibration control. But in the above research, it was still limited to the single training target of head acceleration. The seat comfort predicted from the single target artificial neural network model may be different from that of the measurement.

Therefore, this chapter aims to establish an ANN model based on the 5-DOF biodynamic seating suspension system model data to predict the peak transmissibility ratio from the seat base to head which represents the ride comfort at the vibration frequency of about 4 Hz and the accuracy of the ANN model will be discussed as well.

6.2 Theoretical background

The backpropagation (BP) algorithm is a common method used in conjunction with optimization methods (such as gradient descent) to train artificial neural networks. This method calculates the gradient of the loss function for all weights and biases in the network. This gradient is fed back to the optimization method to update the weights and bias to minimize the loss function.

The BP algorithm requires a known output expected for each input value to calculate the gradient of the loss function. Therefore, it is generally regarded as a supervised learning method. The BP algorithm requires that the activation function of neurons is different. The input-output relationship of the BP network is essentially a mapping relationship, and this mapping is highly nonlinear. A BP neural network is usually composed of multiple layers, each layer has a different number of neurons, in general, the input data is the input layer, the layer following is called the hidden layer, and finally the data output layer; The connection between the neurons of the layer represents the weighting factors. To enable the network to simulate complex relationships, after multiplying the output of the neurons in the previous layer by the weight matrix to obtain the neurons in the next layer, it is necessary to perform a non-linear process on the value of each node through the "activation function".

The learning process of BP-ANN model consists of the forward propagation process and backpropagation process. In the forward propagation process, the input information passes through the hidden layer through the input layer, and is processed layer by layer and passed to the output layer. If the expected output value cannot be obtained at the output layer, the sum of the mean square error is taken as the objective function, which is transferred to the backpropagation, and the partial derivative of the objective function to the weight of each neuron is obtained layer by layer to form the target. The gradient of the function to the weight vector is used as the basis for modifying the weight. The learning of the network is completed during the weight modification process. When the error becomes small and reaches the expected value, the network learning ends.

The forward propagation can be calculated by the equation shown as:

$$S = \sum_{i=1}^{n} x_i w_i + b \tag{6.1}$$

where x_i represents input variables, w_i is weighting factor and b is bias

In the ANN model, the most commonly used activation functions for regression problems are PURELIN, LOGSIG, and TANSIG. The LOGSIG activation function can be written as:

$$logsig\ (S) = \frac{1}{1+e^{-s}} \tag{6.2}$$

In the back propagation, the total error can be calculated by the equation shown as:

$$C = \sqrt{\frac{\sum_{i}^{n} (y_i - S_i)^2}{n}} \tag{6.3}$$

where y_i is expected output value.

The process of the backpropagation is to find the partial derivative of the error function to the weighting factor ($\frac{\partial C}{\partial w_i}$) and bias values ($\frac{\partial C}{\partial b_i}$) to calculate the impact of both the values on the final output. When the result is close to 0, the current weight and deviation value are considered to be close to the optimal result. The network is considered to converge.

6.3 Predictive modeling using ANN

In this study, the ANN model was established to predict the vibration transmissibility with different design parameters settings. As shown in Table 4.2, a total of 26 groups of data were obtained from the 5-DOF biodynamic model to develop the ANN model. The input of the ANN model is the same as the encoded input variable used in the RSM model, namely the seat stiffness, seat damping, seat cushion stiffness, seat cushion damping coefficient, and seat mass. The peak vibration transmissibility Y at 4 Hz is also regarded as the target data for ANN model training. The original 26 groups of the RSM encoded input variable samples are used for training, validation, and testing subsets, where 20 groups for training, 3 groups for validation, and 3 groups for testing. The neural network toolbox of MATLAB has been used for the development of ANN models. In this study, the number of hidden layers and neurons is established by training a multi-layer back-propagation network (MLBP) and selecting the best network topology based on the minimization of the MSE. The design of the MLBP model initially is with four inputs, two hidden layers, and a linear output layer. The best topology architecture of the ANN model obtained after eradication experiments shows that the network topology in this study is expressed as 4: 6: 2: 1, where the numbers represent the number of neurons in the input layer, two hidden layers, and the output layer respectively. Table 6.1 shows the best structure and parameter usage of the developed ANN model. Neurons in all the hidden layers use the LOGSIG transfer function, while the output layer neurons use the linear PURELIN transfer function. The connections between neurons from different layers by weights and bias are shown in Table 6.2. The IW (1,1) represents the input weight matrix of size (6 × 4). LW (2,1) and LW (3,2) represent the layer weight matrix. To determine the optimal values of weights and biases, the network has been trained using the back-propagation method (BP) based on the Levenberg–Marquardt algorithm (LMA). Training is performed by adjusting the weights and deviations of the entire network to minimize the performance function (MSE). In the training phase, each neuron receives input signals, summarizes them using weights and deviations, and finally passes them as outputs after proper transformation.

Table 6.1 The structure of the multi-layers BP Neural networks

NN structure			
Network Type	Feed-forward backprop		
Number of layers	3		
Layers	1st	2nd	3rd
Number of neurons	6	2	1
Transfer function	LOGSIG	LOGSIG	PURELIN
Training function	Trainlm		
Adaption learning function	LearnGDM		
Performance function	MSE		

When the network error (MSE) becomes sufficiently small, training should end. In this study, training stops after 15 iterations. Fig 6.1 shows the mean square error of training, verification, and testing for the ANN model. In the training step, the MSE of the training is reaching a value of 10^{-16}. Also, as shown in Fig 6.2, the plots demonstrate that the training regression correlation coefficient is close to 0.99289, which means the training process is considered to have been completed, and the obtained optimal values of weights and deviations are summarized in Table 6.2.

Table 6.2 The optimal values of weights and biases obtained for ANN Model

iw{1,1}	**3.3854 -2.5049 1.7607 1.6845** **-2.3503 -2.9912 1.1767 -1.5631** **2.5321 0.59918 1.9949 -2.2729** **-1.5316 4.0981 -0.27832 1.2929** **2.1295 -0.36139 4.4552 0.49997** **-1.6905 -0.19127 -1.4105 0.14724**
b{1}	-3.3045 2.6423 -1.4535 -1.153 2.6027 -6.6051
lw{2,1}	2.0433 1.3558 0.32533 4.3262 2.9557 0.2389; 2.6095 1.0275 2.7991 -1.4618 1.7928 2.3404
b{2}	-4.823

	-3.4542
lw{3,2}	1.2424 0.90675
b{3}	-0.96276

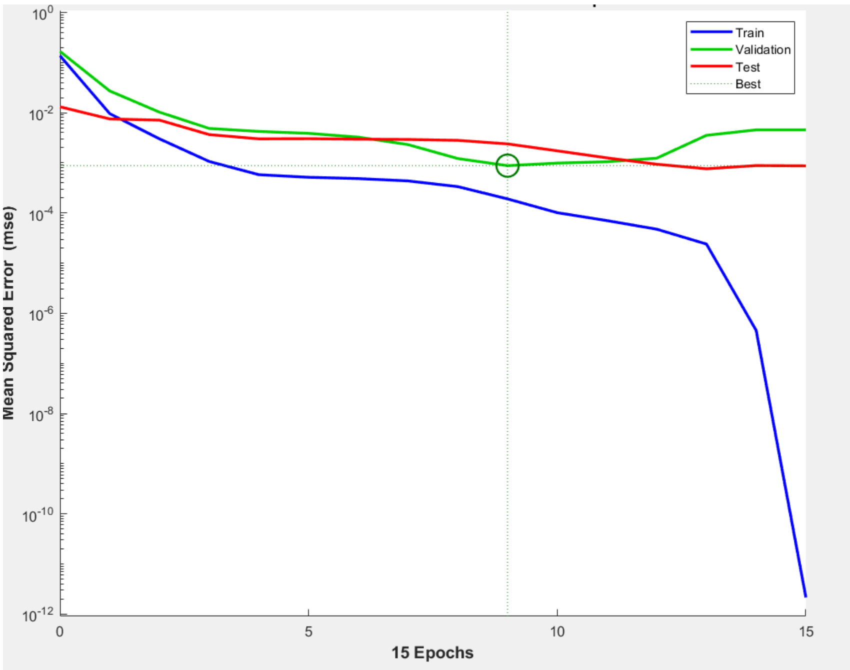

Figure 6.1 Training performance for the ANN model.

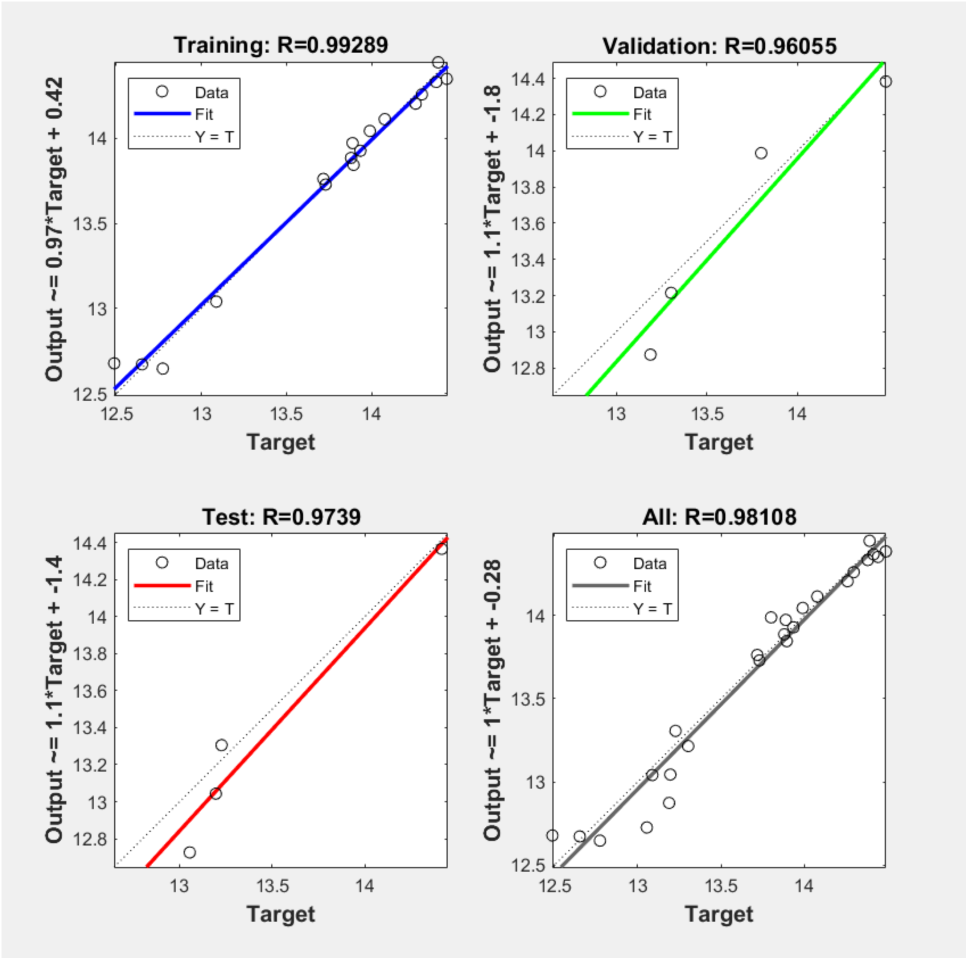

Figure 6.2 The regression performance of the ANN model.

6.4 Results and discussion

According to the data in Table 6.3, compared with the original response factor Y calculated from the frequency response of the 5-DOF bio-dynamic model, the prediction result of the RSM model has the smallest root mean square error (RMSE) value of only 0.53%, while the results of the LRM and ANN model compared with the original response factor, show their RMSEs of 1.335% and 1.279% which are greater than that of the RSM model. Therefore, it can be considered that the RSM model is the most accurate among the three prediction models and the predictive results of the RSM model are more accurate for the seating suspension system than the other prediction models. The prediction accuracy of the LRM model is between that of the RSM and ANN models. Although the accuracy of the ANN model is relatively low, the ANN model has extremely high capabilities compared with the complex mathematical or theoretical models of the first two, the rapid modeling ability of the ANN algorithm is one of the certain advantages.

Table 6.3 The results of different models and their root mean square error values

No.	***Y*** **Response factor**	***Y*** **RSM**	***Y*** **LRM**	***Y*** **ANN**
1	196.2549	197.1140185	200.403661	196.552
2	192.5295	193.7143427	192.0552506	192.5295
3	200.0782	200.9173007	198.612649	200.0782
4	185.9323	187.2773091	190.302025	185.9323
5	187.5914	185.9642234	189.172516	187.5914
6	184.0336	182.9329286	181.063936	184.0336
7	191.3823	189.912378	187.4325284	191.3823
8	177.8676	176.9237836	179.3617348	177.8676
9	198.0127	196.7474713	199.317924	198.0127
10	194.3013	193.4956115	190.9924	192.3714
11	200.6501	199.4837038	197.5317812	212.0402
12	186.5929	186.0351419	189.2440436	186.5929
13	184.2073	185.1104466	188.1176834	184.2073
14	180.76	182.2265108	180.0319898	180.76
15	186.8826	188.0170243	186.3825648	186.9837

16	173.8627	175.2322005	178.3346576	173.8627
17	195.1302	196.4154061	195.0321179	195.1302
18	186.1888	184.8144564	183.4727139	181.7212
19	191.792	192.0822915	190.4399172	191.792
20	190.018	189.6123927	187.9806346	190.018
21	194.8984	194.5985803	197.0932964	194.8984
22	178.9147	179.0906508	181.4842221	178.9147
23	190.8515	191.5885554	189.9537779	190.8515
24	190.9537	190.092613	188.464244	187.0767
25	190.625	190.7464832	189.2082781	189.2248
26	190.625	190.7464832	189.2082781	189.2248
RMS Error		0.53% (<1%)	1.335% (>1%)	1.279% (>1%)

According to the data shown in Table 6.4, with the same optimal input parameter combination of (10000N.m 5000 Ns/m, 10000N/m 5000 Ns/m), the prediction results of the neural network model are very close to the prediction results of the RSM model and the LRM model. The prediction results of the three models are 13.25, 13.2, and 13.36 respectively. The differences are less than 2%. According to the results in Table 6.3, the RSM model has the highest prediction accuracy, followed by LRM. However, in the comparison of optimization results, the predicted peak transmissibility calculated from the ANN model is closer to the maximum peak transmissibility calculated from the RSM model, showing that the ANN model is more reliable for the optimal target prediction than the LRM model. Besides, the ANN model has more powerful capabilities than the LRM model on the system nonlinearity. Therefore, it can be concluded that the RSM model and the ANN model with nonlinear processing capabilities have more accurate predictions than the LRM model in terms of design parameter optimization.

As shown in Table 6.3, although the final predicted values of the transmissibility based on these three methods are different, the trends of the optimal output variables are the same. Reducing the stiffness and damping coefficient of the seat while reducing the stiffness and damping coefficient of the seat cushion as well can make the seat system obtain minimum vibration transmissibility peak, which means increase the riding comfort.

Table 6.4 The comparison of the optimization results with different prediction methods

Method	K_1 **(N/m)**	C_1 **(Ns/m)**	K_{2c} **(N/m)**	C_{2c} **(Ns/m)**	Y
RSM	10000	5000	10000	5000	13.2
Linear regression	10000	5000	10000	5000	13.36
ANN	10000	5000	10000	5000	13.25

6.5 Conclusions

The ANN algorithm provides a powerful framework for solving multiple regression, nonlinear and linear problems. In this chapter, the well-trained ANN model is shown to be able to well simulate the dynamic characteristics of the 5-DOF occupant seating suspension system model. In the vibration frequency range of about 4 Hz, the ANN model can accurately predict the peak transmissibility from the seat base to the head. Compared with the peak transmissibility predicted from the 5-DOF biodynamic occupant seating suspension system model. Although the prediction accuracy of the ANN model is worse than that of the RSM model and the LRM model, the ANN model simulation is reliable. Moreover, the optimization results of the ANN model and the RSM model are closer, which also shows that the ANN model has an advantage over the LRM model in dealing with nonlinear problems. Also, the ANN model is more convenient to apply than the other models in terms of modeling.

7 The Mechanical Design of Active Seat Suspension System

7.1 Introduction

As a vibration isolation device, vehicle seat systems, especially commercial vehicle seats, should protect the human body from the adverse effect of low-frequency vibration. Traditional passive seat suspension systems can only be effective against the vibration of a certain specific frequency, and generally cannot work perfectly with too complicated road conditions, resulting in poor vibration isolation effects. Semi-active vibration isolation measures can mitigate the vibration in a small range of frequency by adjusting the stiffness and damping of the equipment so that a seating system with the semi-active seat suspension can cope with more complicated road conditions than passive vibration isolation. But overall, the working frequency range of the semi-active seat suspension is close to that of the passive vibration isolation, therefore, the improvement is limited. Active vibration isolation equipment is recognized as the most ideal vibration control solution for commercial vehicle seats. The active seat suspension uses an actuator to generate a force or moment that is opposite to the vibration direction to achieve a vibration cancellation effect.

The research on active seat suspension mainly includes three directions, hydraulic, pneumatic, and electric. As shown in Fig. 7.1, in Ref. [56], the vibration control system uses a hydraulic servo system to generate a compensation force to mitigate vibrations. The advantage of the hydraulic system is that it can generate a huge actuation force, so the loading capacity of the seat system will be very large, which increases the scope of application to some extent. However, the disadvantages of the hydraulic system are also obvious, including the bulky system, the need for a special hydraulic pressure generating mechanism, high processing accuracy requirements, and slow response speed. Therefore, the practical application possibility of hydraulic active seat suspension is very limited.

Figure 7.1 Contents page from paper Active Vibration Control System for the Driver's Seat for Off-Road Vehicles. *Veh. Syst. Dyn.* 1991, *20*, 57–78. Stein, G.J.; Ballo, I.

<Image removed due to copyright restrictions>

Figure 7.1 Schematic diagram of the hydraulic active seat suspension system [56].

The use of pneumatic springs gives an alternative to the actuator of the active seat suspension. In Fig 7.2, a pneumatic spring system with a special proportional valve is used in the seat system to generate compensation force to control vibrations [52]. According to the experimental results, the system has good vibration isolation performance for low-frequency vibration. The advantage of the pneumatic system is its inherently good vibration isolation performance. After all, most of the passive vibration isolation seats used in automobiles are pneumatically driven for their height adjustment. Most commercial vehicles have pneumatic pressure generation mechanisms, so no additional equipment is required if the pneumatical active seat suspension is applied. Pneumatic spring technology has been developed over decades, so it is reliable and has no technical application limitation. But the problem of pneumatic springs cannot be ignored. The noise of the pneumatic system, especially during the inflation and deflation stage, cannot be avoided. Long-term use may cause other discomfort effects.

The accuracy of pneumatic control is another problem. Because of the compressibility of the gas, it is difficult to achieve precise control, and the pneumatic is affected by temperature.

Figure 7.2 Contents page from paper The vibration damping effectiveness of an active seat suspension system and its robustness to varying mass loading. *J. Sound Vib.* 2010, *329*, 3898–3914. Maciejewski, I.; Meyer, L.; Krzyżyński, T.

<Image removed due to copyright restrictions>

Figure 7.2 Pneumatic active seat suspension system [52].

Therefore, electric motors that have advantages of rapid response and accurate control become a better choice for an active seat suspension system. It can be seen from Fig 7.3 that two linear motors were used as two actuators in an active seat suspension system [63]. The very high motion accuracy of the linear motor can well suppress vibrations of different amplitudes. However, due to the limitation of the size, the output of the linear motor is greatly restricted. Therefore, it is impossible to have a large loading capacity with a small size linear motor. Therefore, in Ref. [58], an active seat suspension that combines a traditional motor, gearbox, and scissor structure was developed (Fig. 7.4). Compared with the weakness of linear motors, the structure of traditional motor acceleration and gearboxes can increase motor output torque and reduce electrical energy consumption.

Figure 7.3 Contents page from paper Adaptive control of an active seat for occupant vibration reduction. *J. Sound Vib.* 2015, *349*, 39–55. Gan, Z.; Hillis, A.J.; Darling, J.

<Image removed due to copyright restrictions>

Figure 7.3 The active seat suspension with linear motors [63].

Figure 7.4 Contents page from paper Active control of an innovative seat suspension system with acceleration measurement based friction estimation. *J. Sound Vib.* 2016, *384*, 28–44. Ning, D.; Sun, S.; Li, H.; Du, H.; Li, W.

<Image removed due to copyright restrictions>

Figure 7.4 The active seat suspension system with a traditional motor and gearbox [58].

In summary, the research and development of active seat suspension are very popular, but so far, the seat system with active suspension still has the problem of bulky and complex structure. Therefore, how to develop a seat with a simple structure, small size, and high practicability is the main reason for this research. In this chapter, the mechanical design principles of the active seat suspension and the corresponding calculations will be explained in detail.

7.2 Active seat suspension design

As a main vibration isolation equipment, the seat system of a commercial vehicle should have a reasonable size to be adapted to the small cabin environment. In addition, excessive power consumption will also disadvantage the design of the seat itself. Therefore, a compact seat system with active suspension is necessary. Timing belt and pulley is widely used in various equipment as a kind of power transmission mechanisms, such as the power transmission structure of machine tools, electric tools, and the synchronous belt used in automobile engines. The timing belt can transmit power smoothly, and due to the material characteristics of the belt itself, it also can reduce vibration and noise transmission. For the active suspension system of commercial vehicle seats, this feature allows the vibration or shock generated by the motor and gear to be almost completely damped out by the drive belt and will not be transmitted to the seat system. The lower working noise greatly enhances the comfort of the seat without any additional impact. The transmission accuracy of the timing belt is very high because there is no transmission slip. It also has a constant transmission ratio, so for the vibration control system, the application of the timing belt can reduce the vibration control failure caused by the transmission error. The transmission efficiency of the timing belt is high, which can reach 98%. Such a high transmission efficiency can effectively reduce energy consumption and make the application of small motors possible. The transmission power of the timing belt can be as high as several hundred kilowatts, which also increases the load capacity of the commercial vehicle seat active suspension.

Therefore, as shown in Fig.7.5 (a), first, the motor drives the reducer, and the reducer drives the small pulley to rotate. The torque will be transmitted to the timing belt through the small pulley, and the belt will drive the large pulley; at the same time, since the ratio of the pulley diameter is 1:2, the torque is enlarged during the delivery process. Finally, the large pulley drives the X-shape structure to rotate, and this rotation is transformed into the up and down movement of the seat through the X-shape structure to offset the displacement caused by the vibration. Also, it can be seen from Fig.7.5 (b), a CATIA design shows a compact active seat suspension system combining the drive motor and speed reduction gearbox with a timing belt – pulley transmission mechanism is more in line with customers' requirements for improving their ride comfort. The suspension is driven by a motor and a speed reducer gearbox, and the amplified torque is transmitted to the centre axis of the scissor-like seat structure by the timing belt and move the seat frame up and down to counteract the vibration.

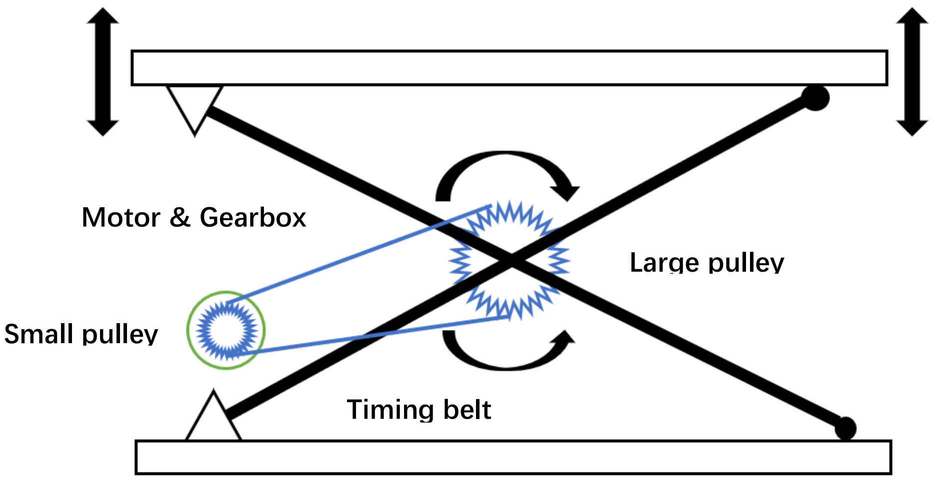

(a)

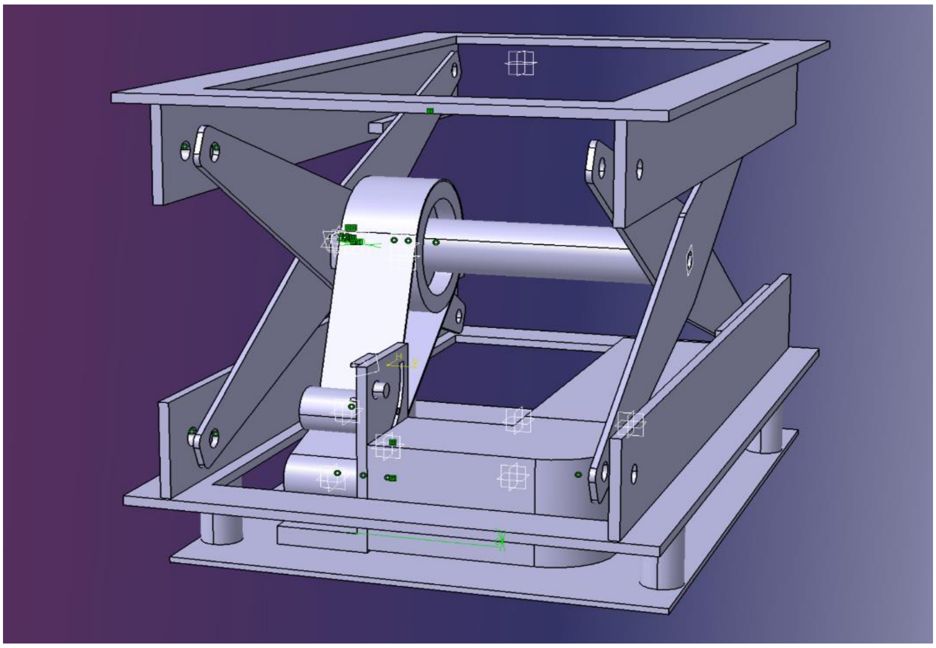

(b)

Figure 7.5 The design drawing of the active seat suspension (a) schematic diagram (b) CATIA design diagram.

The passive seat system with an X-shape scissor-like frame structure is very commonly used on commercial vehicles. In this study, an IVECO truck seat (A6800-16 RH) was used as the baseline for the design modification to be able to implement the active seat suspension system to reduce vibration. According to the general requirement of the seat design, 80 kg is used as the targeted payload, so the magnitude of the compensation torque required of 79.29 Nm to reduce vibration can be calculated from Eq. 7.1 [61]

$$T = \frac{F}{2}W = \frac{F}{2}\sqrt{L^2 - H^2} \qquad (7.1)$$

where T is torque as shown in Fig. 7.6; L=350mm, H=195mm.

Table 7.1 The parameters of the active seating suspension system

Motor (60CST-M0193)

Rated Power (W)	600
Rated Speed (rpm)	3000
Output torque (Nm)	1.91
Gearbox (Planet Gear)	
Reduction Ratio	1:50
Timing belt	
Pulley diameter (small) (mm)	50
Pulley diameter (large) (mm)	100
Belt mode	14m
Width (mm)	50
Round Pitch (mm)	260
Max power transmission (kW)	60

As the main power source, the motor is selected to generate a torque that fully compensates the force demanded active vibration control of the seat. A 600W AC motor xdf600s together with the gearbox was selected to generate the torque and the resistance force through the X-shape scissor-like frame. According to Table 7.1, it can be seen that the motor can generate 1.91Nm of torque at 3000 revolutions. With a 1:50 gearbox reducer, the final output torque can reach 97Nm. According to the calculation result of Eq 7.1, it can be known that the power combination can meet the design needs. The 90-angle speed reducer gearbox can make full use of the small space inside the seat system, and place the motor vertically to minimize the space occupation.

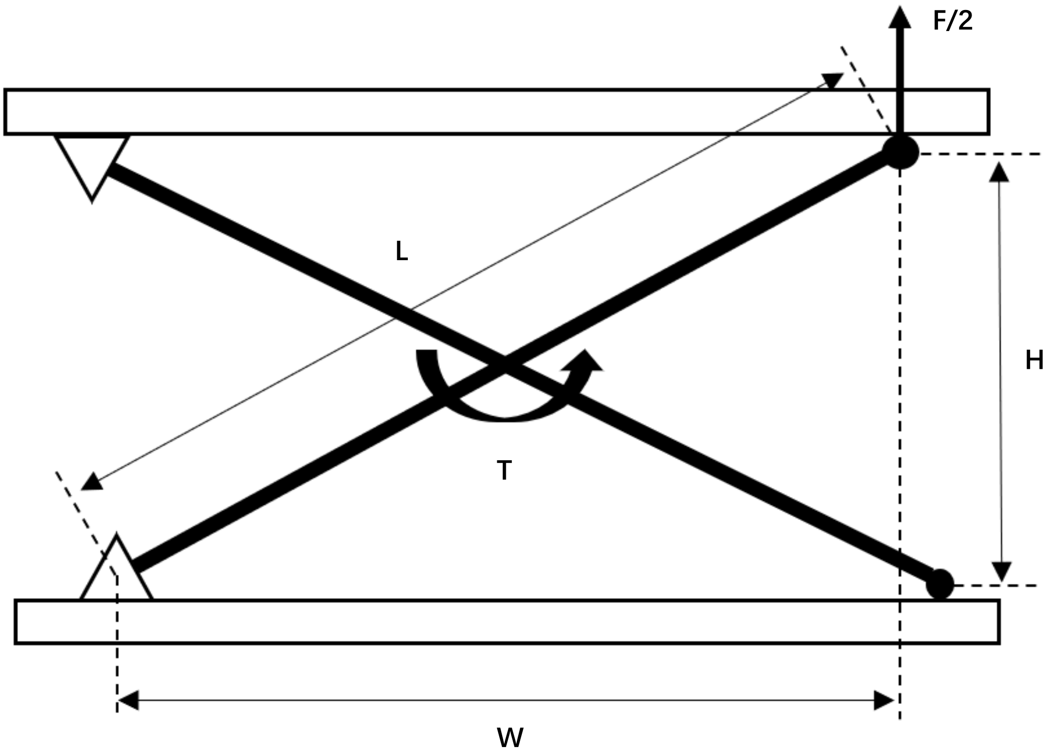

Figure 7.6 Force analysis of seat suspension system.

The selection of the timing belt can be done by looking up the specific data table and calculation. According to Eq. 7.2, the maximum power that the timing belt-pulley mechanism needs to transmit can be calculated

$$P_d = \frac{T \times n(RPM)}{9550} \tag{7.2}$$

where *n* is the rotate speed of the motor.

The belt model selection can be done by looking up the table. As can be seen in Fig. 7.7 the vertical axis represents the maximum speed, and the horizontal axis represents the maximum transmission power. According to the maximum transmission power requirement of 30 kW, the final belt model is determined to be 14m. Another advantage of using a timing belt is that the transmission ratio can be enlarged by adjusting the size of the pulley. In the design, the size of the pulley is set to 50mm and 100mm, so that the torque can be doubled during transmission and increase the payload.

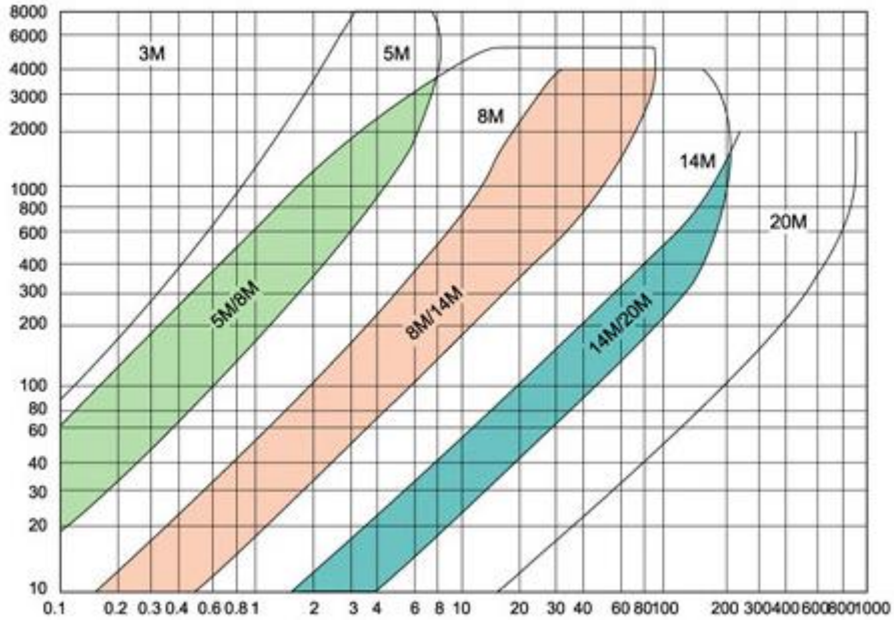

Figure 7.7 Timing belt selection table.

There are two main aspects to the modification of the seat. One is to remove the original structure, such as seat pneumatic springs, shock absorbers, and horizontal shafts.

To ensure that the package room/space of the seat meets the requirements, the IEVCO truck seat will undergo a series of modifications. First, the pneumatic springs and shock absorbers originally used in the seat will be removed. As shown in Fig. 7.8, the L-shape mount block is designed to support the motor and speed reduction gearbox, and the bottom is fixed on a 5mm thick steel plate. At the same time, the seat itself is also supported by four columns. The column itself is also fixed on the same steel plate. The belt tensioning system composed of springs and idle pulley will also be fixed onto the L-shape mount to provide additional belt tension to ensure the tightness of the belt so that the belt will not be loosened or slackened to negatively affect the power transmission. Also, due to the X-shape scissor-like structure of the seat, the trajectory or arrangement of the belt pulley mechanism will affect the belt tension of the timing belt system. Therefore, a tensioning mechanism or tensioner pulley also ensures that the timing belt does not have the tooth skipping or slipping due to its tension changes.

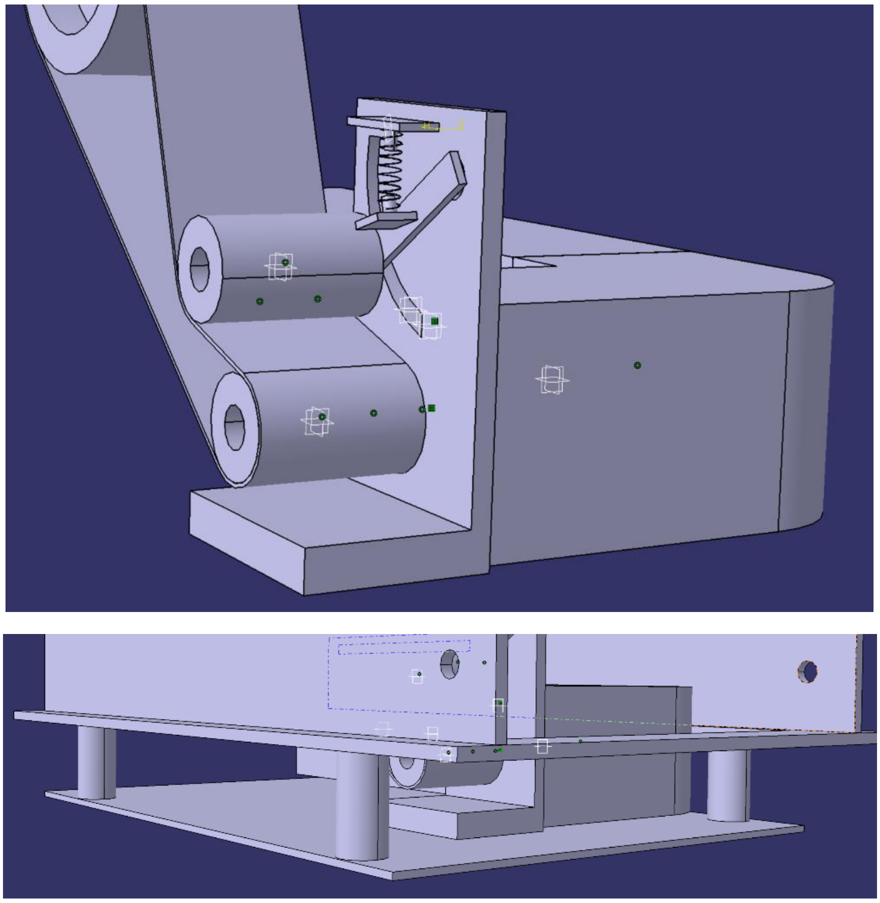

Figure 7.8 The L-shape mount block design and the seat frame bottom support design.

7.3 Summary

As currently the most efficient vibration isolation equipment, vehicle seats with active suspension can better protect people from low-frequency vibrations than the other methods of vibration mitigation. In summary, this design of the active seat suspension has the following three advantages:

1. The seat frame structure is compact, which can pack all the components of the seat system within the seat frame structure and make the implementation feasible. The active seat suspension system with the same size as the existing seat is essential for design package and implementation.
2. The timing belt can transmit power smoothly and quietly. Meanwhile, by adjusting

the size of the input pulley and output pulley to further amplify the torque output and increase the payload.

3. Compared with the other mechanical connection, the timing belt pulley transmission system can reduce additional vibration and noise caused by mechanical transmission.

8 A 7-DOF Vehicle-Seating Suspension System Model for validating the 5-DOF Quarter Car RSM Model

8.1 Introduction

In the research of vehicle seat vibration mitigation, how to replay the real working conditions of the seat system is an essential step that people should carefully consider. No matter how excellent the vibration control performance of the vehicle seat system is, if the vehicle seat system cannot be studied in the vibration environment of the whole vehicle, the vibration control performance of the seat system cannot be verified. In reality, simulation methods of the seating suspension system, vehicle suspension system are applied under random road excitations to reproduce the seat vibration environment in addition to vehicle road tests. In the research [1], the mass-damper-spring model of the whole vehicle was established to evaluate the vibration control capability of the vehicle suspension which was optimized by the Artificial Bee Colony algorithm. The artificial bee colony algorithm (ABC) is an optimization algorithm based on the intelligent foraging behaviour of honey bee swarm, proposed by Derviş Karaboğa (Erciyes University) in 2005. However, in this study, the occupant-seat system was simplified into a single block with mass, spring, and damper, so the dynamic characteristics of the human body under vibration excitation was not able to be predicted.

In Ref. [2], an occupant-seat model combined with a quarter vehicle model was simulated for design analysis of the passive seat system. The study fully considered the seat structure itself and the dynamic characteristics of the human body. In Ref. [3], the half-vehicle model was simulated, considering the vibration characteristics of the half vehicle in the vertical and pitching directions and developing corresponding design analysis. However, the road surface excitation used in these researches were limited to some regular sinusoidal signal inputs, which cannot effectively reflect the real road surface.

Therefore, the main purpose of this chapter is to verify the optimal results of the response surface method (RSM) modeling in the previous chapter through simulation results of a 7-DOF vehicle-seating suspension system model which combines the five degrees of freedom (5-DOF) seating suspension system combined with a quarter vehicle suspension system under random road excitations. As mentioned in the previous chapters and literature, the pitch and roll modes do cause discomfort of the passengers, the vertical heave around 4 Hz causes most discomfort of the passengers, and it is studied in the research in this thesis.

8.2 Simulation design

The verification process will be carried out through the simulations in the time domain and frequency domain respectively. In the frequency domain, under different design parameter settings, the transmissibility from head to the seat base and SEAT values will be calculated separately and compared with the 5-DOF RSM simulation results. In the time domain, the model that replay different road roughness through the white noise and ISO road power spectral density (PSD) will be applied to generate the random vibration excitation in MATLAB/Simulink. A 7-DOF model combining the 5-DOF seating suspension system with a quarter vehicle suspension system will be used to simulate the seating suspension system vibration mitigation performance under random road excitations. The results will be used to verify the RSM results of the 5-DOF seating suspension system.

8.2.1 Frequency domain analysis and simulation

A 7-DOF mass-spring-dashpot lumped parameter model combining the 5-DOF seating suspension system with a quarter vehicle suspension system has been established to predict the vibration control performance of the seating suspension system in the whole vehicle vibration environment. Like the method introduced in Chapter 3, Fig.8.1 shows the details of the 7-DOF mass-spring-dashpot lumped parameter model including its components.

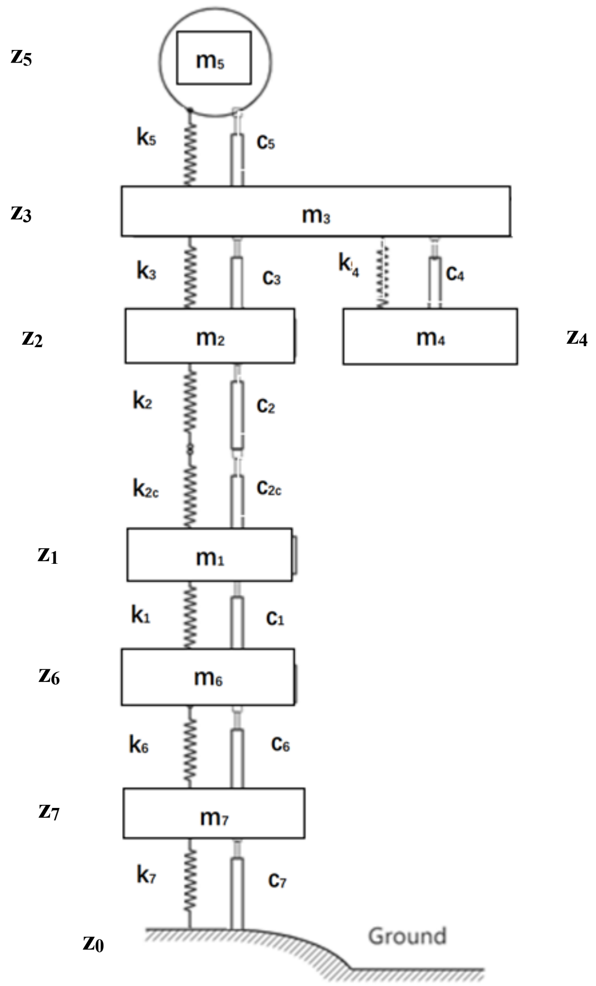

Figure 8.1 7-DOF model combining seat, quarter vehicle, and the human body.

The added m_6 represents the quarter vehicle mass; k_6 represents the stiffness of the vehicle suspension spring; and c_6 represents the damping coefficient of the suspension shock absorber. In addition, m_7 represents the mass of the wheel and tire, k_7 represents the stiffness of the tire, and c_7 represents the damping coefficient of the wheel and tire. m_1-m_5, k_1-k_5, c_1-c_5, c_{2c}, k_{2c} are defined in the previous chapter.

The specific model parameters of the 7-DOF system are listed in Table 8.1. The motion equations of the 7-DOF system are given by:

$$\begin{cases} m_7 \cdot \ddot{z}_7 + c_7 \cdot (\dot{z}_7 - \dot{z}_0) + k_7 \cdot (z_7 - z_0) + c_6 \cdot (\dot{z}_7 - \dot{z}_6) + k_6 \cdot (z_7 - z_6) = 0 \\ m_6 \cdot \ddot{z}_6 + c_1 \cdot (\dot{z}_6 - \dot{z}_1) + k_1 \cdot (z_6 - z_1) + c_6 \cdot (\dot{z}_6 - \dot{z}_7) + k_6 \cdot (z_6 - z_7) = 0 \\ m_5 \cdot \ddot{x}_5 + c_5 \cdot (\dot{x}_5 - \dot{x}_3) + k_5 \cdot (x_5 - x_3) = 0 \\ m_4 \cdot \ddot{x}_4 + c_4 \cdot (\dot{x}_4 - \dot{x}_3) + k_4 \cdot (x_4 - x_3) = 0 \\ m_3 \cdot \ddot{x}_3 + c_4 \cdot (\dot{x}_3 - \dot{x}_4) + k_4 \cdot (x_3 - x_4) + c_5 \cdot (\dot{x}_3 - \dot{x}_5) + k_5 \cdot (x_3 - x_5) + c_3 \cdot (\dot{x}_3 - \dot{x}_2) + k_3 \cdot (x_3 - x_2) = 0 \\ m_2 \cdot \ddot{x}_2 + c_3 \cdot (\dot{x}_2 - \dot{x}_3) + k_3 \cdot (x_2 - x_3) + \frac{c_2 \cdot c_{2c}}{c_2 + c_{2c}} \cdot (\dot{x}_2 - \dot{x}_1) + \frac{k_2 \cdot k_{2c}}{k_2 + k_{2c}} \cdot (x_2 - x_1) = 0 \\ m_1 \cdot \ddot{x}_1 + c_1 \cdot (\dot{x}_1 - \dot{x}_6) + k_1 \cdot (x_1 - x_6) + \frac{c_2 \cdot c_{2c}}{c_2 + c_{2c}} \cdot (\dot{x}_1 - \dot{x}_2) + \frac{k_2 \cdot k_{2c}}{k_2 + k_{2c}} \cdot (x_1 - x_2) = 0 \end{cases} \tag{8.1}$$

From Equation 8.1, the mass and stiffness matrixes of $[M]$ and $[K]$ are:

$$[M] = \begin{bmatrix} m_1 & 0 & 0 & 0 & 0 & 0 & 0 \\ 0 & m_2 & 0 & 0 & 0 & 0 & 0 \\ 0 & 0 & m_3 & 0 & 0 & 0 & 0 \\ 0 & 0 & 0 & m_4 & 0 & 0 & 0 \\ 0 & 0 & 0 & 0 & m_5 & 0 & 0 \\ 0 & 0 & 0 & 0 & 0 & m_6 & 0 \\ 0 & 0 & 0 & 0 & 0 & 0 & m_7 \end{bmatrix}$$

$$[K] = \begin{bmatrix} k_1 + \frac{k_2 \cdot k_{2c}}{k_2 + k_{2c}} & -\frac{k_2 \cdot k_{2c}}{k_2 + k_{2c}} & 0 & 0 & 0 & -k_1 & 0 \\ -\frac{k_2 \cdot k_{2c}}{k_2 + k_{2c}} & k_3 + \frac{k_2 \cdot k_{2c}}{k_2 + k_{2c}} & -k_3 & 0 & 0 & 0 & 0 \\ 0 & -k_3 & k_3 + k_4 + k_5 & -k_4 & -k_5 & 0 & 0 \\ 0 & 0 & -k_4 & k_4 & 0 & 0 & 0 \\ 0 & 0 & -k_5 & 0 & k_5 & 0 & 0 \\ -k_1 & 0 & 0 & 0 & 0 & k_1 + k_6 & -k_6 \\ 0 & 0 & 0 & 0 & 0 & -k_6 & k_6 + k_7 \end{bmatrix}$$

$$
[C]=\begin{bmatrix}
c_1+\dfrac{c_2\cdot c_{2c}}{c_2+c_{2c}} & -\dfrac{c_2\cdot c_{2c}}{c_2+c_{2c}} & 0 & 0 & 0 & -c_1 & 0\\
-\dfrac{c_2\cdot c_{2c}}{c_2+c_{2c}} & c_3+\dfrac{c_2\cdot c_{2c}}{c_2+c_{2c}} & -c_3 & 0 & 0 & 0 & 0\\
0 & -c_3 & c_3+c_4+c_5 & -c_4 & -c_5 & 0 & 0\\
0 & 0 & -c_4 & c_4 & 0 & 0 & 0\\
0 & 0 & -c_5 & 0 & c_5 & 0 & 0\\
-c_1 & 0 & 0 & 0 & 0 & c_1+c_6 & -c_6\\
0 & 0 & 0 & 0 & 0 & -c_6 & c_6+c_7
\end{bmatrix} \tag{8.2}
$$

$$
[M]\{\ddot{z}\}+[C]\{\dot{z}\}+[K]\{z\}=\begin{Bmatrix} 0\\ 0\\ 0\\ 0\\ 0\\ 0\\ c_7\cdot\dot{z}_0+k_7\cdot z_0 \end{Bmatrix} \tag{8.3}
$$

Fourier transform is applied to Equation (8.3), leading to

$$
\left([K]-[M]\cdot\omega^2+i\cdot\omega\cdot[C]\right)\begin{Bmatrix} Z_1\\ Z_2\\ Z_3\\ Z_4\\ Z_5\\ Z_6\\ Z_7 \end{Bmatrix}=\begin{Bmatrix} 0\\ 0\\ 0\\ 0\\ 0\\ 0\\ c_7\cdot i\cdot\omega+k_7 \end{Bmatrix}\cdot Z_0
$$

and

$$\begin{Bmatrix} \frac{Z_1}{Z_0} \\ \frac{Z_2}{Z_0} \\ \frac{Z_3}{Z_0} \\ \frac{Z_4}{Z_0} \\ \frac{Z_5}{Z_0} \\ \frac{Z_6}{Z_0} \\ \frac{Z_7}{Z_0} \end{Bmatrix} = \left([K]-[M]\cdot\omega^2+i\cdot\omega\cdot[C]\right)^{-1}\cdot\begin{Bmatrix} 0 \\ 0 \\ 0 \\ 0 \\ 0 \\ 0 \\ c_7\cdot i\cdot\omega+k_7 \end{Bmatrix} \tag{8.4}$$

As introduced in Chapter 3, the Laplace transform is applied to Equation (8.3). When $s=i\omega$, the Laplace transform becomes the Fourier transform. Equation (8.4) is derived from Equation (8.3) in the frequency domain as the results of the Fourier transform. The displacement transmissibility ratios of the seven lumped mass in the model (z_1/z_0, z_2/z_0, z_3/z_0, z_4/z_0, z_5/z_0, z_6/z_0, and z_7/z_0) can be calculated from Equation (8.4) where

$$\frac{z_i}{z_0}=\frac{Z_i\cdot e^{i\cdot\omega}}{Z_0\cdot e^{i\cdot\omega}}=\frac{Z_i}{Z_0} \quad (i=1,2,3,4,5,6,7)$$

Table 8.1 The parameters of 7-DOF model

Parameter	Value
k_1	24854.31
k_2	28723.1
k_{2c}	14794.2
k_3	4587.43
k_4	159537.93

k_5	2857.13
k_6	26000
k_7	130000
c_1	8041.5
c_2	3848.75
c_{2c}	2024.2
c_3	195.425
c_4	758.5
c_5	4.59
c_6	520
c_7	264.7
m_1	13
m_2	25.15
m_3	20.92
m_4	3.3
m_5	4.59
m_6	40
m_7	264.7

The parameters of the 7-DOF mass-spring-dashpot lumped parameter system are listed in Table 8.1 The ratio of Z_1/Z_0 is plotted in Figure 8.2 where the first peak frequency is identified as 1.21 Hz and the peak value is identified as 12.77 (dB). The reason for Figure 8.2 having two resonant peaks instead of three resonant peaks is the seat may happen to be the node of the third resonant peak mode. The two resonant peak frequencies are close to the natural resonant frequencies of the vehicle suspension bouncing and hopping modes. This may be caused by the damping and stiffness of the seating suspension system are much larger than those of the vehicle suspension system. The modes of the seating suspension system are hidden. Therefore, vehicle suspension bouncing mode dominates the ride comfort which has common senses and coincides with the conclusions from the literature. The MATLAB code for solving Equation (8.4) is given in Figure A1 in Appendix A. The first section of the code in Figure A1 is to apply numerical values to the mass, spring stiffness, and damping coefficients of the 7-DOF biodynamic vehicle and seating suspension system. The second section is to define the matrices of mass, stiffness, and damping of the 7-DOF system. The third section of the code is to calculate the RHS matrices of Equation (8.4). The last section of the code is to plot the curves of the calculated transmissibility ratio of the seven mass points (7-DOF). The peak frequencies f_1-f_7 and corresponding amplitude ratios Z_1/Z_0 - Z_7/Z_0 of the frequency responses of the mass points m_1-m_7 are listed in Table 8.2.

Table 8.2 The peak transmissibility ratio and corresponding peak frequency

	Frequency (Hz)	**Transmissibility ratio (dB)**
Z_1/Z_0	1.21	12.7677
Z_2/Z_0	1.21	14.129
Z_3/Z_0	1.22	17.5874
Z_4/Z_0	1.22	17.598
Z_5/Z_0	1.23	18.4728
Z_6/Z_0	1.21	12.7449
Z_7/Z_0	9.69	8.3821

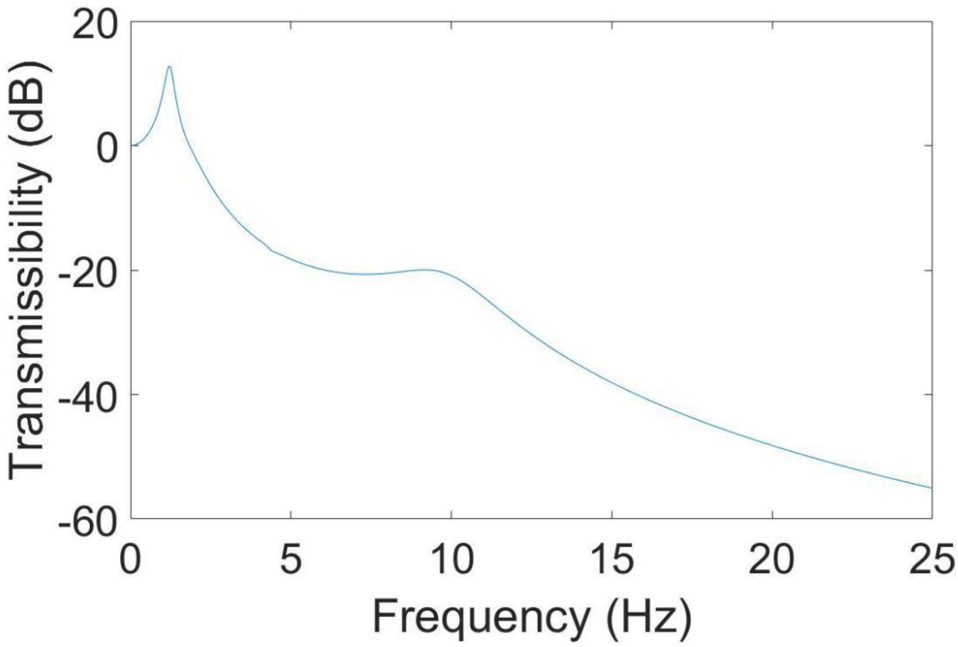

Figure 8.2 The transmissibility ratio from the seat to floor is calculated by the frequency response method (z1/z0).

As mentioned in the previous chapters, the seat effective amplitude transmissibility (SEAT) value is used to evaluate vibration isolation performance and comfort. $G_5(f)$ is given by

$$G_5(f)=G_{\dot{q}}(f)\cdot\left|H_{\dot{q}5}(f)\right|^2 \tag{8.5}$$

where $G_{\dot{q}}(f)$ is the velocity auto-power spectrum density of the white noise random road profile; $H_{\dot{q}5}(f)$ is the velocity frequency response function between the road profile excitation and the driver's head. $G_1(f)$ is given by

$$G_1(f)=G_{\dot{q}}(f)\cdot\left|H_{\dot{q}1}(f)\right|^2 \tag{8.6}$$

where $H_{\dot{q}1}(f)$ is the velocity frequency response function between the road profile excitation and the seat. Equation (8.5) is then given by

$$SEAT\ (\%)=\sqrt{\frac{\int G_{\dot{q}}(f)\cdot\left|H_{\dot{q}5}(f)\right|^2\cdot W_k^2(f)\mathrm{d}f}{\int G_{\dot{q}}(f)\cdot\left|H_{\dot{q}1}(f)\right|^2\cdot W_k^2(f)\mathrm{d}f}}\times 100\% \tag{8.7}$$

where $H_{\dot{q}5}(f)=\dfrac{Z_5}{Z_0}$; $H_{\dot{q}1}(f)=\dfrac{Z_1}{Z_0}$ which can be calculated from Equation (8.4).

8.2.2 Time domain

To solve Equation (8.1) in the time domain by the integration method, Equation (8.1) is written as

$$\begin{cases}
\ddot{z}_7=-\dfrac{c_7+c_6}{m_7}\cdot\dot{z}_7-\dfrac{k_7+k_6}{m_7}\cdot z_7+\dfrac{c_7}{m_7}\cdot\dot{z}_0+\dfrac{k_7}{m_7}\cdot z_0+\dfrac{c_6}{m_7}\cdot\dot{z}_6+\dfrac{k_6}{m_7}\cdot z_6\\
\ddot{z}_6=-\dfrac{c_1+c_6}{m_6}\cdot\dot{z}_6-\dfrac{k_1+k_6}{m_6}\cdot z_6+\dfrac{c_1}{m_6}\cdot\dot{z}_1+\dfrac{k_1}{m_6}\cdot z_1+\dfrac{c_6}{m_6}\cdot\dot{z}_7+\dfrac{k_6}{m_6}\cdot z_7\\
\ddot{z}_5=-\dfrac{c_5}{m_5}\cdot\dot{z}_5+\dfrac{c_5}{m_5}\cdot\dot{z}_3-\dfrac{k_5}{m_5}\cdot z_5+\dfrac{k_5}{m_5}\cdot z_3\\
\ddot{z}_4=-\dfrac{c_4}{m_4}\cdot\dot{z}_4+\dfrac{c_4}{m_4}\cdot\dot{z}_3-\dfrac{k_4}{m_4}\cdot z_4+\dfrac{k_4}{m_4}\cdot z_3\\
\ddot{z}_3=-\dfrac{c_3+c_4+c_5}{m_3}\cdot\dot{z}_3-\dfrac{k_3+k_4+k_5}{m_3}\cdot z_3+\dfrac{c_4}{m_3}\cdot\dot{z}_4+\dfrac{k_4}{m_3}\cdot z_4+\dfrac{c_5}{m_3}\cdot\dot{z}_5+\dfrac{k_5}{m_3}\cdot z_5+\dfrac{c_3}{m_3}\cdot\dot{z}_2+\dfrac{k_3}{m_3}\cdot z_2\\
\ddot{z}_2=-\dfrac{c_3+\dfrac{c_2\cdot c_{2c}}{c_2+c_{2c}}}{m_2}\cdot\dot{z}_2-\dfrac{k_3+\dfrac{k_2\cdot k_{2c}}{k_2+k_{2c}}}{m_2}\cdot z_2+\dfrac{c_3}{m_2}\cdot\dot{z}_3+\dfrac{k_3}{m_2}\cdot z_3+\dfrac{c_2\cdot c_{2c}}{\left(c_2+c_{2c}\right)\cdot m_2}\cdot\dot{z}_1+\dfrac{k_2\cdot k_{2c}}{\left(k_2+k_{2c}\right)\cdot m_2}\cdot z_1\\
\ddot{z}_1=-\dfrac{c_1+\dfrac{c_2\cdot c_{2c}}{c_2+c_{2c}}}{m_1}\cdot\dot{z}_1-\dfrac{k_1+\dfrac{k_2\cdot k_{2c}}{k_2+k_{2c}}}{m_1}\cdot z_1+\dfrac{c_1}{m_1}\cdot\dot{z}_6+\dfrac{k_1}{m_1}\cdot z_6+\dfrac{c_2\cdot c_{2c}}{\left(c_2+c_{2c}\right)\cdot m_1}\cdot\dot{z}_2+\dfrac{k_2\cdot k_{2c}}{\left(k_2+k_{2c}\right)\cdot m_1}\cdot z_2
\end{cases} \tag{8.8}$$

Table 8.3 The maximum displacement of the 7-DOF model calculated by the frequency response method and time-domain integration method

	Frequency (Hz)	**Frequency response method (m)**	**Time-domain integration method (m)**
Z_1	1.21	0.0087	0.00852

Z_2	1.21	0.01	0.01015
Z_3	1.22	0.01515	0.0151
Z_4	1.22	0.015167	0.0152
Z_5	1.23	0.0167	0.0166
Z_6	1.21	0.008675	0.00858
Z_7	9.69	0.00525	0.00522

A MATLAB Simulink code has been developed based on Equation (8.9) as shown in Figure A2 where a sinusoidal wave signal is used as the displacement excitation input. The amplitude of the sinusoidal wave signal is set as 0.002 m and the frequency of the sinusoidal wave signal is set as the same as the first peak frequency of 1.23 Hz as shown in Figure 8.2 where the radial frequency is $2\pi f$=7.73 rad/s is used for the input frequency of the sinusoidal wave excitation signal. The simulation duration is set as 10 seconds, the Runge–Kutta numerical integration method of the stiff trapezoidal algorithm is applied to solve Equation (8.1) or (8.9). The time-domain displacement response z_5 of the head mass m_5 is calculated and shown in Figure 8.3(a) where the peak amplitude of the time domain displacement response z_5 is identified as 0.0166 m which is divided by the sinusoidal wave excitation signal of 0.002 m giving the transmissibility ratio of the head displacement over the road profile displacement. The maximum displacement of 0.0166 m calculated from the time-domain integration as shown in Figure 8.3(a) coincides with that calculated from the frequency response as shown in Figure 8.3(b) at the same excitation frequency. In the same way, the peak displacement amplitudes or the transmissibility ratios Z_1/Z_0 - Z_7/Z_0 of the mass points m_1-m_7 are calculated by the time domain integration method for the peak frequencies f_1-f_7 are also listed in Table 8.3. The maximum displacement transmissibility ratio response can be calculated using both the frequency and time-domain techniques. If the 7-DOF biodynamic vehicle and seat suspension system are linear. The results calculated from the time domain should be the same as those calculated from the frequency domain in the same frequency. The difference, if there is, may be caused by the nonlinearity of the 7-DOF biodynamic vehicle and seat suspension system. For example, suspension spring and damping nonlinearity, gaps, clearances between the parts or components may all cause the nonlinearity. The nonlinearity of the system is out of the research scope of this thesis and will be the future work. The results in Table 8.3 have verified the system linearity and validated the simulation models in both the time and frequency domain. It is seen from Table 8.3 that the peak displacement calculated from the time-domain integration coincide well with those calculated from the frequency response at the same excitation frequency. The time-domain integration and frequency response method has been validated by each other.

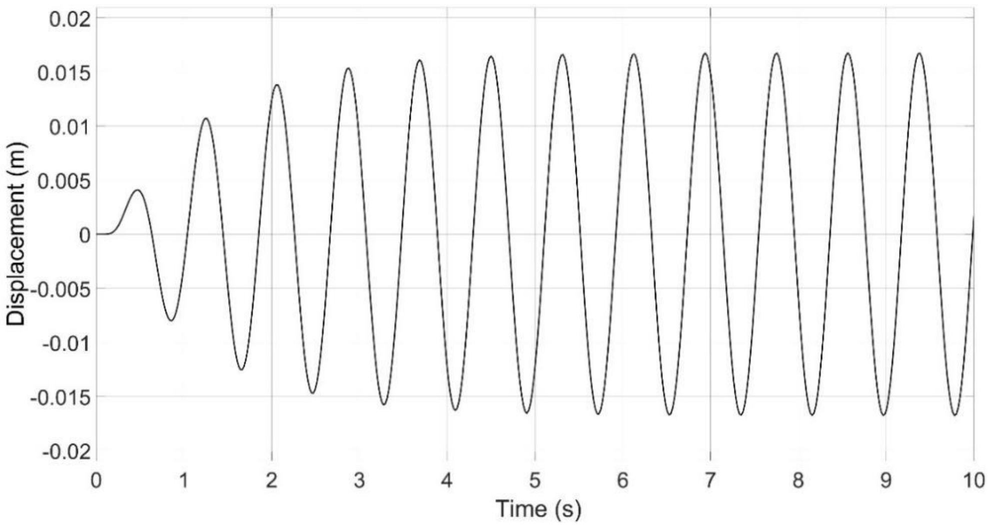

(a)

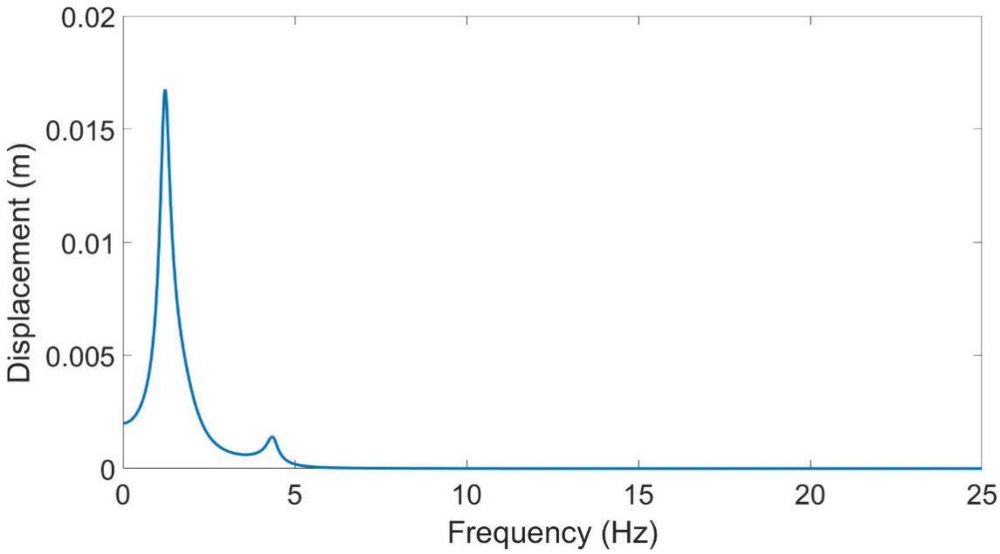

(b)

Figure 8.3 The amplitude of displacement calculated in different methods (a) Time-domain integration method (b) Frequency response method.

To reduce the seat system vibration, the 7-DOF model has been simulated under random road profile excitations. The road excitation comes from the unevenness of the road surface. For the evaluation of seat vibration mitigation performance, the precise road surface profile excitation information is essential. Therefore, how to precisely generate the road surface profile excitation in the time domain according to the road power spectral density has become an important step for simulation of the seat vibration mitigation performance. According to the research [4], the expression formula of the highway random road profile power spectrum density is given by

$$G_q(n) = G_q(n_0)\left(\frac{n}{n_0}\right)^{-w} \tag{8.9}$$

where n is the wavenumber (or spatial frequency), and n_0 is the reference wave number. In this study, $n_0 = 0.1\ m^{-1}$, and G is the power spectrum density of the road surface profile at the reference wavenumber, which can also be considered as the road surface roughness coefficient. w is the wavenumber index that is the slope of the power spectrum density versus the relative wave number ratio under the double logarithmic coordinate, which determines the wavelength/number structure of the road power spectrum density.

In the wavenumber domain of the power spectrum density, the vehicle speed factor is not considered. When the vehicle speed v is applied to simulate the road profile displacement response with a wavenumber of n, the wave frequency becomes:

$$f = vn$$

Therefore, the frequency-domain power spectrum density can be expressed as:

$$G_q(f) = G_q(n) = G_q(n_0) \cdot \left(\frac{n}{n_0} \right)^{-2} = G_q(n_0) \cdot n_0^{\ 2} \cdot \frac{v^2}{f^2} \tag{8.10}$$

In the same way, the power spectrum density of the vertical road surface velocity $\dot{q}$ due to the unevenness of the road profile in the frequency domain can be obtained as:

$$G_{\dot{q}}(f) = G_q(f)\left(2\pi f\right)^2 = 4\pi^2 G_q(n_0) n_0^{\ 2} v^2 \tag{8.11}$$

where $G_{\dot{q}}(f)$ is the velocity auto-power spectrum density of white noise signal, and only related to the road roughness and vehicle speed. This means that the velocity auto-power spectrum density function of the white noise random road profile is a constant value. Equation (8.8) is then given by

$$SEAT\ (\%) = \sqrt{\frac{\int \left| \frac{Z_5(f)}{Z_0(f)} \right|^2 \cdot W_k^2(f) \mathrm{d}f}{\int \left| \frac{Z_1(f)}{Z_0(f)} \right|^2 \cdot W_k^2(f) \mathrm{d}f}} \times 100\% \tag{8.12}$$

According to ISO 8606 [5], the time domain displacement response of the random road profile should satisfy the following equation:

$$\frac{d}{dt}z(t) = -\alpha \cdot v \cdot z(t) + \omega(t) \tag{8.13}$$

where v is the vehicle travel speed, α is dependent on the road type and given by in Table 8.4, $\omega(t)$ is the white noise signal of the power spectrum density ψ_ω which is given by

$$\psi_\omega = 2 \cdot \alpha \cdot v \cdot \sigma^2 \tag{8.14}$$

Table 8.4 The road roughness of the different road class

Road class	σ	α
A	2×10^{-3}	0.127
B	4×10^{-3}	0.127
C	8×10^{-3}	0.127
D	1.6×10^{-2}	0.127
E	3.2×10^{-2}	0.127

For example, for the road Class A, and the vehicle speed of 20 km/h (5.556 m/s), α=0.127; $\sigma=2\times10^{-3}$

Equation (8.8) can be written as

$$\frac{d}{dt}z(t) = -0.7056 \cdot z(t) + \omega(t) \tag{8.15}$$

the power spectrum density of the white noise signal is given by

$$\psi_\omega = 2 \times 0.127 \times 5.556 \times 4 \times 10^{-6} = 5.6449 \times 10^{-6} \tag{8.16}$$

Equation (8.16) can be solved by the integration method using a MATLAB Simulink code as shown in Figure 8.4.

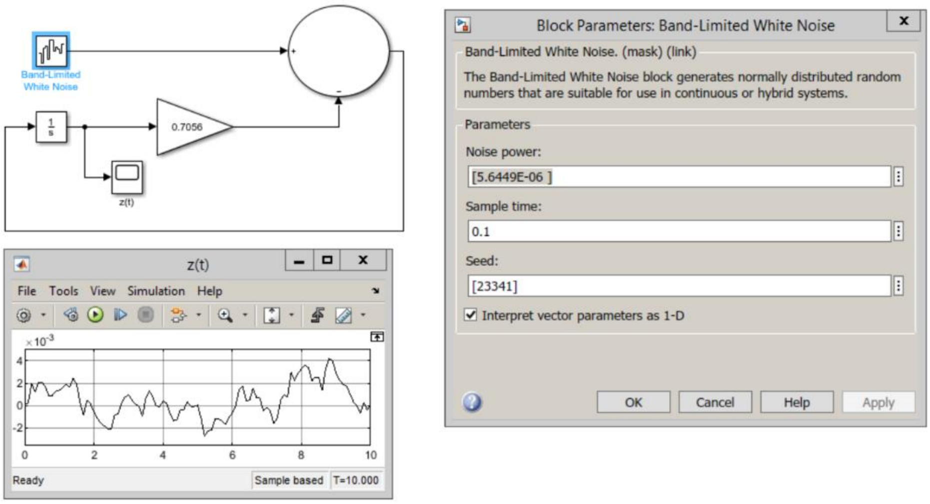

Figure 8.4 MATLAB Simulink code for solving the time-domain displacement response of the Class A random road profile through the integration method.

It is seen from Figure 8.4 that the band-limited white noise $\omega(t)$ is generated where power spectrum density of ψ_{ω}=5.6449×10^{-6} is entered as the noise power parameter in the RHS table of Figure 8.4. The solved displacement time response of the Class A random road profile is shown in the LHS bottom of Figure 8.4. In the same way, the time-domain displacement responses of Class A-E random road profiles can be solved by the MATLAB Simulink code as shown in Figure 8.5. If the displacement time responses of Class A-E random road profiles are used as the excitation inputs of the 7-DOF model as shown in Figure 8.1, the dynamic responses of the human body in the time domain under different random road profile conditions or displacement excitations can be simulated and used to verify the seat vibration control performance. In this study, the road surface roughness profiles applied are Class A, C, and E, and the vehicle speed is 20 km/h. In Figure 8.6, Class E road random road profile has the largest peak displacement amplitude, that is, the road condition is worst; and Class A road random road profile represents the smoothest road surface.

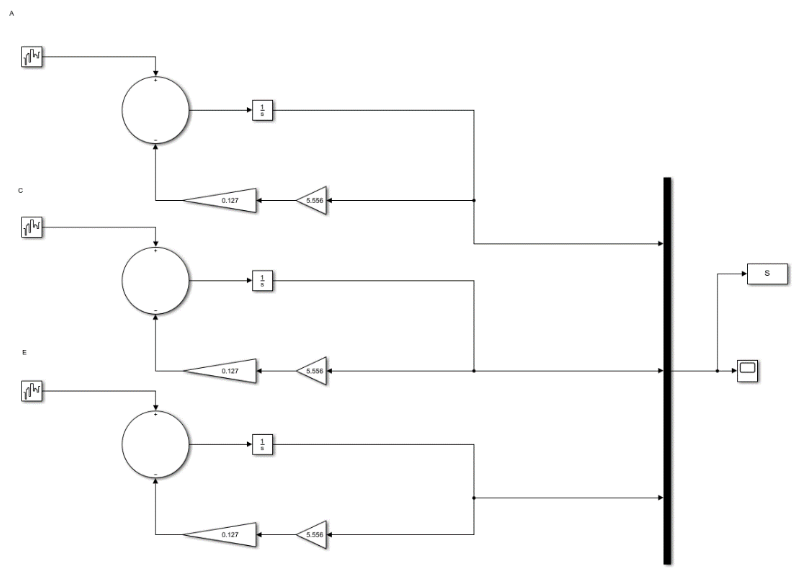

Figure 8.5 MATLAB Simulink code for solving the time-domain displacement responses of the Classes A, C, and E random road profiles through the integration method.

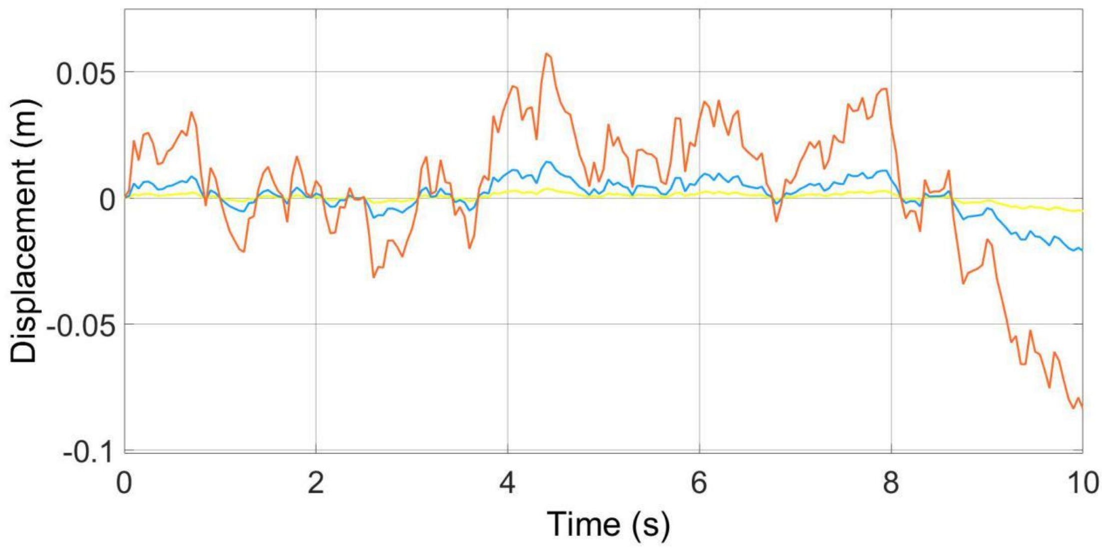

Figure 8.6 The time-domain displacement responses of the Classes A, C, and E random road profiles at the vehicle speed of 20 km/h calculated through the integration method.

To calculate the displacement responses of the mass points m_1-m_7 in the 7-DOF model under the random road profile excitations, the sinusoidal excitation signal in Figure A2 has to be replaced by the time-domain displacement response signals of the Classes A, C, and E random road profiles calculated through the integration method as shown in Figure A3.

8.3 Result and discussion

The parameters of k_1, c_1, k_{2c}, and c_{2c} are adjusted or changed, the peak transmissibility is calculated by the frequency response method based on Equation (8.4) and the MATLAB code in Figure A1.

As shown in Table 8.5, with the original parameter settings, the peak transmissibility from the seat to head is 18.47. When k_1 is reduced by 50%, the peak transmissibility responsively reduces to 18.26; when k_1 is 30% of the original value, the transmissibility also reduces to 18. Same as the former, when c_1 is decreased to 50% and 30% of the original value, the peak transmissibility values become 18.27 and 18.25 respectively. This change is very small. By reducing k_{2c} to 50% and 30% of the original value, the peak transmissibility is greatly reduced to 17.39 and 16.51. Unlike the results of the 5-DOF RSM model, decreasing c_{2c} to 50% and 30% of the original value will increase the peak transmissibility to 18.49 and 19.76. The results of the 5-DOF RSM model show that the seat cushion damping coefficient has the least influence on the peak transmissibility ratio where when the seat cushion damping coefficient increases, the peak transmissibility ratio slightly increases. As shown in Figure 8.7, when the design parameters k_1 and c_1 are accordingly reduced by 50% and 70%, the peak vibration transmissibility is also decreased, but the amplitude is slight. But as k_{2c} is reduced, the peak vibration transmissibility is significantly reduced. The situation of c_{2c} is just the opposite, the peak vibration transmissibility increases with the design parameters decreased.

Table 8.5 The comparison of the peak transmissibility results between the original parameter and adjusted parameter settings

Original k_1 (Peak transmissibility)	**Reduced k_1 by 50%**	**Reduced k_1 by 70%**
18.47	18.26	18.01
Original c_1 (Peak transmissibility)	**50% reduction of c_1**	**70% reduction of c_1**
18.47	18.27	18.25
Original k_{2c} (Peak transmissibility)	**50% reduction of k_{2c}**	**30% reduction of k_{2c}**
18.47	17.39	16.51
Original c_{2c} (Peak transmissibility)	**50% reduction of c_{2c}**	**30% reduction of c_{2c}**
18.47	18.49	19.76

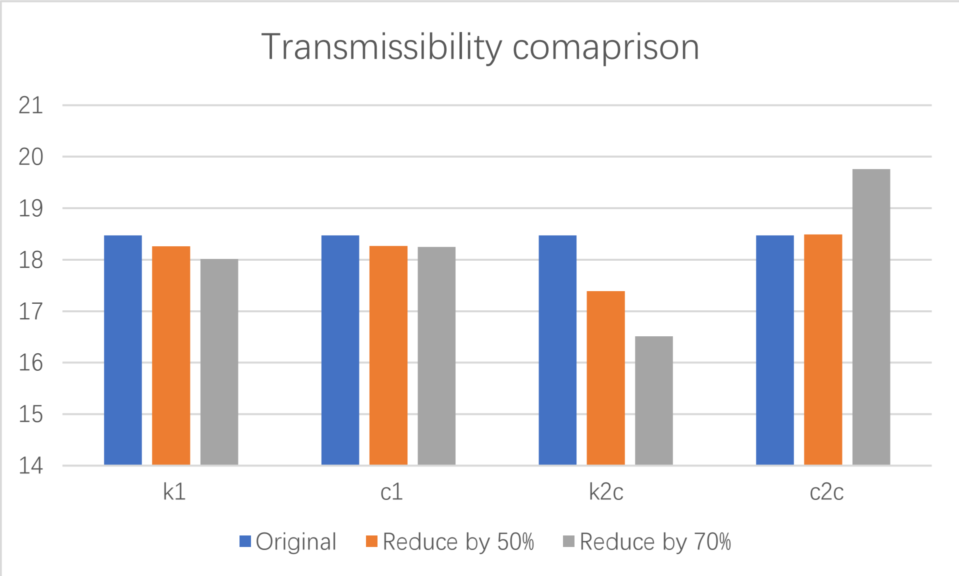

Figure 8.7 The comparison of the peak transmissibility ratio with different design parameters

As shown in Table 8.6 that when the four sets of design parameters (k_1, c_1, k_{2c}, c_{2c}) are reduced by 50% at the same time, the peak transmissibility value is reduced to 16.27; when the design parameters are 30% of the original values, the peak transmissibility value is the lowest of 14.07. At the same time, reducing the stiffness and damping of the seat structure to 50% and 30% of the original values will also decrease the peak transmissibility values to 17.67 and 16.59, respectively; reducing the stiffness and damping of the seat cushion to 50% and 30% of the original value, the peak transmissibility values become 17.09 and 15.43 respectively, leading to a better vibration isolation performance.

Table 8.6 The comparison of the peak transmissibility results between different groups of parameter settings

Original (Peak transmissibility)	50% (k_1, c_1, k_{2c}, c_{2c})	30% (k_1, c_1, k_{2c}, c_{2c})
18.47	16.27	14.07

	50% (k_1, c_1)	30% (k_1, c_1)
18.47	17.67	16.49
	50% (k_{2c}, c_{2c})	30% (k_{2c}, c_{2c})
18.47	17.09	15.43

After comparing the results of the 5-DOF RSM model with the results of the 7-DOF model simulation, it can be found that the overall trend of the two method results is the same, although there is a slight difference in some aspects. For example, reducing the value of c_{2c} does not reduce the peak transmissibility, which is different from the 5-DOF RSM model prediction. Also, in terms of the parameter combination analysis, in the 5-DOF RSM model, increasing the stiffness and damping of seat structure (k_1, c_1) will have a greater improvement on vibration control than increasing the stiffness and damping of the seat cushion (k_{2c}, c_{2c}). However, in 7-DOF model simulation, decreasing the stiffness and damping of the seat cushion (k_{2c}, c_{2c}) is more effective than reducing the stiffness and damping of the seat structure (k_1, c_1) to achieve a better vibration control. The reasons for these differences may be the following two points. First, the 5-DOF RSM model may not be accurate or have errors. Because the 5-DOF RSM model is based on the regression algorithm, there is an inevitable error in the prediction process, which causes the difference between the results of the two methods. Second, because the vehicle suspension system and wheel/tire system are included in 7-DOF model, the degree of freedom of the simulation model has been increased, and the additional system coupling can also cause the difference in the results. Although some results are different, however, according to the optimization results of the 5-DOF RSM simulation, the optimization method of improving the seat vibration control by reducing the stiffness and damping coefficients of the seat and the cushion is still valid in the simulation of the 7-DOF model. By decreasing the values of these design parameters, the seat vibration control performance can be enhanced.

In Simulink, the head acceleration of the 7-DOF model is simulated in the time domain and can directly validate the vibration control performance or passenger comfort under three different random road profile excitations. The results are displayed in Figure 8.8. Under three different random road profile excitations, by reducing the value of the parameter (k1, c1, k2c, c2c), the head acceleration of the model was significantly decreased. With original parameters, the largest head acceleration appears in the random road profile excitation of Class E, when the peak head acceleration reaches 1.417 m/s^2. When the values of the parameters are reduced by half, the peak head acceleration decreases to 1.126 m/s^2. Under the random road profile excitation of Class C, the largest head acceleration is reduced from 0.3543 m/s^2 to 0.2815 m/s^2 after the values of the parameters are reduced by 50%. Under the random road profile excitation of Class A, the peak head acceleration is decreased from 0.08857 m/s^2 to 0.07738 m/s^2

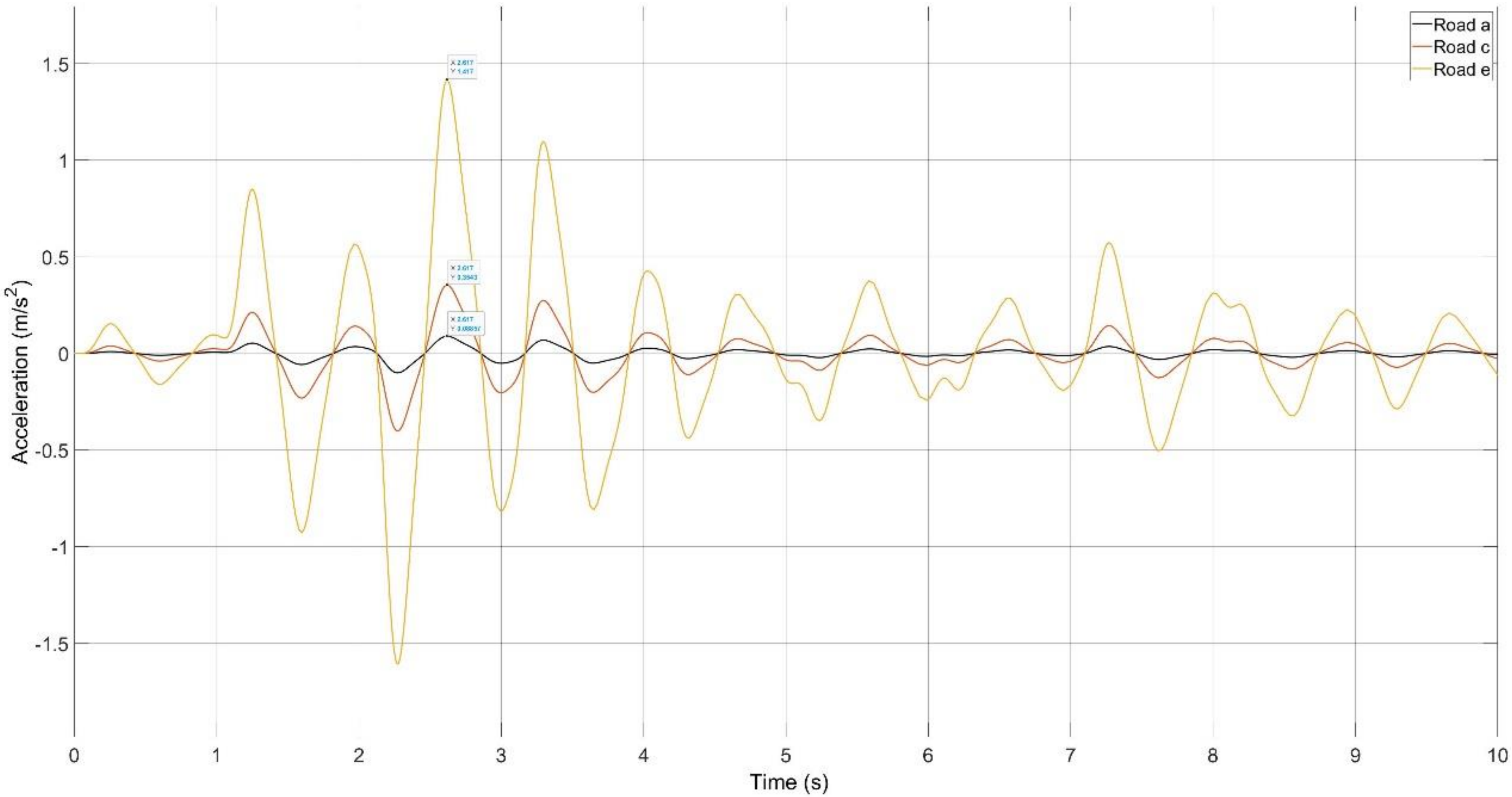
Road a
Road c
Road e
Acceleration (m/s^2)
Time (s)
1.5
1
0.5
0
-0.5
-1
-1.5
0
1
2
3
4
5
6
7
8
9
10

(a)

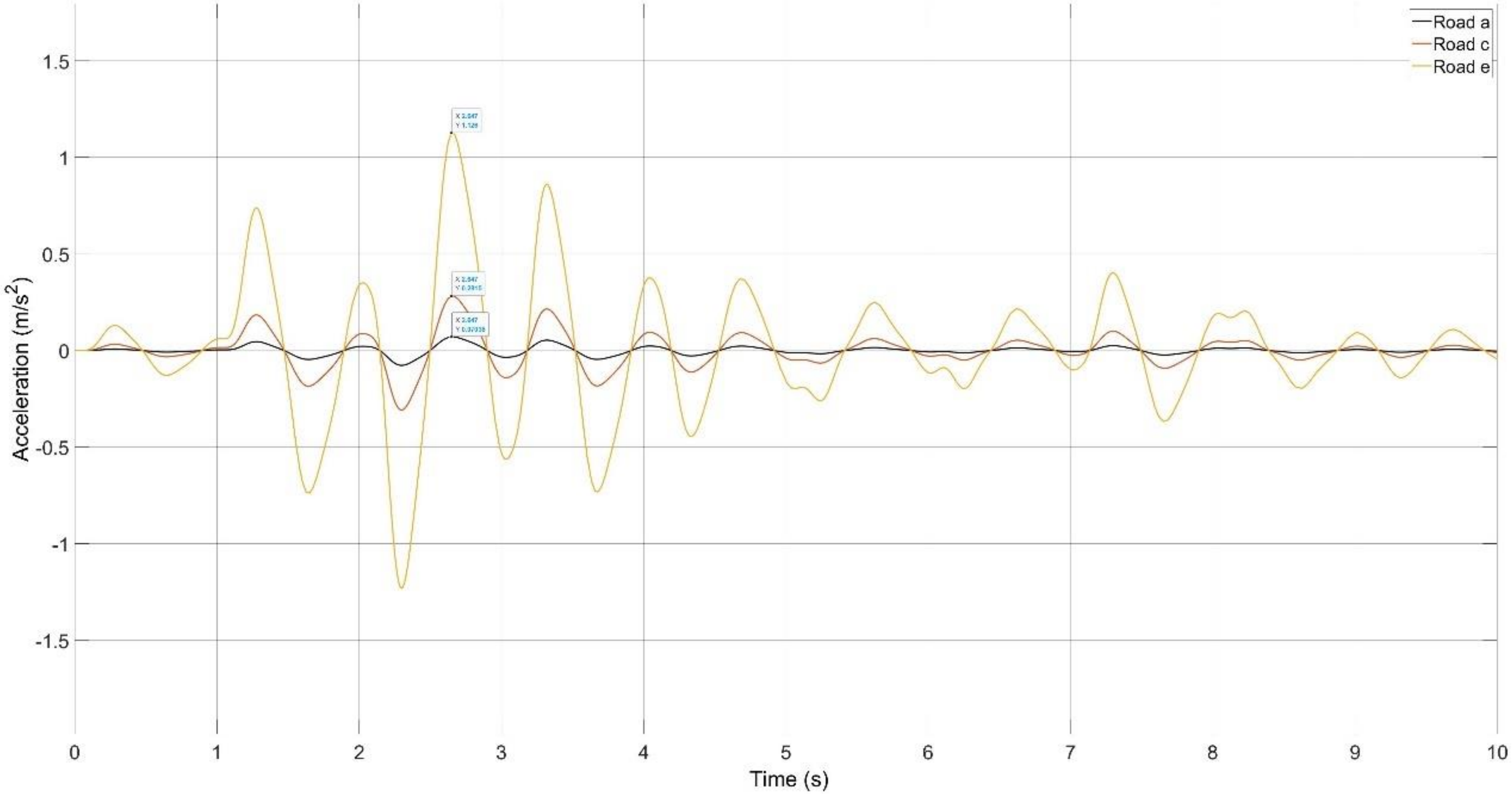

(b)

Figure 8.8 The simulation results of the head acceleration in the time domain (a) 100% of the original parameter value (b) 50% of the original parameter value.

The SEAT values of the 7-DOF model are calculated from Equations (8.4) and (8.13) in the frequency domain where the transmissibility ratios are calculated using the frequency response method under the random road profile excitations. The results are listed in Table 8.7. It can be seen from Table 8.5 that with the original parameters of k_1, c_1, k_{2c}, c_{2c}, the SEAT value reaches 187%. With the seat parameters ($\boldsymbol{k_1}$, $\boldsymbol{c_1}$, $\boldsymbol{k_{2c}}$, $\boldsymbol{c_{2c}}$) are reduced by 50%, that is, after reducing the stiffness and damping, the SEAT value is reduced to 174%.

Table 8.7 The comparison of the SEAT values

SEAT value **Original parameters (%)**	**SEAT value** **Adjusted parameters （%）**
187	174

On the whole, the head acceleration and SEAT value analysis results have also verified the 5-DOF RSM prediction results. Reducing the stiffness and damping coefficients of the seat and cushion can improve the vibration control performance of the seat system. Also, according to the result of the head acceleration simulation, as the unevenness of the road surface increases, the effect of vibration reduction becomes more obvious.

8.4 Conclusions

The 5-DOF seating system has been combined with a quarter truck vehicle suspension system leading to a 7-DOF mass-spring-dashpot lumped parameter system model. The motion equations of the 7-DOF system model have been developed and solved in both the time and frequency domain. The time-domain results have verified the frequency domain results. The time-domain integration method and frequency response method have been validated by each other.

The simulation results of the 5-DOF RSM model and the 7-DOF system model have been compared. It can be seen that the simulation results of the two models have the same trend, that is, under low-frequency vibration excitation, the peak transmissibility value and SEAT value can be reduced by reducing the stiffness and damping of the seat and cushion, which means that the seat vibration control performance can be improved. In addition, in the 7-DOF model, reducing the cushion damping will reduce the vibration isolation effect, which is contrary to the trend of the 5-DOF RSM prediction. The reason for this result may be caused by the inherent error of the 5-DOF RSM method or the model degree of freedom change which leads to the change of the system coupling. However, the overall results prove that the simulation and optimization results of the 5-DOF RSM model apply to the vibration control of the seating system even in the whole vehicle context. To improve the accuracy of the simulation and optimization results of the 5-DOF RSM model, the RSM should be applied to the 7-DOF vehicle-seating suspension system model, which will be our future work.

Conclusions

In summary, this thesis introduces a novel method and process of seat design and development in detail. In the literature review, the related research of active seat vibration control is analyzed and reviewed, including different active suspension actuators, controller designs, and new neural network controls. The research gaps and research direction are determined. Based on the research gaps, the research questions have been raised.

A new and compact active vibration control seat has been designed to reduce the damage to the human body from vibration under the important premise of saving packaging space. The second chapter introduces the experimental test method of the research in detail and provides test results and comparative information for the modelings in the later chapters. The model development process has been illustrated. As an important step and tool for the seat system design and development, an accurate mathematical model for prediction and optimization can save a lot of research time and effort. Through the collection of real truck test data, the multi-target genetic algorithm is applied to quickly identify the system parameters and accurately predict the dynamic response of the seat human body system. The mathematical model has been proved to be able to accurately predict the dynamic response of the seat human body system at about 4Hz. The experimental results have verified the analytical results. The analytical model has been validated by the experimental tests and measurements. The establishment of the RSM model simplifies the analysis process. By comparing the prediction results of the linear regression model and the ANN model with those of the RSM model, it can be concluded that the RSM model has the highest prediction accuracy. Another advantage of this RSM method is being able to establish the relationship formula between design parameters and target peak transmissibility response and to provide design optimization solutions. The advantage of the regression method is that the formula is simple and the method is easy to implement. The ANN method has its advantage of powerful regression calculation ability, which can directly predict the results according to the input parameters without relying on any formulas. The main significance of the model established through the three methods is that it validates and simplifies the research method, and provides an accurate seat human body system model based on real truck test data, which can be used to predict the dynamic response of the human seat suspension system under low-frequency excitation conditions. The model combining the human seating suspension system with the quarter truck suspension system is validated by experimental measurements to predict the dynamic characteristics of the seat suspension system in a real field test environment. The validated model can be applied to identify the seat design parameters and to predict the human head acceleration transmissibility at the same time. According to the analysis of this RSM relationship model, the optimal design parameter combination is determined for the minimum vibration transmissibility and best vibration isolation performance.

The thesis has successfully answered all three research questions. For future research work, the manufacturing of the seat will be completed, and related controller design work will also be implemented.

Appendix A

```
clc
k1=24854.31*0.3;
c1=8041.5*0.3;
m1=13;
k2=28723.1;
c2=3848.75;
k2c=14794.20*0.3;
c2c=2024.2;
m2=25.15;
k3=4587.43;
c3=195.425;
m3=20.92;
k4=159537.93;
c4=758.5;
m4=3.3;
k5=2857.13;
c5=0.8;
m5=4.59;
m6=260;
k6=26000;
c6=520;
m7=40;
k7=130000;
c7=264.7;
M=[m1 0 0 0 0 0 0;0 m2 0 0 0 0 0;0 0 m3 0 0 0 0;0 0 0 m4 0 0 0;0 0 0 0 m5 0 0;0 0 0 0 0 m6 0;0 0 0 0 0 0 m7];
K=[k1+k2*k2c/(k2+k2c) -k2*k2c/(k2+k2c) 0 0 0 -k1 0;-k2*k2c/(k2+k2c) k3+k2*k2c/(k2+k2c) -k3 0 0 0 0;
    0 -k3 k3+k4+k5 -k4 -k5 0 0;0 0 -k4 k4 0 0 0;0 0 -k5 0 k5 0 0;-k1 0 0 0 0 k1+k6 -k6;0 0 0 0 0 -k6 k6+k7];
C=[c1+c2*c2c/(c2+c2c) -c2*c2c/(c2+c2c) 0 0 0 -c1 0;-c2*c2c/(c2+c2c) c3+c2*c2c/(c2+c2c) -c3 0 0 0 0;
    0 -c3 c3+c4+c5 -c4 -c5 0 0;0 0 -c4 c4 0 0 0;0 0 -c5 0 c5 0 0;-c1 0 0 0 0 c1+c6 -c6;0 0 0 0 0 -c6 c6+c7];
[V,D]=eig(K,M)
FF=sqrt(D)/2/pi
f=0:0.01:25;
w=2*f*pi;
for n=1:length(w)
s=1i*w(n);
E=[m1*s^2+(c1+c2*c2c/(c2+c2c))*s+k1+k2*k2c/(k2+k2c) -c2*c2c*s/(c2+c2c)-k2*k2c/(k2+k2c) 0 0 0 -c1*s-k1 0;
    -c2*c2c*s/(c2+c2c)-k2*k2c/(k2+k2c) m2*s^2+(c3+c2*c2c/(c2+c2c))*s+k3+k2*k2c/(k2+k2c) -c3*s-k3 0 0 0 0;
    0 -c3*s-k3 m3*s^2+(c3+c4+c5)*s+k3+k4+k5 -c4*s-k4 -c5*s-k5 0 0;0 0 -c4*s-k4 m4*s^2+c4*s+k4 0 0 0;
    0 0 -c5*s-k5 0 m5*s^2+c5*s+k5 0 0;
    -c1*s-k1 0 0 0 0 m6*s^2+(c1+c6)*s+k1+k6 -c6*s-k6;0 0 0 0 0 -c6*s-k6 m7*s^2+(c6+c7)*s+k6+k7];
F=[0;0;0;0;0;0;c7*s+k7];
Z=E\F;
z1(n)=Z(1); % x1/y
z2(n)=Z(2); % x2/y
z3(n)=Z(3); % x3/y
z4(n)=Z(4); % x1/y
z5(n)=Z(5); % x2/y
z6(n)=Z(6); % x3/y
z7(n)=Z(7); % x3/y
end
```

Figure A1. The MATLAB code of the frequency response method.

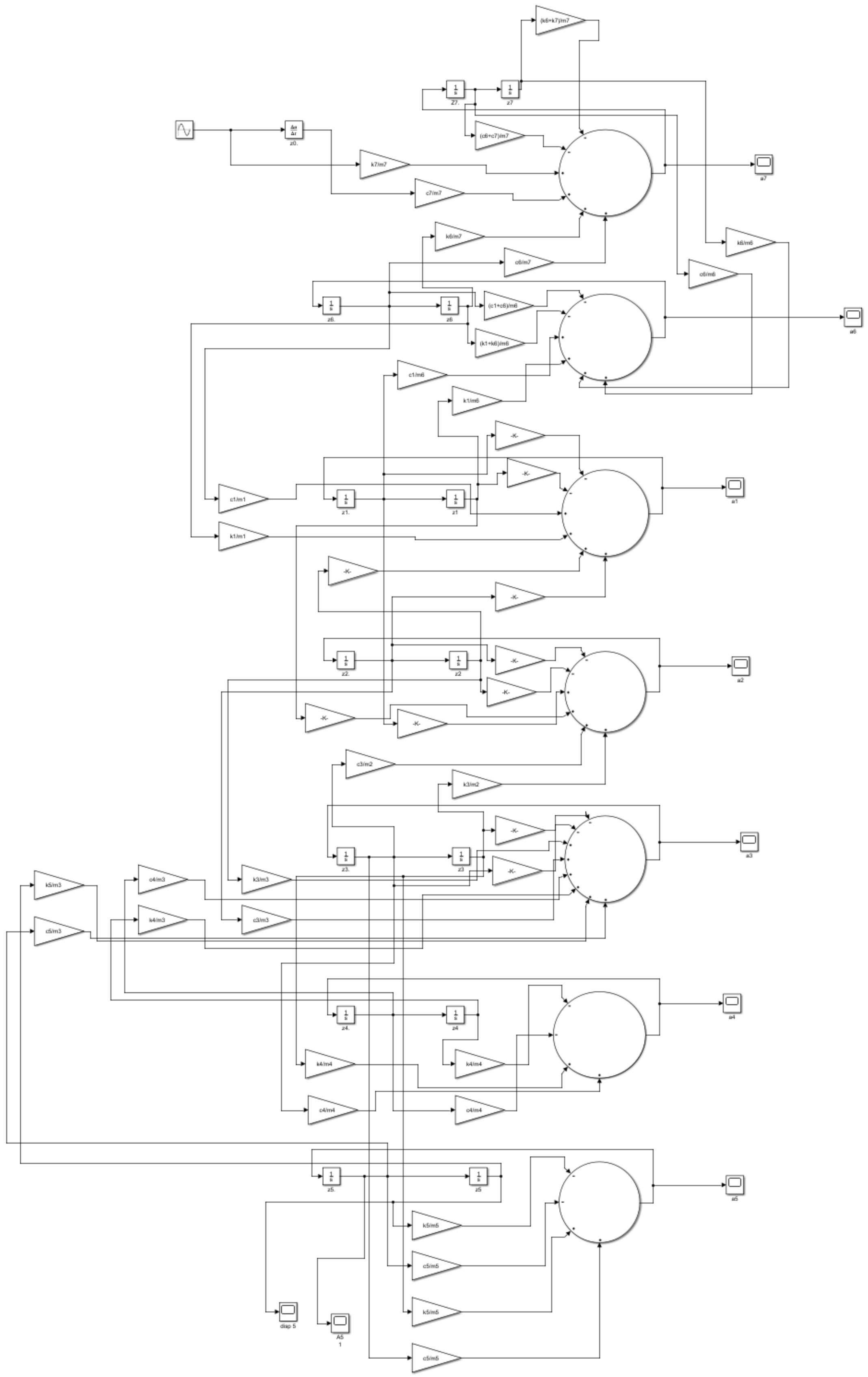
(k6+k7)/m7
z7.
z7
(c6+c7)/m7
z0.
k7/m7
c7/m7
a7
k6/m7
c6/m7
k6/m6
c6/m6
z6.
z6
(c1+c6)/m6
(k1+k6)/m6
a6
c1/m6
k1/m6
-K-
z1.
z1
c1/m1
k1/m1
a1
z2.
z2
a2
c3/m2
k3/m2
z3.
z3
a3
k5/m3
c5/m3
c4/m3
k4/m3
k3/m3
c3/m3
z4.
z4
a4
k4/m4
c4/m4
z5.
z5
a5
k5/m5
c5/m5
disp 5
A5
1

Figure A2. The 7-DOF model with the sinusoidal signal source.

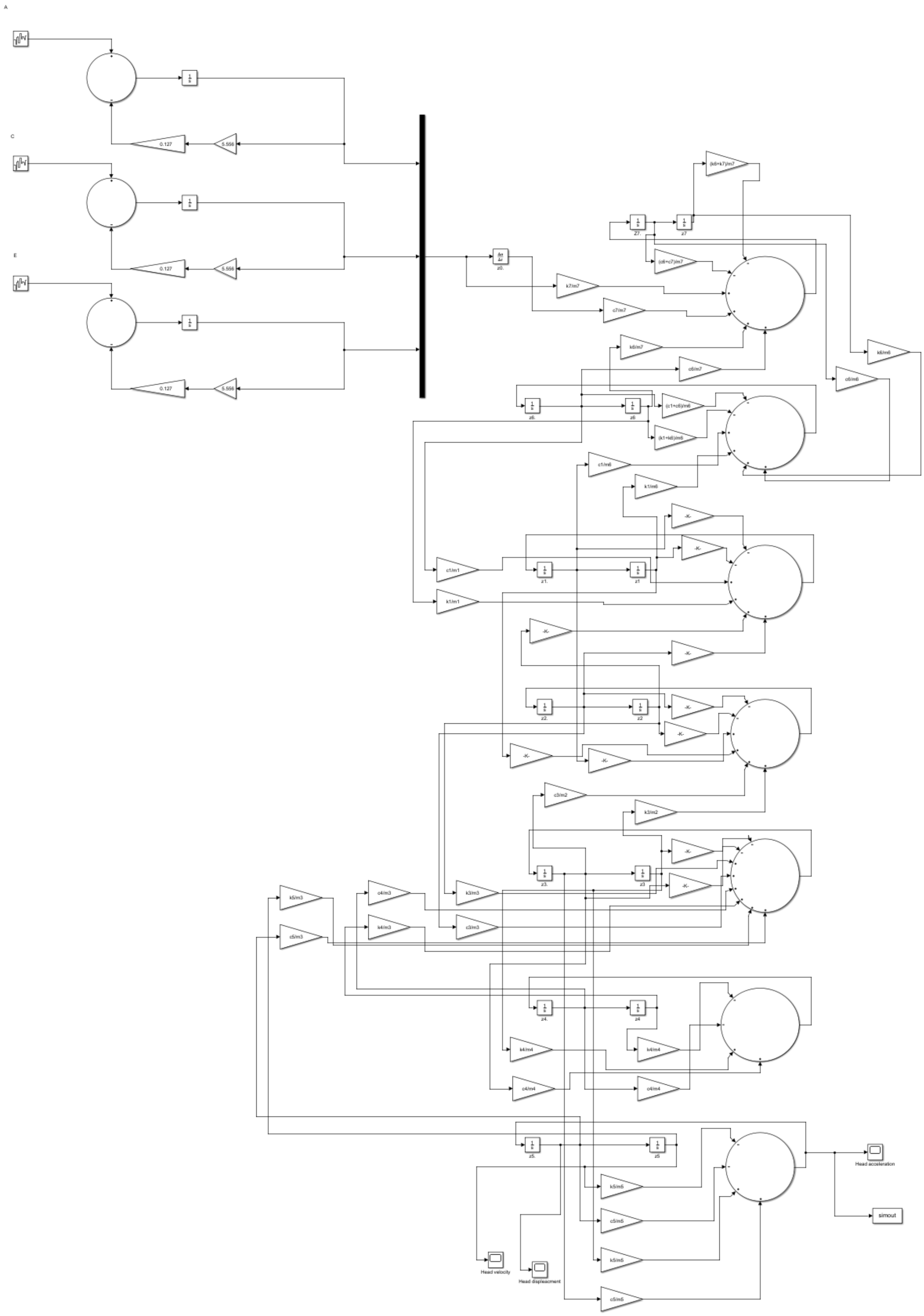

Figure A3. The 7-DOF model with three different classes random road excitation.

Appendix B

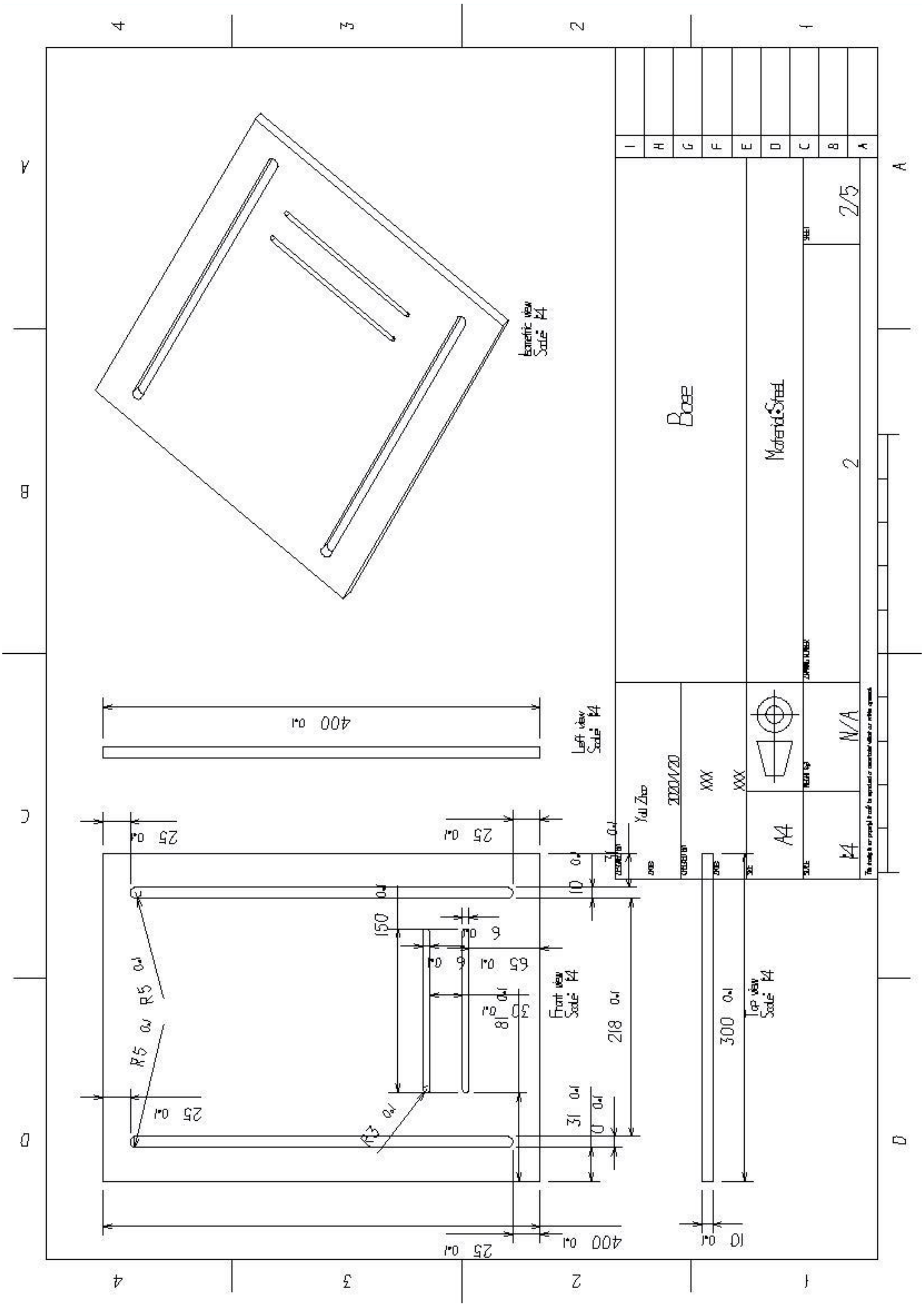

Base
Material:Steel
2/5
Yuli Zhao
2020/1/20
XXX
XXX
A4
N/A
Isometric view
Left view
Front view
Top view

Figure B1. The draft drawing of the seat base.

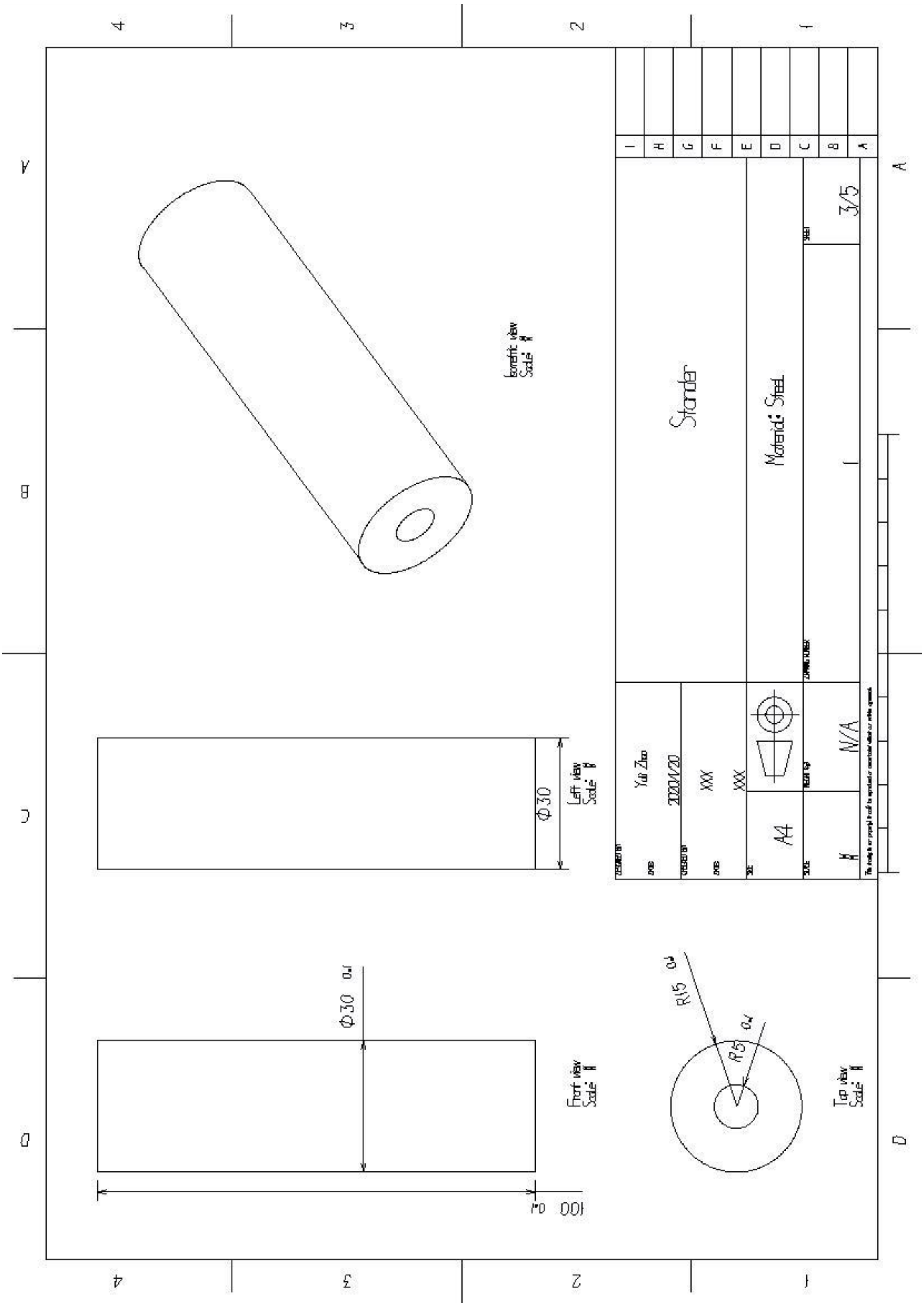

Figure B2. The draft drawing of the seat stander.

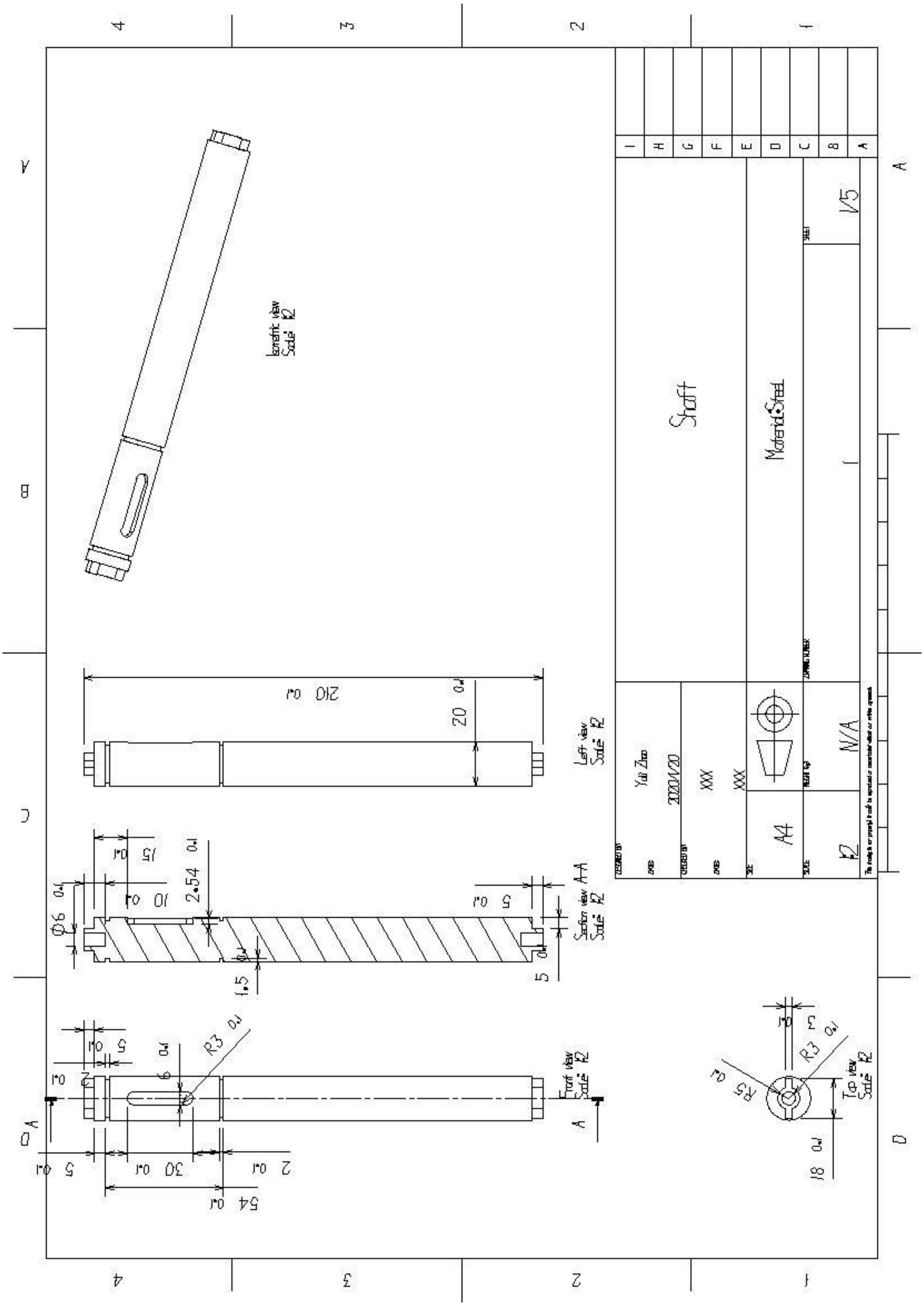

Figure B3. The draft drawing of the seat shaft.

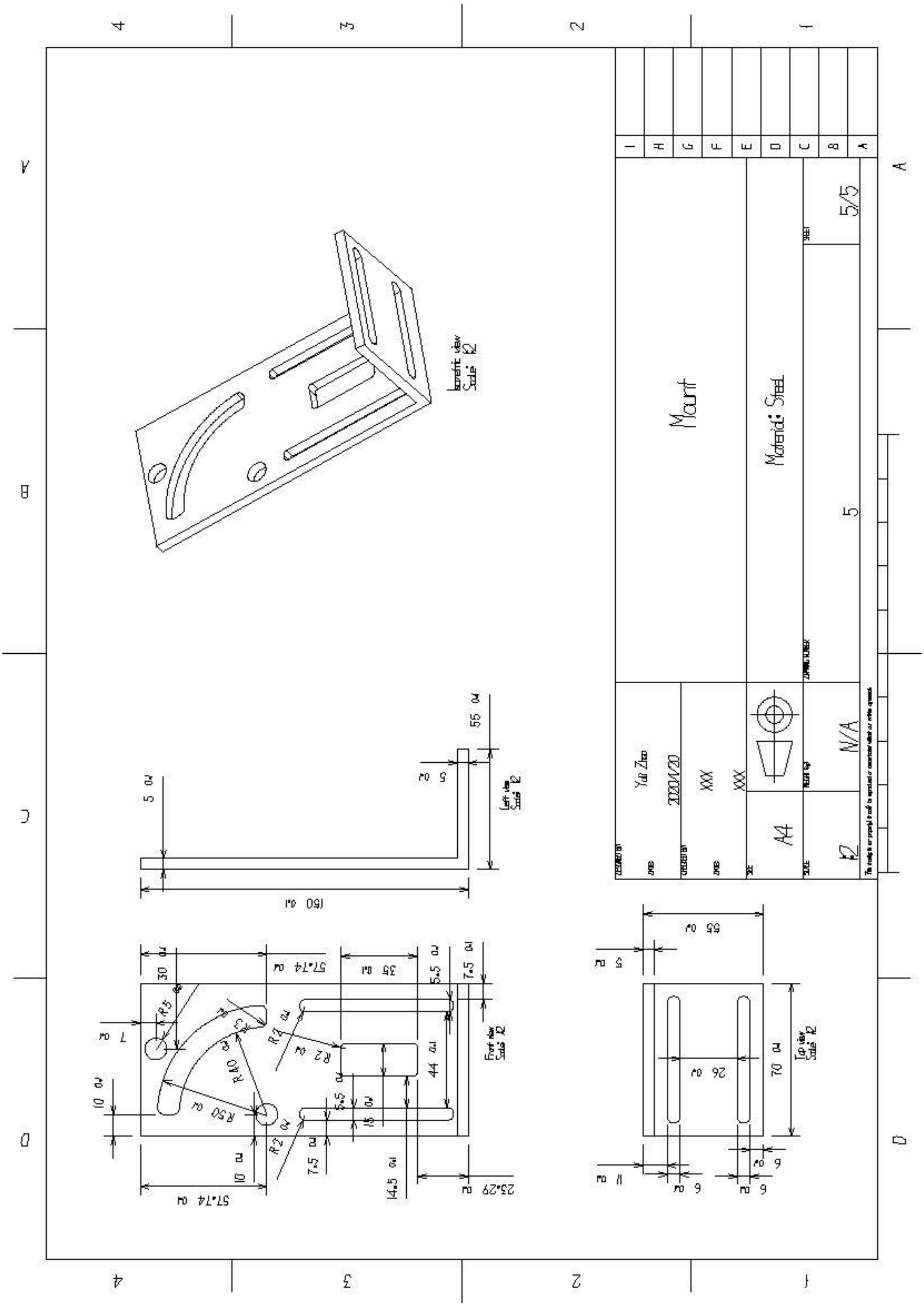

Figure B4. The draft drawing of the L-mount.

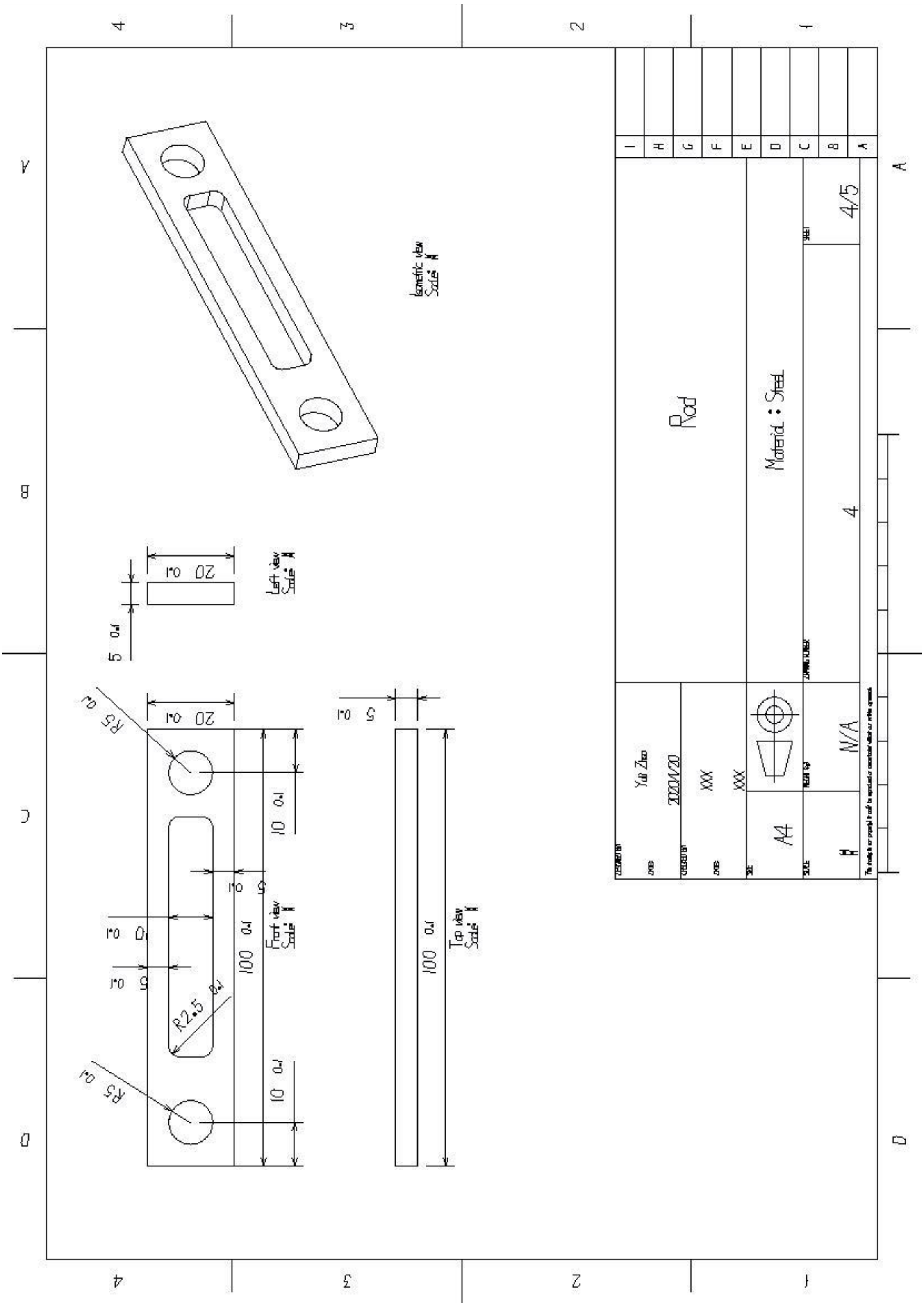

Figure B5. The draft drawing of the rod.

Appendix C First author publications

Applied Acoustics 173 (2021) 107697

Contents lists available at ScienceDirect

Applied Acoustics

journal homepage: www.elsevier.com/locate/apacoust

Parameter identification and robust vibration control of a truck driver's seat system using multi-objective optimization and genetic algorithm

Yuli Zhao [a], Mohammed Alashmori [a], Fengrong Bi [b], Xu Wang [a,*]

[a] School of Engineering, RMIT University, Australia
[b] School of Mechanical Engineering, Tianjin University, Australia

ARTICLE INFO

Article history:
Received 14 July 2020
Received in revised form 3 September 2020
Accepted 24 September 2020

ABSTRACT

This paper has developed a 5-DOF driver and seat suspension system model for active vibration control. A novel fast system parameter identification method from vibration measurement data has been proposed for the seat-occupant system based on the multi-objective Genetic Algorithm optimization (GA). This sys-tem parameter identification method can identify the seat system parameters of a 5-DOF lumped mass-

Open Access Review

A Review of Low-Frequency Active Vibration Control of Seat Suspension Systems

by Yuli Zhao and Xu Wang *

School of Engineering, RMIT University, Bundoora, VIC 3083, Australia

* Author to whom correspondence should be addressed.

Appl. Sci. **2019**, *9*(16), 3326; https://doi.org/10.3390/app9163326

Received: 17 July 2019 / Revised: 4 August 2019 / Accepted: 8 August 2019 / Published: 13 August 2019

View Full-Text | Download PDF | Browse Figures | Review Reports | Cite This Paper

Abstract

As a major device for reducing vibration and protecting passengers, the low-frequency vibration control performance of commercial vehicle seating systems has become an attractive research topic in recent years. This article reviews the recent developments in active seat suspensions for vehicles. The features of active seat suspension actuators and the related control algorithms are described and discussed in detail. In addition, the vibration control and reduction performance of active seat suspension systems are also reviewed. The article also discusses the prospects of the application of machine learning, including artificial neural network (ANN) control algorithms, in the development of active seat suspension systems for vibration control. View Full-Text

Keywords: vibration; active control; low frequency; suspension; seating system; machine learning

Reference

1. Krajnak, K. Health effects associated with occupational exposure to hand-arm or whole body vibration. *J. Toxicol. Environ. Health Part B* 2018, *21*, 320–334.
2. Coyte, J.L.; Stirling, D.; Du, H.; Ros, M. Seated Whole-Body Vibration Analysis, Technologies, and Modeling: A Survey. *IEEE Trans. Syst. Man Cybern. Syst.* 2016, *46*, 725–739.
3. Tiemessen, I.J.; Hulshof, C.T.; Frings-Dresen, M.H. An overview of strategies to reduce whole-body vibration exposure on drivers: A systematic review. *Int. J. Ind. Ergon.* 2007, *37*, 245–256.
4. Slota, G.P.; Granata, K.P.; Madigan, M.L. Effects of seated whole-body vibration on postural control of the trunk during unstable seated balance. *Clin. Biomech.* 2008, *23*, 381–386.
5. Burdorf, A.; Swuste, P. The effect of seat suspension on exposure to whole-body vibration of professional drivers. *Ann. Occup. Hyg.* 1993, *37*, 45–55.
6. Johanning, E. Diagnosis of whole-body vibration related health problems in occupational medicine. *J. Low Freq. Noise Vib. Act. Control* 2011, *30*, 207–220.
7. Paddan, G.; Griffin, M.; Griffin, M. Effect of seating on exposures to whole-body vibration in vehicles. *J. Sound Vib.* 2002, *253*, 215–241.
8. Toward, M.G.; Griffin, M.J. The transmission of vertical vibration through seats: Influence of the characteristics of the human body. *J. Sound Vib.* 2011, *330*, 6526–6543.
9. Wu, X, Rakheja, S & Boileau, P-É 1999, 'Study of Human-Seat Interactions for Dynamic Seating Comfort Analysis', paper presented to <https://doi.org/10.4271/1999-01-1303>.
10. Mozaffarin, A.; Pankoke, S.; Wölfel, H.-P. MEMOSIK V—An active dummy for determining three-directional transfer functions of vehicle seats and vibration exposure ratings for the seated occupant. *Int. J. Ind. Ergon.* 2008, *38*, 471–482.

11. Le, T.D.; Ahn, K.K. Experimental investigation of a vibration isolation system using negative stiffness structure. *Int. J. Mech. Sci.* 2013, *70*, 99–112.

12. Maciejewski, I.; Meyer, L.; Krzyzynski, T. Modelling and multi-criteria optimization of passive seat suspension Vibro-isolating properties. *J. Sound Vib.* 2009, *324*, 520–538.

13. McManus, S.; Clair, K.S.; Boileau, P.; Boutin, J.; Rakheja, S. Evaluation of vibration and shock attenuation performance of a suspension seat with a semiactive magnetorheological fluid damper. *J. Sound Vib.* 2002, *253*, 313–327.

14. Bai, X.-X.; Jiang, P.; Qian, L.-J. Integrated semiactive seat suspension for both longitudinal and vertical vibration isolation. *J. Intell. Mater. Syst. Struct.* 2017, *28*, 1036–1049.

15. Li, W.; Zhang, X.; Du, H. Development and simulation evaluation of a magnetorheological elastomer isolator for seat vibration control. *J. Intell. Mater. Syst. Struct.* 2012, *23*, 1041–1048.

16. Sireteanu, T.; Stancioiu, D.; Stammers, C.W. Use of magnetorheological fluid dampers in semi-active driver seat vibration control. In Proceedings of the ACTIVE 2002, Southampton, UK, 15–17 July 2002.

17. Choi, S.-B.; Han, Y.-M. Vibration control of electrorheological seat suspension with a human-body model using sliding mode control. *J. Sound Vib.* 2007, *303*, 391–404.

18. Lee, C.-M.; Bogatchenkov, A.; Goverdovskiy, V.; Shynkarenko, Y.; Temnikov, A. Position control of seat suspension with minimum stiffness. *J. Sound Vib.* 2006, *292*, 435–442.

19. Kim, J.H.; Marin, L.S.; Dennerlein, J.T. Evaluation of commercially available seat suspensions to reduce whole body vibration exposures in mining heavy equipment vehicle operators. *Appl. Ergon.* 2018, *71*, 78–86.

20. Ning, D.; Sun, S.; Yu, J.; Zheng, M.; Du, H.; Zhang, N.; Li, W. A rotary variable admittance device and its application in vehicle seat suspension vibration control. *J. Frankl. Inst.* 2019, doi:10.1016/j.jfranklin.2019.04.015.

21. Ning, D.; Sun, S.; Du, H.; Li, W.; Zhang, N. Vibration control of an energy regenerative seat suspension with variable external resistance. *Mech. Syst. Signal Process.* 2018, *106*, 94–113.

22. Choi, S.-B.; Lee, B.; Nam, M.H.; Cheong, C. Vibration control of an MR seat damper for commercial vehicles. *J. Intell. Mater. Syst. Struct.* 2000, *11*, 936–944.

23. Han, Y.M.; Nam, M.H.; Han, S.S.; Lee, H.G.; Choi, S.B.; Choi, S. Vibration Control Evaluation of a Commercial Vehicle Featuring MR Seat Damper. *J. Intell. Mater. Syst. Struct.* 2002, *13*, 575–579.

24. Song, X.; Ahmadian, M. *Study of Semiactive Adaptive Control Algorithms with Magneto-Rheological Seat Suspension*; SAE Technical Paper; SAE International in United States: Warrendale, PA, USA, 2004.

25. Jung, J.Y.; Choi, S.B.; Wereley, N.M.; Han, Y.M.; Choi, Y.T. Ride quality investigation of an electrorheological seat suspension to minimize human body vibrations. *Proc. Inst. Mech. Eng. Part D J. Automob. Eng.* 2006, *220*, 139–150.

26. Zhao, Y.; Zhao, L.; Gao, H. Vibration Control of Seat Suspension using $H\infty$ Reliable Control. *J. Vib. Control* 2010, *16*, 1859–1879.

27. Zhao, Y.; Sun, W.; Gao, H. Robust control synthesis for seat suspension systems with actuator saturation and time-varying input delay. *J. Sound Vib.* 2010, *329*, 4335–4353.

28. Choi, S.-B.; Lee, Y.-S.; Han, M.-S.; Phu, D.X. Vibration control of a vehicle’s seat suspension featuring a magnetorheological damper based on a new adaptive fuzzy sliding-mode controller. *Proc. Inst. Mech. Eng. Part D J. Automob. Eng.* 2015, *230*, 437–458.

29. Gao, H.; Zhao, Y.; Sun, W. Input-Delayed Control of Uncertain Seat Suspension Systems with Human-Body Model. *IEEE Trans. Control Syst. Technol.* 2010, *18*, 591–601.

30. Yao, H.J.; Fu, J.; Yu, M.; Peng, Y.X. Semi-active control of seat suspension with MR damper. *J. Phys. Conf. Ser.* 2013, *412*, 012054.

31. Ning, D., Du, H., Sun, S., Li, W., Zhang, N., Dong, M. A novel electrical variable stiffness device for vehicle seat suspension control with mismatched disturbance compensation', IEEE/ASME Transactions on Mechatronics, 2019, vol., pp. 1-1.

32. Ning, D., Sun, S., Du, H., Li, W., Zhang, N., Zheng, M., Luo, L. An electromagnetic variable inertance device for seat suspension vibration control. *Mech. Syst. Signal Process.* 2019, *133*, 106259.

33. Wu, X.; Griffin, M. A semi-active control policy to reduce the occurrence and severity of end-stop impacts in a suspension seat with an electrorheological fluid damper. *J. Sound Vib.* 1997, *203*, 781–793.

34. Sathishkumar, P.; Jancirani, J.; John, D. Reducing the seat vibration of vehicle by semi active force control technique. *J. Mech. Sci. Technol.* 2014, *28*, 473–479.

35. Metered, H.; Šika, Z. Vibration control of a semi-active seat suspension system using magnetorheological damper. In Proceedings of the 2014 IEEE/ASME 10th International Conference on Mechatronic and Embedded Systems and Applications (MESA), Senigallia, Italy, 10–12 September 2014; pp. 1–7.

36. Huseinbegovic, S.; Tanovic, O. Adjusting stiffness of air spring and damping of oil damper using a fuzzy controller for vehicle seat vibration isolation. In Proceedings of the 2009 International Siberian Conference on Control and Communications, Tomsk, Russia, 27–28 March 2009, pp. 83–92.

37. Kawana, M.; Shimogo, T. Active Suspension of Truck Seat. *Shock Vib.* 1998, *5*, 35–41.

38. Choi, Y.-T.; Wereley, N.M. Mitigation of biodynamic response to vibratory and blast-induced shock loads using magnetorheological seat suspensions. *Proc. Inst. Mech. Eng. Part D J. Automob. Eng.* 2005, *219*, 741–753.

39. Sun, S.S.; Ning, D.H.; Yang, J.; Du, H.; Zhang, S.W.; Li, W.H. A seat suspension with a rotary magnetorheological damper for heavy duty vehicles. *Smart Mater. Struct.* 2016, *25*, 105032.

40. Park, C.; Jeon, D. Semiactive vibration control of a smart seat with an mr fluid damper considering its time delay. *J. Intell. Mater. Syst. Struct.* 2002, *13*, 521–524.

41. Qiang, Z.; Yaxun, Y. Improved single neuron PID control for heavy-duty vehicle magnetorheological seat suspension. In Proceedings of the 2008 IEEE Vehicle Power and Propulsion Conference, Harbin, China, 3–5 September 2008; pp. 1–3.
42. Liu, P.; Xia, X.; Zhang, N.; Ning, D.; Zheng, M. Torque response characteristics of a controllable electromagnetic damper for seat suspension vibration control. *Mech. Syst. Signal Process.* 2019, *133*, 106238.
43. Phu, D.X.; Shin, D.K.; Choi, S.-B. Design of a new adaptive fuzzy controller and its application to vibration control of a vehicle seat installed with an MR damper. *Smart Mater. Struct.* 2015, *24*, 85012.
44. Phu, D.X.; An, J.-H.; Choi, S.-B. A Novel Adaptive PID Controller with Application to Vibration Control of a Semi-Active Vehicle Seat Suspension. *Appl. Sci.* 2017, *7*, 1055.
45. Phu, D.X.; Choi, S.-M.; Choi, S.-B. A new adaptive hybrid controller for vibration control of a vehicle seat suspension featuring MR damper. *J. Vib. Control* 2017, *23*, 3392–3413.
46. Nguyen, S.D.; Nguyen, Q.H.; Choi, S.-B. A hybrid clustering based fuzzy structure for vibration control – Part 2: An application to semi-active vehicle seat-suspension system. *Mech. Syst. Signal Process.* 2015, *56*, 288–301.
47. Phu, D.X.; Hung, N.Q.; Choi, S.-B. A novel adaptive controller featuring inversely fuzzified values with application to vibration control of magneto-rheological seat suspension system. *J. Vib. Control* 2017, *24*, 5000–5018.
48. Guclu, R. Fuzzy Logic Control of Seat Vibrations of a Non-Linear Full Vehicle Model. *Nonlinear Dyn.* 2005, *40*, 21–34.
49. Bouazara, M.; Richard, M.; Rakheja, S. Safety and comfort analysis of a 3-D vehicle model with optimal non-linear active seat suspension. *J. Terramech.* 2006, *43*, 97–118.
50. Stein, G.J. A Driver's Seat with Active Suspension of Electro-pneumatic Type. *J. Vib. Acoust.* 1997, *119*, 230–235.

51. Stein, G.J. Vibration control system with a proportionally controlled pneumatic actuator. In Proceedings of the 1997 European Control Conference (ECC), Brussels, Belgium, 1–7 July 1997; pp. 1814–1818.

52. Maciejewski, I.; Meyer, L.; Krzyżyński, T. The vibration damping effectiveness of an active seat suspension system and its robustness to varying mass loading. *J. Sound Vib.* 2010, *329*, 3898–3914.

53. Maciejewski, I. Control system design of active seat suspensions. *J. Sound Vib.* 2012, *331*, 1291–1309.

54. Maciejewski, I.; Glowinski, S.; Krzyżyński, T. Active control of a seat suspension with the system adaptation to varying load mass. *Mechatronics* 2014, *24*, 1242–1253.

55. Maciejewski, I.; Krzyżyński, T.; Meyer, H. Modeling and vibration control of an active horizontal seat suspension with pneumatic muscles. *J. Vib. Control* 2018, *24*, 5938–5950.

56. Stein, G.J.; Ballo, I. Active Vibration Control System for the Driver's Seat for Off-Road Vehicles. *Veh. Syst. Dyn.* 1991, *20*, 57–78.

57. Ning, D.; Sun, S.; Zhang, J.; Du, H.; Li, W.; Wang, X. An active seat suspension design for vibration control of heavy-duty vehicles. *J. Low Freq. Noise Vib. Act. Control* 2016, *35*, 264–278.

58. Ning, D.; Sun, S.; Li, H.; Du, H.; Li, W. Active control of an innovative seat suspension system with acceleration measurement based friction estimation. *J. Sound Vib.* 2016, *384*, 28–44.

59. Ning, D.; Sun, S.; Wei, L.; Zhang, B.; Du, H.; Li, W. Vibration reduction of seat suspension using observer based terminal sliding mode control with acceleration data fusion. *Mechatronics* 2017, *44*, 71–83.

60. Ning, D.; Sun, S.; Zhang, F.; Du, H.; Li, W.; Zhang, B. Disturbance observer based Takagi-Sugeno fuzzy control for an active seat suspension. *Mech. Syst. Signal Process.* 2017, *93*, 515–530.

61. Ning, D.; Sun, S.; Du, H.; Li, W.; Li, W. Control of a multiple-DOF vehicle seat suspension with a roll and vertical vibration. *J. Sound Vib.* 2018, *435*, 170–191.

62. Ning, D.; Du, H.; Sun, S.; Li, W.; Zhang, B. An Innovative Two-Layer Multiple-DOF Seat Suspension for Vehicle Whole Body Vibration Control. *IEEE/ASME Trans. Mechatron.* 2018, *23*, 1787–1799.

63. Gan, Z.; Hillis, A.J.; Darling, J. Adaptive control of an active seat for occupant vibration reduction. *J. Sound Vib.* 2015, *349*, 39–55.

64. Frechin, M.M.; Ariño, S.B.; Fontaine, J. ACTISEAT: Active vehicle seat for acceleration compensation. *Proc. Inst. Mech. Eng. Part D J. Automob. Eng.* 2004, *218*, 925–933.

65. Du, H.; Li, W.; Zhang, N. Vibration Control of Vehicle Seat Integrating with Chassis Suspension and Driver Body Model. *Adv. Struct. Eng.* 2013, *16*, 1–9.

66. Wang, L. and Kazmierski, T., 2005. VHDL-AMS modeling of an automotive vibration isolation seating system.

67. Al-Junaid, H.; Kazmierski, T.; Wang, L. SystemC-A Modeling of an Automotive Seating Vibration Isolation System. In Proceedings of the Forum on Specification and Design Languages (FDL 2006), Darmstadt, Germany, 19–22 September 2006.

68. Wang, X.; Bi, F.; Du, H. Reduction of low-frequency vibration of a truck driver and seating system through system parameter identification, sensitivity analysis, and active control. *Mech. Syst. Signal Process.* 2018, *105*, 16–35.

69. Ali, S.A., Metered, H., Bassiuny, A.M. and Abdel-Ghany, A.M., 2019. *Vibration Control of an Active Seat Suspension System Integrated Pregnant Woman Body Model* (No. 2019-01-0172). SAE Technical Paper.

70. Wu, J.D. and Chen, R.J., 2004. Application of an active controller for reducing small-amplitude vertical vibration in a vehicle seat. *Journal of Sound and Vibration*, *274*(3-5), pp.939-951.

71. Sun, W., Li, J., Zhao, Y. and Gao, H., 2011. Vibration control for active seat suspension systems via dynamic output feedback with limited frequency characteristic. *Mechatronics*, *21*(1), pp.250-260.

72. Du, H.; Li, W.; Zhang, N. Integrated Seat and Suspension Control for a Quarter Car With Driver Model. *IEEE Trans. Veh. Technol.* 2012, *61*, 3893–3908.

73. Guclu, R.; Gulez, K. Neural network control of seat vibrations of a non-linear full vehicle model using PMSM. *Math. Comput. Model.* 2008, *47*, 1356–1371.

74. Tahmasebi, M.; Gohari, M. Active Off-Road Seat Suspension System Using Intelligent Active Force Control. *J. Low Freq. Noise Vib. Act. Control* 2015, *34*, 475–489.

75. Sammonds, G. M. Fray, M. and Mansfield, N. J. Effect of long term driving on driver discomfort and its relationship with seat fidgets and movements (SFMs), *Applied Ergonomics,* vol. 58, pp. 119-127, Jan 2017.

76. Choi, Y. T. and Wereley, N. M. Mitigation of biodynamic response to vibratory and blast-induced shock loads using magnetorheological seat suspensions, *Proceedings of the Institution of Mechanical Engineers Part D-Journal of Automobile Engineering,* vol. 219, no. D6, pp. 741-753, Jun 2005.

77. Nahvi, H., Nor, M.J.M., Fouladi, M.H. and Abdullah, S., 2006, July. Evaluating automobile road vibrations using BS 6841 and ISO 2631 comfort criteria. In *1st Regional Conference on Vehicle Engineering & Technology* (pp. 1-8).

78. ISO, I., 1997. Mechanical Vibration and Shock--Evaluation of human exposure to wholebody vibrations (2631-1). *International Standards Organization*.

79. Saraswat, M., 2013. Genetic Algorithm for optimization using MATLAB. *International Journal of Advanced Research in Computer Science*, *4*(3).

80. Askarzadeh, Z. and Moradi, H., 2016. Multivariable control of transmitted vibrations to the seat model of the human body. *International Journal of Industrial Ergonomics*, *56*, pp.69-83.

81. Pan, G.Y. and Hao, X.L., 2011, June. Research on modeling and simulation of active seat suspension system based on LQG control. In *2011 International Conference on Remote Sensing, Environment and Transportation Engineering* (pp. 656-659). IEEE.

82. Srdjevic, Z. and Cveticanin, L., 2012. Identifying nonlinear biomechanical models by multicriteria analysis. *Journal of sound and vibration*, *331*(5), pp.1207-1216.Wang, X., Bi, F. and Du, H., 2018. Reduction of low frequency vibration of truck driver and seating system through system parameter identification, sensitivity analysis and active control. *Mechanical Systems and Signal Processing*, *105*, pp.16-35.

83. Chen, S., Wang, D., Zuo, A., Chen, Z., Li, W. and Zan, J., 2010, August. Vehicle ride comfort analysis and optimization using design of experiment. In *2010 Second International Conference on Intelligent Human-Machine Systems and Cybernetics* (Vol. 1, pp. 14-18). IEEE.

84. Moradi, A., Nafchi, A.M., Ghanbarzadeh, A. and Soodmand, E., 2011, December. Optimization of linear and nonlinear full vehicle model for improving ride comfort vs. road holding with the Bees Algorithm. In *2011 IEEE Colloquium on Humanities, Science and Engineering* (pp. 17-22). IEEE.

85. Deprez, K., Maertens, K. and Ramon, H., 2002, May. Comfort improvement by passive and semi-active hydropneumatic suspension using global optimization technique. In *Proceedings of the 2002 American Control Conference (IEEE Cat. No. CH37301)* (Vol. 2, pp. 1497-1501). IEEE.

86. Gunston, T.P., Rebelle, J. and Griffin, M.J., 2004. A comparison of two methods of simulating seat suspension dynamic performance. *Journal of Sound and Vibration, 278*(1-2), pp.117-134.

87. Segla, S. and Trisovic, N., 2013. Modelling and Optimization of Passive Seat Suspension. *American Journal of Mechanical Engineering*, *1*(7), pp.407-411.

88. Gündoğdu, Ö., 2007. Optimal seat and suspension design for a quarter car with driver model using genetic algorithms. *International Journal of Industrial Ergonomics*, *37*(4), pp.327-332.

89. Abbas, W., Emam, A., Badran, S., Shebl, M. and Abouelatta, O., 2013. Optimal seat and suspension design for a half-car with driver model using genetic algorithm.

90. ALIZADEH, H.H., SEDAGHAT, A., MEHR, M.S. and NADERI, D., 2008. Determining and Optimization of Mass, Stiffness and Damping Coefficients of Tractor Seat by Quasi-Newton Method Using Coupled Human-Seat Model. *Tarım Makinaları Bilimi Dergisi*, *4*(1), pp.51-55.

91. Aydın, M. and Ünlüsoy, Y.S., 2012. Optimization of suspension parameters to improve impact harshness of road vehicles. *The International Journal of Advanced Manufacturing Technology*, *60*(5-8), pp.743-754.

92. Reddy, M.S., Vigneshwar, P., Ram, M.S., Sekhar, D.R. and Harish, Y.S., 2017. Comparative optimization study on vehicle suspension parameters for rider comfort based on RSM and GA. *Materials Today: Proceedings*, *4*(2), pp.1794-1803.

93. Reddy, M.S., Rao, S.S., Vigneshwar, P., Akhil, K. and RajaSekhar, D., 2016. An Intelligent Optimization Approach to Quarter Car Suspension System Through RSM Modeled Equation. In *Proceedings of First International Conference on Information and Communication Technology for Intelligent Systems: Volume 2* (pp. 97-108). Springer, Cham.

94. Banerjee, A., Mallick, P. and Mitra, A., 2018. *Analysis and optimization of seat and suspension parameters for occupant ride comfort in a passenger vehicle* (No. 2018-01-1404). SAE Technical Paper.

95. Gohari, M., Rahman, R.A., Tahmasebi, M. and Nejat, P., 2014. Off-road vehicle seat suspension optimisation, part I: derivation of an artificial neural network model to predict seated human spine acceleration in vertical vibration. *Journal of Low Frequency Noise, Vibration and Active Control*, *33*(4), pp.429-441.

96. Mani, R., Milosavljevic, S. and John Sullivan, S., 2011. The influence of body mass on whole-body vibration: a quad-bike field study. *The Ergonomics Open Journal*, *4*(1).

97. Gulez, K. and Guclu, R., 2008. CBA-neural network control of a non-linear full vehicle model. *Simulation Modelling Practice and Theory*, *16*(9), pp.1163-1176.

98. Tanovic, O. and Huseinbegovic, S., 2009, December. Hybrid fuzzy-neural network structure for vehicle seat vibration isolation. In *2009 IEEE International Conference on Control and Automation* (pp. 2354-2359). IEEE.

99. Huy, T.D., Mien, V. and Choi, S.B., 2018. A new composite adaptive controller featuring the neural network and prescribed sliding surface with application to vibration control. *Mechanical Systems and Signal Processing*, *107*, pp.409-428.

100. Eski, I. and Yıldırım, Ş., 2009. Vibration control of vehicle active suspension system using a new robust neural network control system. *Simulation Modelling Practice and Theory*, *17*(5), pp.778-793.

101. Gohari, M., Rahman, R.A. and Tahmasebi, M., 2014. Prediction head acceleration from hand and seat vibration via artificial neural network model. In *Applied Mechanics and Materials* (Vol. 471, pp. 161-166). Trans Tech Publications Ltd.

102. Gohari, M., Rahman, R.A., Raja, R.I. and Tahmasebi, M., 2012. A novel artificial neural network biodynamic model for prediction seated human body head acceleration in vertical direction. *Journal of Low Frequency Noise, Vibration and Active Control*, *31*(3), pp.205-216.

103. Tanovic, O., Huseinbegovic, S. and Lacevic, B., 2008, December. Road type recognition using neural networks for vehicle seat vibration damping. In *2008 IEEE International Symposium on Signal Processing and Information Technology* (pp. 320-323). IEEE.

104. International Organization for Standardization, Mechanical vibration and shock—evaluation of human exposure to whole body vibration—part 1: general requirements, ISO 2631-1:1997, 1997.